

# Photopolarimetric Monitoring of Blazars in the Optical and Near-Infrared Bands with the Kanata Telescope.I. Correlations between Flux, Color, and Polarization

Yuki IKEJIRI<sup>1</sup>, Makoto UEMURA<sup>2</sup>, Mahito SASADA<sup>1</sup>, Ryosuke ITO<sup>1</sup>, Masayuki YAMANAKA<sup>1</sup>, Kiyoshi SAKIMOTO<sup>1</sup>, Akira ARAI<sup>3</sup>, Yasushi FUKAZAWA<sup>1</sup>, Takashi OHSUGI<sup>2</sup>, Koji S. KAWABATA<sup>2</sup>, Michitoshi YOSHIDA<sup>2</sup>, Shuji SATO<sup>4</sup>, and Masaru KINO<sup>4</sup>

<sup>1</sup>*Department of Physical Science, Hiroshima University, Kagamiyama 1-3-1,  
Higashi-Hiroshima 739-8526*

<sup>2</sup>*Hiroshima Astrophysical Science Center, Hiroshima University, Kagamiyama 1-3-1,  
Higashi-Hiroshima 739-8526  
uemuram@hiroshima-u.ac.jp*

<sup>3</sup>*Faculty of Science, Kyoto Sangyo University, Motoyama, Kamigamo, Kita-Ku, Kyoto-City 603-8555*

<sup>4</sup>*Department of Physics, Nagoya University, Furo-cho, Chikusa-ku, Nagoya 464-8602*

(Received 2011 January 19; accepted 2011 March 7)

## Abstract

We report on the correlation between the flux, color and polarization variations on time scales of days–months in blazars, and discuss their universal aspects. We performed monitoring of 42 blazars in the optical and near-infrared bands from 2008 to 2010 using TRISPEC attached to the “Kanata” 1.5-m telescope. We found that 28 blazars exhibited “bluer-when-brighter” trends in their whole or a part of time-series data sets. This corresponds to 88% of objects that were observed for  $> 10$  days. Thus, our observation unambiguously confirmed that the “bluer-when-brighter” trend is common in the emission from blazar jets. This trend was apparently generated by a variation component with a constant and relatively blue color and an underlying red component. Prominent short-term flares on time scales of days–weeks tended to exhibit a spectral hysteresis; their rising phases were bluer than their decay phases around the flare maxima. In contrast to the strong flux–color correlation, the correlation of the flux and polarization degree was relatively weak; only 10 objects showed significant positive correlations. Rotations of polarization were detected only in three objects: PKS 1510–089, 3C 454.3, and PKS 1749+096, and possibly in S5 0716+714. We also investigated the dependence of the degree of variability on the luminosity and the synchrotron peak frequency,  $\nu_{\text{peak}}$ . As a result, we found that lower luminosity and higher  $\nu_{\text{peak}}$  objects had smaller variations in their amplitudes both in the flux, color, and polarization degree. Our observation suggests the presence of several distinct emitting sources, which have different variation time-scales, colors, and polarizations. We propose that the energy injection by, for example, internal shocks in relativistic shells is a major factor for blazar variations on time scales of both days and months.

**Key words:** galaxies:active — galaxies: BL Lacertae objects: general — galaxies: jets

## 1. Introduction

Blazars are a subgroup of active galactic nuclei (AGN). They have relativistic jets that are believed to be directed along the line of sight (e.g. Blandford, Rees 1978). The emission from blazars can be detected in a very wide range of wavelengths from radio to TeV  $\gamma$ -ray regions, with strong variability on various time-scales (e.g. Hufnagel, Bregman 1992). Their spectral energy distribution (SED) is characterized by non-thermal continuum spectra that consist of low and high-energy components. The low-energy component is believed to be synchrotron radiation from relativistic electrons in the jet. The emission of this component is highly polarized (Angel, Stockman 1980; Mead et al. 1990). The origin of the high-energy component is not fully understood. The most plausible scenario is that it is emission via inverse Compton scat-

tering of synchrotron emission and/or external photons (e.g. Dermer et al. 1992; Sikora et al. 1994).

Blazars are classified into two categories: BL Lac objects and flat spectrum radio quasars (FSRQs) (Angel, Stockman 1980). Non-thermal continuum emission is dominant in BL Lac objects, while broad emission lines from AGN characterize FSRQs. BL Lac objects are further classified into three subtypes based on the peak frequency of synchrotron emission: high-, intermediate-, and low-energy peaked BL Lac objects (HBL, IBL, and LBL). The peak frequency lies higher than, around, and lower than the optical band in HBL, IBL, and LBL, respectively.

Multi-wavelength observations are essential to study blazars because of their emission in a wide range of wavelengths. The multi-wavelength study of blazars has recently entered a new era owing to  $\gamma$ -ray observations obtained with the Fermi satellite (Abdo et al. 2010a; Abdo

et al. 2010b). The origin of the high-energy component, for example, is expected to be revealed by the study of temporal variations in SEDs obtained with Fermi. Among the multi-wavelength study, optical data is important to understand the SED variations, because the optically-thin synchrotron emission in this band allows us to estimate basic physical parameters in the emitting region. For follow-up ground-based observations of Fermi blazars, we executed photopolarimetric monitoring of 42 blazars from 2008 to 2010. We obtained simultaneous optical and near-infrared (NIR) data using the “Kanata” 1.5-m telescope. Our observation provides one of the largest data sets of blazars in terms of variations in color and polarization on a time scale of days–months (Ikejiri et al. 2009). In this paper, we report on the results of simple correlation studies between the flux (,or luminosity), color, polarization degree ( $PD$ ), and polarization angle ( $PA$ ). We also discuss the implications for the mechanism of time variations in blazars obtained from our observations. A detailed study of polarization and the data, itself, will be published in a forthcoming paper.

The behavior of colors gives us a clue to understand the mechanism of time variations in blazars. Carini et al. (1992) report a possible feature that both BL Lac and OJ 287 became bluer when they were brighter (also see, Clements, Carini 2001). Ghisellini et al. (1997) observed S5 0716+714, and found that a bluer-when-brighter trend was seen only in its faint state. Its bluer-when-brighter trend was later confirmed in variations on a time scale shorter than days in its bright state (Wu et al. 2007a; Sasada et al. 2008). Villata et al. (2002) and Villata et al. (2004) report that the bluer-when-brighter trend in BL Lac was only observed in short-term variations, and not prominent in long-term ones. Raiteri et al. (2001) performed multi-band photometric observations of AO 0235+164 for four years, and found a bluer-when-brighter trend. As reported in those past studies, the bluer-when-brighter trend has been a well-observed feature in blazars, while its universality has not been established.

Systematic observations of multiple sources have also been performed in order to establish a characteristic feature of color variations in blazars. Ghosh et al. (2000) performed observations of five blazars. Their observation showed that 3C 66A only exhibited a bluer-when-brighter trend, while the other objects showed no significant correlation of the flux and color. Gu et al. (2006) investigated variations in color of eight blazars. The bluer-when-brighter trend was confirmed in five blazars. Among the other three objects, 3C 345 showed no correlation of the flux and color, and 3C 454.3 and PKS 0420–01 showed a reddening trend when they brightened. This “redder-when-brighter” trend in 3C 454.3 was confirmed in later observations (Raiteri et al. 2008b, Villata et al. 2006a). Thus, it is currently unclear whether the bluer-when-brighter trend is universal in blazars.

As well as the color variation, the polarimetric variation in the optical band has been extensively investigated in blazars. The temporal variation in polarization

has, in general, been considered to be erratic in blazars (e.g. Moore et al. 1982). On the other hand, a few cases have been reported in which the increase in  $PD$  was associated with flares of the total flux. For example,  $PD$  of Mrk 421 increased to  $\sim 14\%$  associated with its outburst in 1997 (Tosti et al. 1998). A significant correlation of the flux and  $PD$  was also detected in AO 0235+164 in 2006 (Hagen-Thorn et al. 2008). Most recently, several rotation episodes of  $PA$  have been found during flares (Marscher et al. 2008; Marscher et al. 2010; Abdo et al. 2010c; Jorstad et al. 2010). In general, the number of polarimetric observations has been much smaller than that of color observations. High-frequency, long-term polarimetric observations are required in order to find universal aspects that are possibly present.

The aim of this paper is to investigate universal aspects in blazar variability in the optical–NIR bands. We search for them with a simple correlation study between the flux, color, and polarization. In section 2, we describe the observation method and reduction processes. In section 3, first, we shortly introduce the basic properties of our sample (subsection 3.1). Then, we report on the results of our correlation studies of the flux and color (subsection 3.2), and the flux and polarization (subsection 3.3). We also search for rotation events of polarization in subsection 3.3. In subsection 3.4, we report on the dependence of the degree of variability on different luminosities and synchrotron peak frequencies. In section 4, we discuss the implication to the mechanism of blazar variability obtained from our observation. Finally, we summarize our findings in section 5.

## 2. Sample and Observation

### 2.1. Sample

We first selected our targets from the catalog, “Extended list of 206 possible AGN/blazar targets for GLAST multi-frequency analysis”<sup>1</sup> with an apparent magnitude of  $R \lesssim 16$ . Then, we performed test observations of those potential targets in early 2008. Objects were included in our sample in the case that the test observation confirmed that they were bright enough to monitor with the photopolarimetric mode ( $R \lesssim 16$ ). The number of selected objects from that catalog was 30. New objects were included in our sample when optical or  $\gamma$ -ray flares of them were detected during our monitoring period. The number of additional objects was 12. The total number of our target is, hence, 42. Table 1 lists our targets. Bright and/or highly variable sources were monitored more frequently than faint and/or stationary ones. This is because one of our aims was follow-up observations of  $\gamma$ -ray flares detected by Fermi.

The objects were classified into four subclasses, defined in Abdo et al. (2010a). Based on high-quality SEDs obtained almost simultaneously from radio to  $\gamma$ -rays, Abdo et al. (2010a) propose a new classification for blazars (FSRQs and BL Lac objects): Low, intermedi-

<sup>1</sup> <http://glastweb.pg.infn.it/blazar/>

**Table 1.** Observation log and list of comparison stars.

Object	Observation period	N	$T_{\text{exp}}$	Comparison star						
(1)	(2)	(3)	(4)	Coordinate	$V$	$J$	$K_s$	Ref.	$\sigma_V$	
				(5)	(6)	(7)	(8)	(9)	(10)	
QSO J0324+3410	08 Nov.20 — 09 Oct.14	2	93,11,1	03 24 33.78 +34 10 53.7	13.322	11.232	10.589	[6]*	0.010	
4C 14.23	09 Oct.15 — 09 Dec.07	16	280,6,0	07 25 20.89 +14 25 04.0	14.805	13.485	13.192	[4]	0.014	
PKS 1222+216	09 Apr.22 — 09 Apr.22	1	153,20,0	12 24 41.03 +21 21 26.5	15.660	14.024	13.500	[1]	0.007	
3EG J1236+0457	09 Jan.02 — 09 Jan.08	5	123,10,1	12 39 30.11 +04 39 52.6	14.095	12.942	12.638	[4]	0.026	
3C 279	08 Dec.09 — 10 Jan.24	64	200,10,1	12 56 16.90 —05 50 43.0	13.660	12.377	11.974	[1]*	0.006	
PKS 0215+015	08 Sep.09 — 09 Aug.25	6	103,20,8	02 17 49.22 +01 48 28.0	11.772	11.320	11.046	[6]	0.056	
QSO 0454–234	08 Oct.17 — 09 Dec.16	53	153,5,1	04 57 00.74 —23 26 05.9	12.184	10.849	10.364	[6]	0.034	
PKS 1510–089	09 Jan.12 — 10 Jan.21	57	200,10,1	15 12 53.19 —09 03 43.6	13.282	12.205	11.919	[3]†	0.013	
PKS 1749+096	08 Jul.18 — 09 Sep.10	78	200,5,1	17 51 37.28 +09 39 07.1	11.950	10.252	9.740	[1]	0.037	
OJ 287	08 May 26 — 10 Jan.31	174	103,15,1	08 54 59.01 +20 02 57.1	13.986	12.811	12.445	[3]	0.026	
3C 273	08 Dec.11 — 10 Jan.29	77	53,8,1	12 29 08.34 +02 00 17.2	12.718	11.345	10.924	[3]	0.039	
AO 0235+164	08 Aug.12 — 09 Jul.22	70	123,8,1	02 38 32.31 +16 35 59.7	12.720	11.248	10.711	[3]†	0.023	
OJ 49	08 Oct.31 — 10 Jan.25	52	183,15,1	08 32 00.74 +04 32 02.5	13.550	12.475	12.189	[1]	0.026	
MisV1436	08 Dec.17 — 10 Jan.19	103	123,10,1	01 36 42.49 +47 51 03.4	14.035	12.223	11.922	[6]*	0.034	
PKS 1502+106	08 Aug.09 — 10 Jan.29	80	200,20,1	15 04 36.51 +10 28 47.0	15.335	14.117	13.678	[4]	0.055	
3C 454.3	08 May 27 — 10 Jan.28	262	123,10,1	22 53 58.18 +16 09 06.9	13.587	11.858	11.241	[3]†	0.037	
PKS 0754+100	08 Nov.05 — 10 Jan.26	29	123,15,1	07 57 16.12 +09 55 47.8	13.000	11.852	11.496	[1]†	0.023	
BL Lac	08 May 26 — 10 Jan.28	196	123,4,1	22 02 45.45 +42 16 35.4	12.938	9.817	8.811	[3]†	0.020	
QSO 0948+002	09 Mar.30 — 09 Apr.10	3	183,20,1	09 49 10.19 +00 21 39.5	14.944	13.500	13.139	[4]	0.029	
S4 0954+658	08 Dec.03 — 09 Dec.14	5	183,12,1	09 58 50.44 +65 32 09.1	14.610	12.927	12.455	[1]	0.045	
S5 1803+784	08 Jul.08 — 09 Oct.18	35	123,15,3	17 59 52.6 +78 28 50.9	13.052	11.761	11.381	[1]*	0.027	
RX J1542.8+612	09 May 13 — 10 Jan.28	65	203,5,0	15 42 40.04 +61 30 25.1	14.000	10.354	9.593	[4]	0.016	
OQ 530	08 Jul.15 — 08 Sep.10	3	123,15,3	14 19 39.70 +54 21 55.0	15.961	13.873	13.131	[4]	0.016	
PKS 0048–097	08 Oct.02 — 09 Sep.23	46	123,10,1	00 50 47.23 —09 30 15.9	14.120	12.455	11.854	[1]	0.020	
ON 231	08 Dec.16 — 10 Jan.28	14	153,15,1	12 21 33.67 +28 13 04.0	12.080	10.921	10.597	[1]	0.068	
S2 0109+224	08 Jul.31 — 09 Oct.29	74	123,10,1	01 12 03.28 +22 43 26.7	12.510	11.245	10.886	[1]	0.031	
S5 0716+714	08 May 26 — 10 Jan.31	242	83,15,1	07 21 52.18 +71 18 16.1	12.475	11.320	10.980	[3]	0.021	
3EG 1052+571	08 Oct.31 — 09 Oct.13	3	103,5,3	10 58 37.99 +56 25 21.5	11.752	10.531	10.207	[4]	0.040	
3C 371	08 Jul.07 — 09 Dec.07	101	43,8,1	18 06 53.72 +69 45 37.4	12.588	12.219	11.856	[7]*	0.023	
3C 66A	08 Jul.09 — 10 Jan.31	227	123,15,1	02 22 55.12 +43 03 15.5	12.809	12.371	12.282	[3]	0.027	
PG 1553+113	08 Jul.08 — 10 Jan.17	22	63,10,1	15 55 52.28 +11 13 18.3	13.828	12.539	12.139	[5]	0.022	
ON 325	08 May 26 — 09 Dec.26	47	133,20,1	12 17 44.51 +30 09 43.6	14.960	13.674	13.232	[1]	0.058	
PKS 0422+004	08 Sep.04 — 09 Nov.11	42	133,10,1	04 24 42.42 +00 37 10.8	12.510	11.217	10.899	[1]	0.044	
H 1722+119	08 Jul.11 — 09 Oct.17	28	63,10,1	17 25 05.27 +11 52 11.0	13.210	11.308	10.710	[1]	0.024	
PKS 2155–304	08 Jul.09 — 09 Dec.22	137	43,5,1	21 59 02.47 —30 10 46.2	12.050	10.775	10.365	[1]	0.031	
1ES 2344+514	08 Jul.07 — 09 Oct.11	17	93,6,5	23 47 02.24 +51 43 17.6	12.610	11.421	11.117	[1]	0.030	
1ES 0806+524	08 Oct.30 — 10 Jan.31	18	123,10,1	08 09 40.65 +52 19 17.2	13.040	11.417	10.867	[1]	0.046	
Mrk 421	08 Jun.30 — 09 Mar.31	42	63,15,1	11 04 18.22 +38 16 30.9	15.570	14.453	14.106	[2]	0.073	
1ES 1959+650	08 Jul.07 — 09 Nov.28	53	103,10,1	20 00 26.51 +65 09 26.4	12.670	11.464	11.135	[2]	0.074	
Mrk 501	08 May 26 — 10 Jan.17	46	63,6,1	16 53 45.85 +39 44 08.8	12.598	10.935	10.399	[3]	0.018	
1ES 0647+250	08 Sep.09 — 10 Jan.29	7	200,10,1	06 50 40.57 +25 03 24.4	12.740	12.053	11.771	[6]*	0.015	
1ES 0323+022	08 Jul.25 — 10 Jan.28	24	153,10,1	03 26 13.42 +02 24 06.1	12.840	11.097	10.485	[1]	0.031	

(1)Object name. (2)Period of our monitoring. (3)Number of observations.

(4)Exposure times for each  $V$ ,  $J$ , and  $K_s$ -band image. (5)Coordinate of comparison stars.

(6),(7),(8) $V$ ,  $J$ , and  $K_s$  band magnitudes of comparison stars.

(9)References for the magnitudes of comparison stars.

(10) Standard deviations of the  $V$ -mag of the comparison stars during our monitoring period. The magnitudes were measured with neighbor check stars in the same field. Note that the check stars are fainter than the blazars in some cases, and hence,  $\sigma_V$  do not indicate the systematic error of the photometry of the blazars. It just indicates the constancy level of the comparison stars.

[1]Skiff (2007); [2]Villata et al. (1998); [3]González-Pérez et al. (2001); [4]Adelman-McCarthy et al. (2008);

[5]Doroshenko et al. (2005); [6]Høg et al. (2000); [7]McGimsey, Miller (1977).

\*We measured the  $V$ -magnitude of our comparison star using the stars listed in the reference.

†The NIR magnitudes were referred from the same reference for the  $V$ -band magnitude.

No symbol: The  $V$ -magnitude of the comparison star was quoted from the reference, and the NIR magnitudes were from the 2MASS catalog.

ate, and high synchrotron peaked blazars (LSP, ISP, and HSP blazars, respectively). LSP, ISP, and HSP blazars are defined as those having a synchrotron peak frequency,  $\nu_{\text{peak}}$ , of  $\nu_{\text{peak}} \lesssim 10^{14}$  Hz,  $10^{14} \lesssim \nu_{\text{peak}} \lesssim 10^{15}$  Hz, and  $\nu_{\text{peak}} \gtrsim 10^{15}$  Hz, respectively. All FSRQs are LSP blazars in their sample, except for one source (J1012.9+2435; ISP), which is not included in our sample. BL Lac ob-

jects are distributed in all three subclasses. According to Abdo et al. (2010a), the mean  $\nu_{\text{peak}}$  of LSP BL Lac objects is higher than that of FSRQs. This indicates that  $\nu_{\text{peak}}$  is lower in the following order: FSRQs < LSP-BL Lac < ISP-BL Lac < HSP-BL Lac. We classified blazars into these four subclasses, namely FSRQs, LSP BL Lac, ISP BL Lac, and HSP BL Lac, and used abbreviated forms of

Table 2. Observational properties of blazars.

Object Class	(log $\nu_{\text{peak}}$ ) <sup>z</sup>	Mag. (ref.)	$A_V$	$V$	$V - J$	PD	$r_{\text{color}}$	$r_{\text{pol.}}$	$r_{\text{col.}} - \text{pol.}$	N
(1)	(2) (3)	(4) (5)	(6)	(7)	(8)	(9)	(10)	(11)	(12)	
QSO J0324+3410	FSRQ (-) <sup>1</sup> 0.063 <sup>7</sup>	14.72V <sup>15</sup> -15.72V <sup>7</sup>	0.65	15.35-15.36	2.01-2.02	0.7-0.8	-	-	-	2
4C 14.23	FSRQ (-) <sup>2</sup> 1.038 <sup>7</sup>	19.0p <sup>16</sup> -17.48V <sup>7</sup>	0.27	16.53-17.48	1.62-1.79	2.6-21.3	-	(+0.13 <sup>+0.55</sup> -0.64)	-	16
PKS 1222+216	FSRQ (-) <sup>3</sup> 0.435 <sup>7</sup>	14.6R <sup>17</sup> -17.50V <sup>18</sup>	0.07	17.46	-	5.9	-	-	-	1
3EG J1236+0457	FSRQ (-) <sup>4</sup> 1.750 <sup>7</sup>	15.98U <sup>19</sup> -20.56V <sup>7</sup>	0.07	16.44-17.59	2.45-2.61	2.5-9.7	-	-	-	4
3C 279	FSRQ (12.6) <sup>5</sup> 0.538 <sup>7</sup>	11.51V <sup>20</sup> -17.75V <sup>7</sup>	0.09	15.45-17.32	2.43-3.01	2.8-36.3	+0.70 <sup>+0.13</sup> -0.20	+0.41 <sup>+0.21</sup> -0.27	-0.38 <sup>+0.31</sup> -0.24	64
PKS 0215+015	FSRQ (12.9) <sup>5</sup> 1.715 <sup>7</sup>	14.45V <sup>21</sup> -> 19.5V <sup>22</sup>	0.10	15.65-17.08	1.88-2.01	15.2-26.6	(-0.40 <sup>+1.14</sup> -0.55)	(+0.91 <sup>+0.09</sup> -1.32)	(+0.13 <sup>+0.34</sup> -1.08)	6
QSO 0454-234	FSRQ (13.1) <sup>5</sup> 1.003 <sup>7</sup>	16.58V <sup>23</sup> -19.84V <sup>23</sup>	0.14	15.16-16.89	1.85-2.22	2.2-12.3	(+0.29 <sup>+0.28</sup> -0.34)	(-0.23 <sup>+0.39</sup> -0.32)	(+0.23 <sup>+0.36</sup> -0.43)	53
PKS 1510-089	FSRQ (13.1) <sup>5</sup> 0.360 <sup>7</sup>	16.52V <sup>24</sup> -16.88V <sup>25</sup>	0.31	13.33-16.65	1.72-2.34	1.1-36.3	(-0.04 <sup>+0.29</sup> -0.23)	+0.83 <sup>+0.08</sup> -0.12	(-0.24 <sup>+0.30</sup> -0.25)	57
PKS 1749+096	LBL (13.1) <sup>5</sup> 0.320 <sup>7</sup>	15.88V <sup>26</sup> -17.88V <sup>15</sup>	0.55	14.06-17.01	2.07-2.83	1.7-25.7	+0.70 <sup>+0.10</sup> -0.14	(+0.15 <sup>+0.24</sup> -0.25)	(-0.17 <sup>+0.23</sup> -0.23)	78
OJ 287	LBL (13.4) <sup>5</sup> 0.306 <sup>7</sup>	12.2V <sup>27</sup> -17.4V <sup>28</sup>	0.09	13.86-15.65	1.87-2.45	10.4-37.8	+0.52 <sup>+0.12</sup> -0.14	(-0.06 <sup>+0.16</sup> -0.16)	(-0.05 <sup>+0.18</sup> -0.18)	174
3C 273	FSRQ (13.5) <sup>5</sup> 0.158 <sup>7</sup>	12.3V <sup>29</sup> -13.2V <sup>29</sup>	0.06	12.51-12.75	0.96-1.19	0.1-1.4	+0.47 <sup>+0.18</sup> -0.23	(+0.19 <sup>+0.22</sup> -0.24)	(+0.07 <sup>+0.27</sup> -0.28)	77
AO 0235+164	LBL (13.5) <sup>5</sup> 0.940 <sup>7</sup>	15.1V <sup>30</sup> -19.8V <sup>31</sup>	0.25	14.81-18.05	2.87-3.66	2.7-34.0	+0.68 <sup>+0.12</sup> -0.17	+0.78 <sup>+0.09</sup> -0.14	-0.55 <sup>+0.22</sup> -0.17	70
OJ 49	LBL (13.5) <sup>6</sup> 0.180 <sup>7</sup>	14.2B <sup>32</sup> -17.8B <sup>32</sup>	0.10	14.73-16.26	1.99-2.30	1.9-21.0	+0.54 <sup>+0.21</sup> -0.30	-0.66 <sup>+0.22</sup> -0.15	(+0.28 <sup>+0.30</sup> -0.37)	52
Mis V1436	FSRQ (13.6) <sup>5</sup> 0.859 <sup>7</sup>	14.1V <sup>33</sup> -19.0V <sup>33</sup>	0.48	15.53-17.81	2.66-3.10	0.5-40.1	(+0.07 <sup>+0.23</sup> -0.17)	+0.53 <sup>+0.14</sup> -0.17	-0.29 <sup>+0.24</sup> -0.17	103
PKS 1502+106	FSRQ (13.6) <sup>5</sup> 1.839 <sup>7</sup>	15.5V <sup>34</sup> -19.5V <sup>35</sup>	0.10	15.92-18.26	1.99-2.63	2.3-45.3	-0.35 <sup>+0.25</sup> -0.21	+0.64 <sup>+0.13</sup> -0.19	+0.30 <sup>+0.22</sup> -0.26	80
3C 454.3	FSRQ (13.6) <sup>5</sup> 0.859 <sup>7</sup>	12.0R <sup>36</sup> -16.96 <sup>37</sup>	0.33	13.59-16.14	1.34-2.41	0.2-22.3	-0.67 <sup>+0.08</sup> -0.07	+0.50 <sup>+0.10</sup> -0.11	+0.34 <sup>+0.12</sup> -0.13	262
PKS 0754+100	LBL (13.6) <sup>6</sup> 0.267 <sup>7</sup>	13.8V <sup>38</sup> -16.8V <sup>39</sup>	0.07	15.07-17.16	1.60-2.40	3.7-21.8	+0.84 <sup>+0.26</sup> -0.08	(-0.23 <sup>+0.45</sup> -0.13)	(-0.09 <sup>+0.57</sup> -0.16)	29
BL Lac	LBL (13.6) <sup>5</sup> 0.069 <sup>7</sup>	12.68B <sup>40</sup> -17.99B <sup>40</sup>	1.02	13.08-14.49	2.06-2.53	2.8-30.7	+0.64 <sup>+0.08</sup> -0.10	(-0.07 <sup>+0.16</sup> -0.15)	(-0.09 <sup>+0.16</sup> -0.15)	196
QSO J0948+0022	FSRQ (13.8) <sup>5</sup> 0.584 <sup>7</sup>	18.61V <sup>7</sup>	0.24	17.03-17.77	1.95	18.8	-	-	-	3
S4 0954+65	LBL (13.8) <sup>6</sup> 0.367 <sup>7</sup>	15.46V <sup>41</sup> -17.21V <sup>41</sup>	0.37	16.11-17.35	2.20-2.37	9.9-16.7	(-0.76 <sup>+1.51</sup> -0.24)	(-0.96 <sup>+0.98</sup> -0.04)	(-0.85 <sup>+1.46</sup> -0.15)	5
S5 1803+784	LBL (13.8) <sup>5</sup> 0.680 <sup>7</sup>	14.43V <sup>42</sup> -17.65V <sup>42</sup>	0.16	15.83-16.83	2.14-2.42	2.6-20.9	(+0.17 <sup>+0.37</sup> -0.39)	(+0.08 <sup>+0.37</sup> -0.39)	(-0.28 <sup>+0.37</sup> -0.39)	35
RX J1542.8+612	IBL (14.1) <sup>5</sup> -	16.25V <sup>7</sup> -16.97V <sup>15</sup>	0.05	14.55-15.24	1.65-1.98	0.4-13.4	+0.36 <sup>+0.23</sup> -0.28	(-0.05 <sup>+0.29</sup> -0.29)	(+0.25 <sup>+0.26</sup> -0.30)	65
OQ 530	IBL (14.2) <sup>6</sup> 0.152 <sup>7</sup>	12.0B <sup>43</sup> -16.8B <sup>44</sup>	0.04	16.06-16.31	2.38-2.48	6.4	-	-	-	3
PKS 0048-097	IBL (14.3) <sup>5</sup> -	15.30B <sup>45</sup> -17.52B <sup>45</sup>	0.10	14.92-16.17	1.69-2.01	0.5-21.5	(+0.23 <sup>+0.29</sup> -0.33)	(+0.12 <sup>+0.30</sup> -0.33)	(+0.10 <sup>+0.33</sup> -0.36)	46
ON 231	IBL (14.5) <sup>5</sup> 0.102 <sup>2</sup>	13B <sup>46</sup> -17.5B <sup>46</sup>	0.07	14.75-15.24	1.95-2.32	3.5-19.6	+0.78 <sup>+0.16</sup> -0.45	-0.56 <sup>+0.54</sup> -0.28	(+0.60 <sup>+0.29</sup> -0.65)	14
S2 0109+224	IBL (14.6) <sup>5</sup> 0.265 <sup>2</sup>	14.34B <sup>32</sup> -17.41B <sup>32</sup>	0.12	14.50-15.90	1.70-2.23	1.6-25.2	+0.33 <sup>+0.20</sup> -0.24	(+0.04 <sup>+0.25</sup> -0.25)	(-0.15 <sup>+0.27</sup> -0.27)	74
S5 0716+714	IBL (14.6) <sup>5</sup> 0.310 <sup>8</sup>	12.43V <sup>47</sup> -15.30V <sup>47</sup>	0.10	12.60-14.71	1.65-2.19	0.5-25.7	+0.66 <sup>+0.07</sup> -0.09	(-0.05 <sup>+0.14</sup> -0.13)	(-0.10 <sup>+0.14</sup> -0.14)	242
3EG 1052+571	IBL (14.6) <sup>5</sup> 0.144 <sup>2</sup>	14.2R <sup>48</sup> -15.63R <sup>48</sup>	0.02	15.52-15.56	2.04-2.11	3.0-3.9	-	-	-	3
3C 371	IBL (14.7) <sup>6</sup> 0.050 <sup>7</sup>	13.53V <sup>49</sup> -14.96V <sup>49</sup>	0.11	13.59-14.46	1.44-1.96	3.5-13.0	+0.92 <sup>+0.03</sup> -0.04	(-0.18 <sup>+0.22</sup> -0.20)	(-0.06 <sup>+0.21</sup> -0.21)	101
3C 66A	IBL (15.1) <sup>5</sup> (0.44) <sup>9,10</sup>	13.50V <sup>26</sup> -16.25V <sup>26</sup>	0.26	13.45-14.84	1.46-1.90	1.0-24.9	+0.50 <sup>+0.10</sup> -0.11	-0.18 <sup>+0.14</sup> -0.13	(+0.03 <sup>+0.15</sup> -0.15)	227
PG 1553+113	HBL (15.4) <sup>5</sup> (0.360) <sup>11,12</sup>	14.62B <sup>45</sup> -15.65B <sup>45</sup>	0.16	13.73-14.49	1.31-1.47	0.5-6.9	(+0.04 <sup>+0.45</sup> -0.46)	(+0.36 <sup>+0.33</sup> -0.45)	(+0.27 <sup>+0.39</sup> -0.50)	22
ON 325	HBL (15.5) <sup>5</sup> 0.130 <sup>7</sup>	13.7B <sup>32</sup> -17.46B <sup>26</sup>	0.07	14.93-15.59	1.63-1.94	5.4-15.0	+0.55 <sup>+0.20</sup> -0.29	-0.40 <sup>+0.30</sup> -0.23	(+0.26 <sup>+0.31</sup> -0.37)	47
PKS 0422+004	HBL (15.7) <sup>6</sup> (0.310) <sup>13</sup>	14.16B <sup>50</sup> -17.45B <sup>32</sup>	0.32	14.99-16.32	1.98-2.31	5.0-20.3	+0.86 <sup>+0.07</sup> -0.12	(-0.08 <sup>+0.34</sup> -0.32)	(+0.31 <sup>+0.32</sup> -0.35)	42
H 1722+119	HBL (15.8) <sup>6</sup> (0.018) <sup>2,14</sup>	15.77V <sup>51</sup> -16.6V <sup>52</sup>	0.53	14.78-15.33	1.37-1.77	1.9-10.3	(+0.15 <sup>+0.38</sup> -0.43)	+0.44 <sup>+0.29</sup> -0.43	(-0.18 <sup>+0.48</sup> -0.41)	28
PKS 2155-304	HBL (16.5) <sup>5</sup> 0.116 <sup>7</sup>	12.27V <sup>53</sup> -14.13V <sup>53</sup>	0.07	12.38-13.91	1.36-1.89	0.2-8.6	+0.41 <sup>+0.14</sup> -0.16	+0.19 <sup>+0.17</sup> -0.18	(+0.05 <sup>+0.18</sup> -0.18)	137
1ES 2344+514	HBL (16.4) <sup>6</sup> 0.044 <sup>7</sup>	15.2V <sup>39</sup> -15.5V <sup>39</sup>	0.65	15.08-15.25	2.58-2.84	0.7-5.4	+0.87 <sup>+0.08</sup> -0.22	(+0.49 <sup>+0.32</sup> -0.34)	(-0.45 <sup>+0.55</sup> -0.54)	17
1ES 0806+524	HBL (16.6) <sup>6</sup> 0.138 <sup>7</sup>	14.72R <sup>54</sup> -15.62R <sup>54</sup>	0.14	15.45-15.91	1.86-2.09	1.1-8.2	+0.69 <sup>+0.20</sup> -0.42	(+0.42 <sup>+0.36</sup> -0.56)	(-0.21 <sup>+0.55</sup> -0.44)	18
Mrk 421	HBL (16.6) <sup>5</sup> 0.031 <sup>7</sup>	11.6B <sup>55</sup> -16B <sup>55</sup>	0.05	13.23-13.69	1.59-1.94	0.1-4.9	+0.73 <sup>+0.18</sup> -0.43	+0.48 <sup>+0.28</sup> -0.43	(-0.49 <sup>+0.58</sup> -0.33)	42
1ES 1959+650	HBL (16.6) <sup>5</sup> 0.047 <sup>7</sup>	12.8V <sup>56</sup> -16V <sup>56</sup>	0.53	14.12-14.64	1.57-1.87	1.4-11.4	+0.80 <sup>+0.08</sup> -0.13	(+0.03 <sup>+0.28</sup> -0.29)	(-0.01 <sup>+0.28</sup> -0.28)	53
Mrk 501	HBL (17.1) <sup>5</sup> 0.033 <sup>7</sup>	13.66B <sup>32</sup> -14.93B <sup>32</sup>	0.06	13.92-14.06	2.36-2.59	0.6-3.9	+0.68 <sup>+0.14</sup> -0.22	(+0.03 <sup>+0.34</sup> -0.34)	(+0.08 <sup>+0.31</sup> -0.32)	46
1ES 0647+250	HBL (18.3) <sup>6</sup> 0.203 <sup>9</sup>	15.30V <sup>7</sup>	0.31	15.50-16.08	1.25-1.54	1.9-5.7	-	(+0.59 <sup>+0.40</sup> -1.45)	-	7
1ES 0323+022	HBL (19.9) <sup>6</sup> 0.147 <sup>7</sup>	15.56V <sup>57</sup> -17.28V <sup>58</sup>	0.34	16.19-16.77	1.84-2.10	3.0-10.5	+0.78 <sup>+0.13</sup> -0.28	+0.50 <sup>+0.29</sup> -0.48	(-0.38 <sup>+0.54</sup> -0.37)	24

(1) Object name. (2) Blazar class and the peak frequency of synchrotron radiation.

(3) Redshift. Those which have been disputed or not been confirmed are indicated by parentheses.

(4) Variation range reported in previous studies. No correction for the interstellar extinction was performed.

(5) V-band interstellar absorption referred from Schlegel et al. (1998). (6) The minimum and maximum values of V-band magnitude in this study.

The correction for the interstellar extinction has been performed. (7) The minimum and maximum values of V - J.

The correction for the interstellar reddening has been performed. (8) The minimum and maximum values of the polarization degree (PD) in percent.

(9) Correlation coefficient between the V-band magnitude and V - J. (10) Correlation coefficient between the V-band flux and PD.

(11) Correlation coefficient between the V - J and PD. The correlation coefficients with parentheses indicate that the correlation was not statistically significant.

(12) The number of observations. References: <sup>1</sup>Zhou et al. (2007); <sup>2</sup>Healey et al. (2008); <sup>3</sup>Burbidge, Kinman (1966); <sup>4</sup>Halpern et al. (2003);

<sup>5</sup>Abdo et al. (2010a); <sup>6</sup>Nieppola et al. (2006); <sup>7</sup>Véron-Cetty, Véron (2010); <sup>8</sup>Nilsson et al. (2008); <sup>9</sup>Massaro et al. (2009);

<sup>10</sup>Bramel et al. (2005); <sup>11</sup>Falomo, Treves (1990); <sup>12</sup>Aharonian et al. (2006); <sup>13</sup>Mickaelian et al. (2006); <sup>14</sup>Sbarufatti et al. (2006);

<sup>15</sup>Souchay et al. (2009); <sup>16</sup>Condon et al. (1977); <sup>17</sup>Hauser et al. (2010); <sup>18</sup>Sandage (1972); <sup>19</sup>Tramacere, Rea (2009);

<sup>20</sup>Webb et al. (1990); <sup>21</sup>Kikuchi (1988); <sup>22</sup>Gaskell (1982); <sup>23</sup>Impey, Tapia (1988); <sup>24</sup>Barbieri et al. (1983); <sup>25</sup>Kataoka et al. (2008);

<sup>26</sup>Fan, Lin (2000a); <sup>27</sup>Sillanpaa et al. (1985); <sup>28</sup>Takalo et al. (1990); <sup>29</sup>Soldi et al. (2008); <sup>30</sup>Raiteri et al. (2008a); <sup>31</sup>Takalo et al. (1998); <sup>32</sup>Zekl et al. (1981);

<sup>33</sup>Yoshida et al. (2008); <sup>34</sup>Wills et al. (1992); <sup>35</sup>Morton et al. (2008); <sup>36</sup>Villata et al. (2006b); <sup>37</sup>Corso et al. (1988); <sup>38</sup>Tapia et al. (1977);

<sup>39</sup>Xie et al. (2002); <sup>40</sup>Fan et al. (1998); <sup>41</sup>Raiteri et al. (1999); <sup>42</sup>Nesci et al. (2002); <sup>43</sup>Miller (1978); <sup>44</sup>Smith et al. (1987);

<sup>45</sup>Pica et al. (1988); <sup>46</sup>Liu et al. (1995); <sup>47</sup>Qian et al. (2002); <sup>48</sup>Bloom et al. (2004); <sup>49</sup>Carini et al. (1998); <sup>50</sup>Massaro et al. (1996);

<sup>51</sup>Brissenden et al. (1990); <sup>52</sup>Griffiths et al. (1989); <sup>53</sup>Fan, Lin (2000b); <sup>54</sup>Kapanadze (2009); <sup>55</sup>Liu et al. (1997); <sup>56</sup>Villata et al. (2000);

<sup>57</sup>Feigelson et al. (1986); <sup>58</sup>Zhang et al. (2008)

the latter three subclasses as LBL, IBL, and HBL.

We identified 27 of our monitoring objects in the catalog presented in Abdo et al. (2010a). The classification of these 27 objects was based on Abdo et al. (2010a). Among the remaining 15 objects, prominent emission lines have been observed in QSO J0324+3410 (Marcha et al. 1996; Zhou et al. 2007), PKS 1222+216 (Burbidge, Kinman 1966), 4C 14.23 (Healey et al. 2008), and 3EG J1236+0457 (Halpern et al. 2003). Hence, these four objects belong

to FSRQs. Then, the classification of the remaining 11 objects was based on Nieppola et al. (2006). According to Nieppola et al. (2006), BL Lac objects are classified into three subgroups: namely LBL, IBL, and HBL, defined by  $\nu_{\text{peak}}$  estimated from radio-optical (with X-rays in several cases) SEDs. Their criteria for subgroups are, however, different from those in Abdo et al. (2010a):  $\nu_{\text{peak}} \lesssim 10^{14.5}$  Hz for LBL,  $10^{14.5} \lesssim \nu_{\text{peak}} \lesssim 10^{16.5}$  Hz for IBL, and  $\nu_{\text{peak}} \gtrsim 10^{16.5}$  Hz for HBL. We classified the



remaining 11 objects by adopting the criteria defined in Abdo et al. (2010a) using  $\nu_{\text{peak}}$  estimated in Nieppola et al. (2006). Table 2 gives  $\nu_{\text{peak}}$  and subclasses of each object. Our sample includes 13 FSRQs, 8 LBLs, 9 IBLs, and 12 HBLs. We note that  $\nu_{\text{peak}}$  can significantly shift, depending on the brightness of blazars (e.g. Costamante et al. 2001). It is possible that the classification of each object changes with time, even with the same criterions. Table 2 also presents the red-shift,  $z$ , and the variation range obtained from previous literature.

## 2.2. Observation and data reduction

We performed photopolarimetric observations of those blazars simultaneously in the optical  $V$ -, and the NIR  $J$ -, and  $K_s$ -bands from 2008. We used TRISPEC attached to the 1.5-m ‘‘Kanata’’ telescope at Higashi-Hiroshima Observatory. TRISPEC is capable of simultaneous three-band (one optical and two NIR bands) imaging or spectroscopy, with or without polarimetry (Watanabe et al. 2005). TRISPEC has a CCD and two InSb arrays. Table 1 presents the observation period, the number of observations, and the typical exposure times of each image. A part of NIR images failed to be obtained because of mechanical errors. The  $K_s$ -band data are, especially, limited, and have a low quality. In this paper, we mainly use  $V$ - and  $J$ -band data for the color and correlation analysis, except for in sub-subsection 3.2.1.

The photometry of blazars was performed in a standard procedure of CCD images; after making dark-subtracted and flat-fielded images, the magnitudes were measured using the aperture photometry technique. The radius of the aperture, which depended on the seeing size of each night, was 3–5 arcsec. These correspond to 3–4 pixels on the optical CCD. Since the pixel scale of the NIR InSb arrays of TRISPEC is large ( $\sim 1.66$  arcsec), the NIR images were slightly de-focused in order to avoid undersampling. On the NIR arrays, the FWHM of a point source was adjusted to be  $\sim 3$  pixels, which correspond to the aperture size of the NIR images. It is well known that the photometry of a part of blazars is complicated by the presence of a host galaxy component. Subtraction of contamination of the host galaxy is, in general, possible if the host galaxy is well resolved on images (e.g. Kotilainen et al. 1998; Nilsson et al. 2007). Unfortunately, the angular resolution of our instrument is too low to accurately estimate the host galaxy contamination. Hence, we performed no correction for it in the present work. The obtained magnitude corresponds to the combined flux from the jet, AGN, and the host galaxy.

We calculated differential magnitudes of blazars using comparison stars located in the same frame. We checked the constancy of the brightness of the comparison stars using the differential photometry between them and neighbor stars in the same field. The standard deviations of the  $V$ -band magnitudes,  $\sigma_V$ , are given in table 1. We confirmed that each comparison star exhibited no significant variation. The  $V$ -band magnitude of the comparison stars were taken from previous literature. The references are given in the ninth column of table 1. The symbol ‘‘\*’’

represents cases that our image includes no comparison stars listed in the reference. In this case, we measured the  $V$ -magnitude of our comparison star using the stars listed in the reference. The  $J$ - and  $K_s$ -band magnitudes were referred from the 2MASS catalog (Skrutskie et al. 2006), except for the cases with the symbol ‘‘†’’ in table 1. The NIR magnitudes with this symbol were taken from the same reference for the  $V$ -band magnitude.

The correction for the interstellar extinction,  $A_V$ , and the color excess were performed according to Schlegel et al. (1998). The magnitude and color presented in this paper are corrected values. The correction was not done for the historical variation range given in table 2.

A set of polarization parameters was calculated from four consecutive images, which were obtained with half-wave-plate angles of  $0^\circ$ ,  $22.5^\circ$ ,  $45.0^\circ$ , and  $67.5^\circ$ . We took 12 sets of images for each object on one night, from which three sets of polarimetric data were obtained. We confirmed that the instrumental polarization was smaller than 0.1 % in the  $V$ -band using observations of unpolarized standard stars. Hence, we applied no correction for it. The zero point of the polarization angle was corrected as the standard system (measured from north to east).

Since we present no discussion about intra-day variability in this paper, we only use nightly-averaged photometric and polarimetric data. Observations were sometimes carried out under bad sky conditions. Some data obtained under such conditions have very large errors. They could just disrupt systematic trends, which may exist in blazar variability. In this paper, we only use photometric data with an error of less than 0.1 mag, color indices with an error less than 0.1, and  $PD$  with an error less than 5%. In Appendix, we show the temporal variation in the flux, color,  $PD$ ,  $PA$ , and the color-magnitude and magnitude- $PD$  diagrams, and the Stokes  $QU$  plane for all objects. Those data will be published in electric form in a forthcoming paper about a detailed analysis of polarization (Paper II).

## 3. Results

### 3.1. Basic Properties of the Sample

#### 3.1.1. Relationship between the red-shift, luminosity, and synchrotron peak frequency, with comments on the blazar sequence

In this subsection, we report on basic properties of our sample. We investigated the relationships between the red-shift,  $z$ , the optical luminosity,  $\nu L_\nu$ , and the synchrotron peak frequency,  $\nu_{\text{peak}}$ , of our sample. We calculated the minimum, average, and maximum  $\nu L_\nu$  during our observation period for our sample whose  $z$  is known. The observed minimum and maximum values of the  $V$ -band magnitudes and  $z$  are presented in table 2. No estimation of  $\nu L_\nu$  was given in the case that  $z$  has not been well determined. Such  $z$  are indicated in parentheses in table 2. We assumed a flat universe with  $H_0 = 71 \text{ km s}^{-1} \text{ Mpc}^{-1}$  and  $\Omega_m = 0.27$  for calculating  $\nu L_\nu$ .

Figure 1 shows the  $z$  distribution of our sample. Our sample is distributed in  $z = 0.02$ –1.75. The  $\nu L_\nu$  rep-

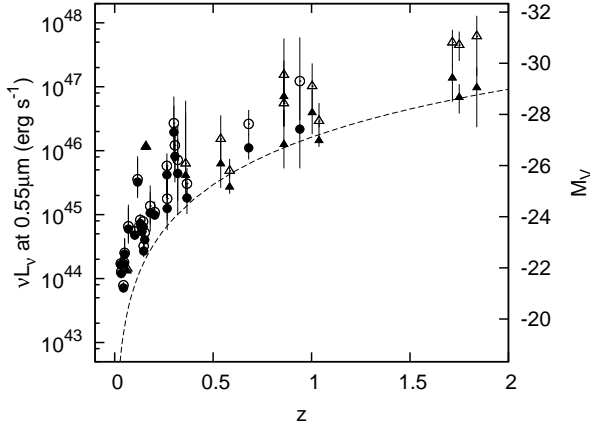


**Fig. 1.**  $z$  distribution of the  $V$ -band luminosity ( $\nu L_\nu$ ) (and absolute magnitude,  $M_V$ ) of our sample. The circles and triangles represent the average  $\nu L_\nu$  during our observation period for BL Lac objects and FSRQs, respectively. The filled and open circles represent the observed and  $K$ -corrected luminosities, respectively. The vertical bars associated with each point show variation ranges defined by the observed minimum and maximum values of the magnitude during our observation period. The dashed line indicates an apparent magnitude of  $V = 17.0$

represented by the open circles were calculated from the observed magnitudes with a  $K$ -correction. For the  $K$ -correction, we assumed SEDs in two power-law forms between the  $V$ – $J$ -band and  $J$ – $K_s$ -band regions. The flux densities at 0.55, 1.22, and 2.16  $\mu\text{m}$  were obtained from our simultaneous  $V$ -,  $J$ -, and  $K_s$ -band observations, respectively. Then, the rest-frame flux densities at 0.55  $\mu\text{m}$  were estimated with those three flux densities and the two-power-law SEDs. The dashed line in figure 1 represents an apparent magnitude of  $V = 17.0$ . This curve indicates that our sample had a limit magnitude of  $V \sim 17$ .

Figure 2 shows the  $\nu_{\text{peak}}$  distribution of the luminosity. In addition to the  $K$ -correction, a red-shift correction was performed to  $\nu_{\text{peak}}$  of the open circles by multiplying  $\nu_{\text{peak}}$  by  $(1+z)$ . An anti-correlation is apparent between  $\nu L_\nu$  and  $\nu_{\text{peak}}$ . The anti-correlation is more emphasized between the corrected  $\nu L_\nu$  and  $\nu_{\text{peak}}$ , as indicated by the open circles.

The anti-correlation between  $\nu L_\nu$  and  $\nu_{\text{peak}}$  is well known as the “blazar sequence”, which was first proposed by Fossati et al. (1998). According to Ghisellini et al. (1998), the blazar sequence can be explained by the idea that a synchrotron cooling works more severely for low-energy electrons in more powerful blazars. As a result, it leads to smaller  $\nu_{\text{peak}}$  in them. However, it has been suspected that the blazar sequence scenario involves serious problems about the selection effects (Costamante et al. 2001; Padovani et al. 2003; Caccianiga, Marchã 2004; Antón, Browne 2005; Nieppola et al. 2006; Padovani 2007). When the blazar sequence is evaluated, a problem is the high variability not only in  $\nu L_\nu$ , but also  $\nu_{\text{peak}}$  (e.g. Costamante et al. 2001). Simultaneous measurements of  $\nu L_\nu$  and  $\nu_{\text{peak}}$  are, hence, required. The

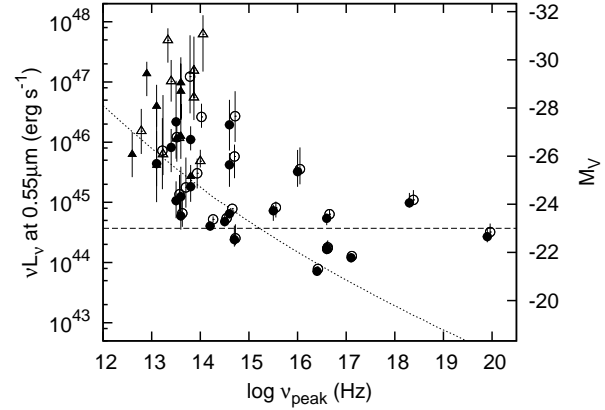
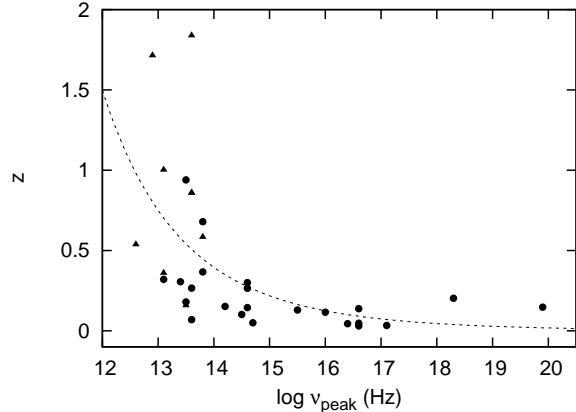


**Fig. 2.**  $\nu_{\text{peak}}$  distribution of the  $V$ -band luminosity ( $\nu L_\nu$ ) (and absolute magnitude,  $M_V$ ) of our sample. The circles and triangles represent BL Lac objects and FSRQs, respectively. The filled and open circles represent the observed and the  $K$ -corrected luminosities, respectively. The redshift-correction was also performed for  $\nu_{\text{peak}}$  of the open circles. The vertical bars associated with each point show the minimum and maximum values of the magnitude during our observation period. The dashed line represents the luminosity of a typical host galaxy (Urry et al. 2000). The dotted line represents an apparent magnitude of  $V = 17$  obtained from the  $z$ – $\nu_{\text{peak}}$  relation in figure 3.

$\nu_{\text{peak}}$  of our sample are mostly quoted from Abdo et al. (2010b), who analyzed multi-wavelength data taken in the almost same observation periods as those of our monitoring. Hence, our data can provide one of the most reliable tests for the blazar sequence scenario in terms of simultaneous measurements of  $\nu L_\nu$  and  $\nu_{\text{peak}}$ .

As shown in figure 2, the result is apparently compatible with the blazar sequence scenario originally proposed by Fossati et al. (1998). The blazars with a high  $\nu_{\text{peak}}$  of  $> 10^{16}$  Hz had  $M_V \sim 6$  mag fainter than those with a low  $\nu_{\text{peak}}$  of  $< 10^{14}$  Hz. It is evident that our observation did not cover the faintest states in several blazars, as can be seen in table 2. The observed faintest states in a part of LBLs and FSRQs are, in particular,  $\sim 3$  mag brighter than the previously recorded faintest states. However, the anticorrelation between  $\nu L_\nu$  and  $\nu_{\text{peak}}$  still appears even if  $\nu L_\nu$  are estimated from the faintest states ever recorded. This indicates that the flux variability actually has no major affect on the blazar sequence scenario.

We comment on the selection effects. Several studies have reported that deep radio observations found sources that have low  $\nu L_\nu$  and low  $\nu_{\text{peak}}$  (Padovani et al. 2003; Caccianiga, Marchã 2004; Antón, Browne 2005). Similar results were also obtained in the optical data collected by Nieppola et al. (2006). The presence of sources having low  $\nu L_\nu$  and low  $\nu_{\text{peak}}$  contradicts the blazar sequence scenario. Figure 3 shows the  $\nu_{\text{peak}}$  distribution of  $z$  of our sample. IBLs and HBLs having  $\nu_{\text{peak}} > 10^{14}$  Hz can be found only in a low  $z$  region of  $z < 0.5$ . In contrast, a part of LBLs and FSRQs can be found in a high  $z$  region of  $z > 0.5$ , as well as in a low  $z$  region. The dashed line in



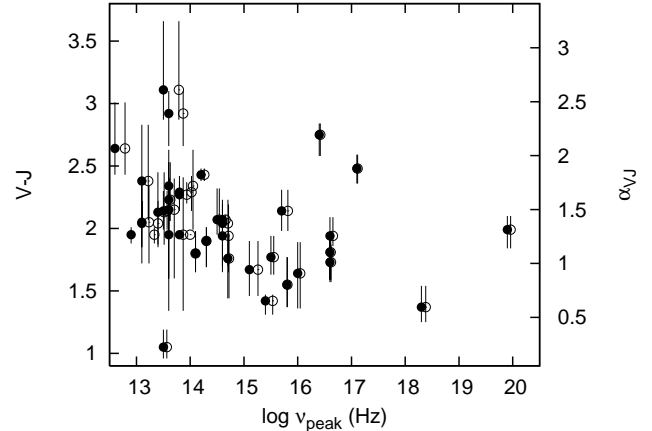
**Fig. 3.**  $\nu_{\text{peak}}$  distribution of the red-shift,  $z$  of our sample. The circles and triangles represent BL Lac objects and FSRQs, respectively. The dashed line represents the best-fitted power-law model of  $z$  against  $\nu_{\text{peak}}$ .

figure 3 represents the best-fitted power-law model of  $z$  against  $\nu_{\text{peak}}$ . While the power-law form has no physical meaning here, this empirical model well represents a trend of  $z$  versus  $\nu_{\text{peak}}$ . In conjunction with the curve, which indicates the apparent magnitude of  $V = 17$  in figure 1, this model for  $z$  provides  $\nu L_\nu$  corresponding to  $V = 17$  in figure 2. The dotted line in figure 2 represents it. Objects are detectable over this curve in a magnitude-limited sample. As suggested by this curve, the apparent lack of low  $\nu L_\nu$  and low  $\nu_{\text{peak}}$  sources could be due to a selection effect present in magnitude-limited samples.

Second, the lack of high  $\nu L_\nu$  and high  $\nu_{\text{peak}}$  blazars is also suspected to be due to a selection effect. Giommi et al. (2005) propose that such blazars, if exist, would have featureless optical spectra, which make it difficult to estimate  $z$  and luminosity (also see, Giommi et al. 2002). Urry et al. (2000) have reported that host galaxies of BL Lac objects have an absolute magnitude of  $M_R = -23.7 \pm 0.6$ . Assuming  $V - R = 0.7$  for elliptical galaxies, we show the  $V$ -band absolute magnitude of the typical host galaxy in figure 2 by the dashed line. It has been reported that the luminosity of the host galaxy is not severely dependent on  $z$  in a region of  $z < 0.5$  (Scarpa et al. 2000; Urry et al. 2000). Our sample includes only a few IBLs and HBLs having luminosities one order higher than that of the typical host galaxy. A significant part of BL Lac objects has such high luminosities in  $\nu_{\text{peak}} \lesssim 10^{14}$  Hz. They are, however, LBLs in  $z > 0.5$ , where the absolute magnitudes of the host galaxy are poorly known. Thus, our observation is compatible with the scenario proposed by Giommi et al. (2005).

### 3.1.2. Relationship between the color and synchrotron peak frequency

Figure 4 shows the  $\nu_{\text{peak}}$  distribution of  $V - J$ . The spectral index between the  $V$ - and  $J$ -band region,  $\alpha_{V,J}$ , defined with  $f_\nu \propto \nu^{-\alpha_{V,J}}$ , is also shown in the right side of the figure. We calculated  $\alpha_{V,J}$  from the flux density at 0.55 and 1.22  $\mu\text{m}$  estimated from the  $V$ - and  $J$ -band obser-



**Fig. 4.**  $\nu_{\text{peak}}$  distribution of the  $V - J$  color index ( $\circ$ , and the spectral index,  $\alpha_{V,J}$ ) of our sample. The filled and open circles represent the observed and the red-shift corrected data, respectively. The vertical bars associated with each point show the minimum and maximum values of  $V - J$  during our observation period.

vations, assuming a power-law form of spectra. The figure indicates an anti-correlation between  $V - J$  and  $\nu_{\text{peak}}$  in a region of  $\nu_{\text{peak}} \lesssim 10^{16}$  Hz. This anti-correlation can be naturally expected if the optical-NIR emission is dominated by synchrotron emission from jets. The overall trend of  $V - J$  ( $\alpha_{V,J}$ ) is qualitatively analogous to that of the spectral index between the radio and optical regions (Fossati et al. 1998; Nieppola et al. 2006).

In the lowest  $\nu_{\text{peak}}$  regime, objects are distributed around  $\alpha_{V,J} = 1.5$ . This is consistent with the model of synchrotron self-Compton emission in blazar jets; the spectral index is predicted to be 1.5 in a high energy region where Compton cooling is efficient (Chiang, Böttcher 2002). The optical band definitely corresponds to this high energy region in low  $\nu_{\text{peak}}$  objects. On the other hand, most objects can reach  $\alpha_{V,J} > 1.5$ , as can be seen from the figure. This might suggest that the Compton cooling actually worked more efficiently than the model predicted. Alternatively, it may suggest that the number of high-energy electrons is much smaller than that expected from the standard power-law form of the energy distribution of electrons.

The anti-correlation of  $V - J$  and  $\nu_{\text{peak}}$  appears to be weak in a high  $\nu_{\text{peak}}$  region of  $\nu_{\text{peak}} \gtrsim 10^{15}$  Hz. In this  $\nu_{\text{peak}}$  region, the spectral index is distributed around  $\sim 1.0$ . There is no object in our sample in which fully self-absorbed synchrotron emission ( $\alpha \lesssim -1$ ) is dominant in the optical-NIR band. These colors of high  $\nu_{\text{peak}}$  sources imply that blazars have nearly flat SEDs ( $\alpha \sim 1$ ) in a region even 4-5 orders of magnitude below  $\nu_{\text{peak}}$ . Alternatively, the contamination of the red host galaxy may be significant, particularly in low-luminosity HBLs. In fact, we found that two low luminosity HBLs, 1ES 2344+514 ( $\nu_{\text{peak}} = 10^{16.4}$  Hz) and Mrk 501 ( $\nu_{\text{peak}} = 10^{17.1}$  Hz), had quite red colors of  $V - J \sim 2.8$  and  $\sim 2.5$ , respectively, which suggest a large contribution of their

host galaxies in the observed fluxes. In addition, it has been reported that the UV–IR emission of Mrk 501 can be reproduced with a strong contribution of an elliptical galaxy (Katarzyński et al. 2001).

Before closing this subsection, we mention the anomalies in a low  $\nu_{\text{peak}}$  region in figure 4. First, the reddest source is AO 0235+164 ( $V - J = 3.1$ ). This object is suggested to be affected by absorption by foreground galaxies (e.g. Yanny et al. 1989). The quite red color of AO 0235+164 is, hence, due to color excess arising from the foreground galaxies. According to Raiteri et al. (2005), the color excess,  $E(V - J)$ , arising from them is estimated to be 0.673. The mean corrected  $V - J$  is, then, calculated as 2.44, which is rather normal for FSRQs and LBLs having  $\nu_{\text{peak}} \sim 10^{13-14}$  Hz. The second reddest source is MisV1436 ( $V - J = 2.9$ ), whose violent variability has been first reported in 2008 by the MISAO project.<sup>2</sup> No detailed study has been performed for this object. Its atypically red color suggests that this blazar is a noteworthy object. Third, the bluest source is 3C 273 ( $V - J = 1.1$ ), one of the most famous QSOs. A large contamination of the big blue bump originated in its AGN component has been confirmed in optical spectroscopy and polarimetric observations (Impey et al. 1989; Smith et al. 1993). The blue color of 3C 273 is due to the strong contribution of the AGN component.

### 3.2. Light Curve and Color Variation

#### 3.2.1. Time lag between variations in the optical and NIR bands

Multi-wavelength studies of blazar variability have shown that variations in different wave-bands occasionally correlate with significant time-lags (e.g. Ulrich et al. 1997). It has been reported that the variation in low-energy synchrotron photons tends to lag behind that in high-energy ones. In HBLs, for example, variations in soft X-rays lag those of hard X-rays by hours (Takahashi et al. 1996; Kataoka et al. 2000) and variations in UV photons lag those of X-rays or  $\gamma$ -rays by 1–2 d (Buckley et al. 1996; Urry et al. 1997). A time lag of low-energy photons indicates a spectral hysteresis in flares; for example, a spectrum becomes hardest before the flare maximum (Kataoka et al. 2000). Such spectral hystereses have also been reported in optical flares (Ciprini et al. 2003; Wu et al. 2007b). The time lag and spectral hysteresis are expected in the case that synchrotron cooling governs temporal variations in a flare region. High-energy electrons diminished more quickly than low-energy ones by cooling (Takahashi et al. 1996; Kirk et al. 1998).

We searched for universal time lags between the optical and NIR variations for each object. We calculated the correlation function between the  $V$ -,  $J$ - and  $K_s$ -band light curves. We used the discrete correlation function ( $DCF$ ) method (Edelson, Krolik 1988). The  $DCF$  method was proposed to estimate a correlation function from unevenly sampled data. For two data streams,  $a_i$  and  $b_i$ , the  $DCF$  method first calculates a set of unbinned discrete correla-

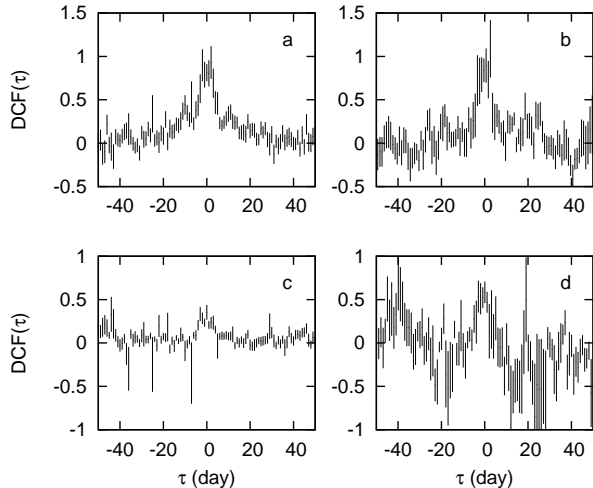


**Fig. 5.**  $DCF$  between the light curves in the  $V$ - and  $J$ -bands (panel a), the  $V$ - and  $K_s$ -bands (panel b), the  $V$ -band light curve and the  $V - J$  color (panel c), and the  $V$ -band light curve and the  $V - K_s$  color (panel d) calculated from the data of BL Lac.

tions,

$$UDCF_{ij} = \frac{(a_i - \bar{a})(b_j - \bar{b})}{\sqrt{(\sigma_a^2 - e_a^2)(\sigma_b^2 - e_b^2)}}, \quad (1)$$

where  $\bar{a}$  and  $\bar{b}$  are the averages of the data values,  $\sigma_a$  and  $\sigma_b$  are their standard deviations, and  $e_a$  and  $e_b$  are the observation error of each data.  $DCF$  for each time lag,  $\tau$ , is defined as an average of  $UDCF$  having the same  $\tau$ : Averaging over the  $M$  pairs for which  $\tau - \Delta\tau/2 \leq \Delta\tau_{ij} < \tau + \Delta\tau/2$ ,

$$DCF(\tau) = \frac{1}{M} \sum UDCF_{ij}. \quad (2)$$

The standard error for each bin is:

$$\sigma(\tau) = \frac{1}{M-1} \left\{ \sum [UDCF_{ij} - DCF(\tau)]^2 \right\}^{1/2}. \quad (3)$$

The upper panels in figure 5 show the  $DCF$  between the light curves in the  $V$ - and  $J$ -bands (panel a) and the  $V$ - and  $K_s$ -bands (panel b) calculated from the data of BL Lac. We also calculated the  $DCF$  between the  $V$ -band light curve and the  $V - J$  or  $V - K_s$  color, as shown in the lower panels in figure 5. We found no significant time-lag in these results for BL Lac. As well as BL Lac, we calculated and checked  $DCF$  for all blazars we observed. We confirmed that no object exhibited a universal significant time-lag between variations in the different bands and the colors.

Then, we searched for time lags in the optical and NIR light curves for each prominent flare, while no clear lag was found between  $V$ - and  $J$ -band light curves of flares in all objects. On the other hand, we found several cases that the bluest phase in  $V - J$  preceded the flare maximum. Panels (a) and (b) of figure 6 present examples for S5 0716+714 and PKS 0048–097, respectively. The

<sup>2</sup> (<http://www.aerith.net/misao/variable/MisV1436.html>)



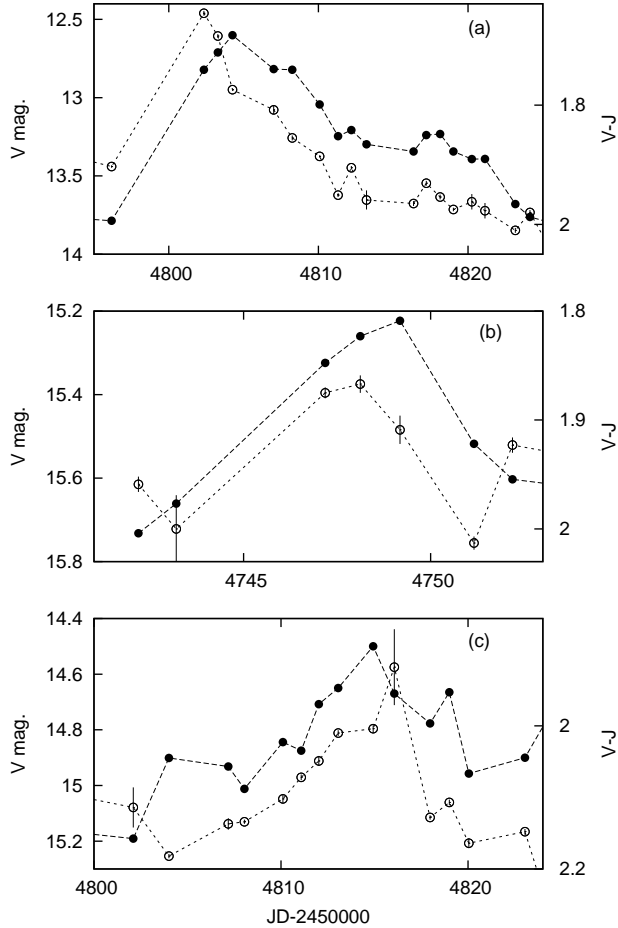


**Fig. 6.** Examples of flares showing time lag between different wave-bands. Panel a, b, and c: The  $V$ -band light curves (filled circles) and  $V - J$  color (open circles) during flares in S5 0716+714, PKS 0048-097, and S2 0109+224, respectively.

lags were 2 and 1 d for S5 0716+714 and PKS 0048-097, respectively. We systematically searched for time lags between the flux and color during such flares. It is expected that a time lag possibly present in small flares would readily disappear by the composition of another small flares. Hence, prominent flares should be selected. We selected such flares with the following criteria: (i) A flare maximum was defined as the brightest point in a period of 15 d before and after the maximum date. (ii) A peak-to-peak amplitude of the flare must be larger than  $V = 1.0$  within 30 d. (iii) A flare maximum must be recorded within 5 d after and before the neighboring observations. The selection with these criteria yielded 17 flares. Among those 17 events, the peak of the flux coincided with the bluest time in nine events. Seven events showed the precedence of the bluest phase against the flare maximum. One event in S2 0109+224 possibly showed a lag of the bluest time behind the flare maximum, which is shown in panel (d) of figure 6. All lags were 1–2 d. These results suggest that the bluest phase of flares tended to precede the flare maximum by  $\lesssim 1$  d.

The spectral hysteresis associated with flares is again discussed in sub-subsection 3.2.3. In the next subsection, we investigate the correlation between the flux and color, neglecting time lags between them.

### 3.2.2. Correlation between the $V$ -band light curve and the $V - J$ color index

We present examples of the light curves, color variations, and color-magnitude diagrams in figure 7. Panel (a) shows those of 3C 371. The color-magnitude diagram clearly indicates that the object became bluer when it was brighter. In this paper, we conclude that an object had a bluer-when-brighter trend in the case that it showed a significant positive correlation between the  $V$ -band magnitude and the  $V - J$  color index. We used the Pearson product-moment correlation coefficient. The significance of the correlation was tested using the Student's  $t$ -test. The correlation coefficient and its 95 % confidence interval of 3C 371, for example, were calculated as  $0.92^{+0.03}_{-0.04}$ . Thus, we conclude that 3C 371 had a bluer-when-brighter trend. We calculated the correlation coefficients using the whole data sets of 42 blazars, as well as 3C 371. The results are listed as  $r_{\text{color}}$  in table 2. We found that 23 blazars had significant bluer-when-brighter trends. The correlation coefficients that are not statistically significant are shown with parentheses in table 2.

Two blazars, 3C 454.3 and PKS 1502+106, had significant negative correlations between the light curve and color, in other words, a redder-when-brighter trend ( $r_{\text{color}} = -0.67^{+0.08}_{-0.07}$  and  $-0.35^{+0.25}_{-0.21}$ , respectively, as shown in table 2). Panel (b) of figure 7 shows the light curve and color-magnitude diagram of 3C 454.3. As reported in Sasada et al. (2010), this object exhibited a redder-when-brighter trend when it was fainter than  $V \sim 15$ , while a bluer-when-brighter trend was observed when it was brighter. This feature can be confirmed in figure 7. A redder-when-brighter trend was detected in the whole data because the object had almost stayed in the faint state during our observation period. As well as 3C 454.3, PKS 1510-089 and PG 1553+113 also exhibited redder-when-brighter trends in their faint states (see, figures 21 and 28). No significant correlation of the flux and color was detected in those two objects when their whole data were used. Bluer-when-brighter trends were significantly detected in 3C 454.3 and PKS 1510-089 in their bright states ( $V < 15.0$  for 3C 454.3 and  $< 15.5$  for PKS 1510-089).

It is widely accepted that the redder-when-brighter trend in the faint state is attributed to a strong contribution of thermal emission from an accretion disk (also see, Smith et al. 1986; Hagen-Thorn, Yakovleva 1994, Pian et al. 1999). The contribution of the thermal disk emission would definitely be small when the flux from the jet increases. Hence, the bluer-when-brighter trends in the bright states of 3C 454.3 and PKS 1510-089 probably have the same origin as those in ordinary objects. Including 3C 454.3 and PKS 1510-089, the number of objects that showed a bluer-when-brighter trend is 25.

PG 1553+113 exhibited a significant redder-when-brighter trend in its faint state ( $V > 13.8$ ), as well

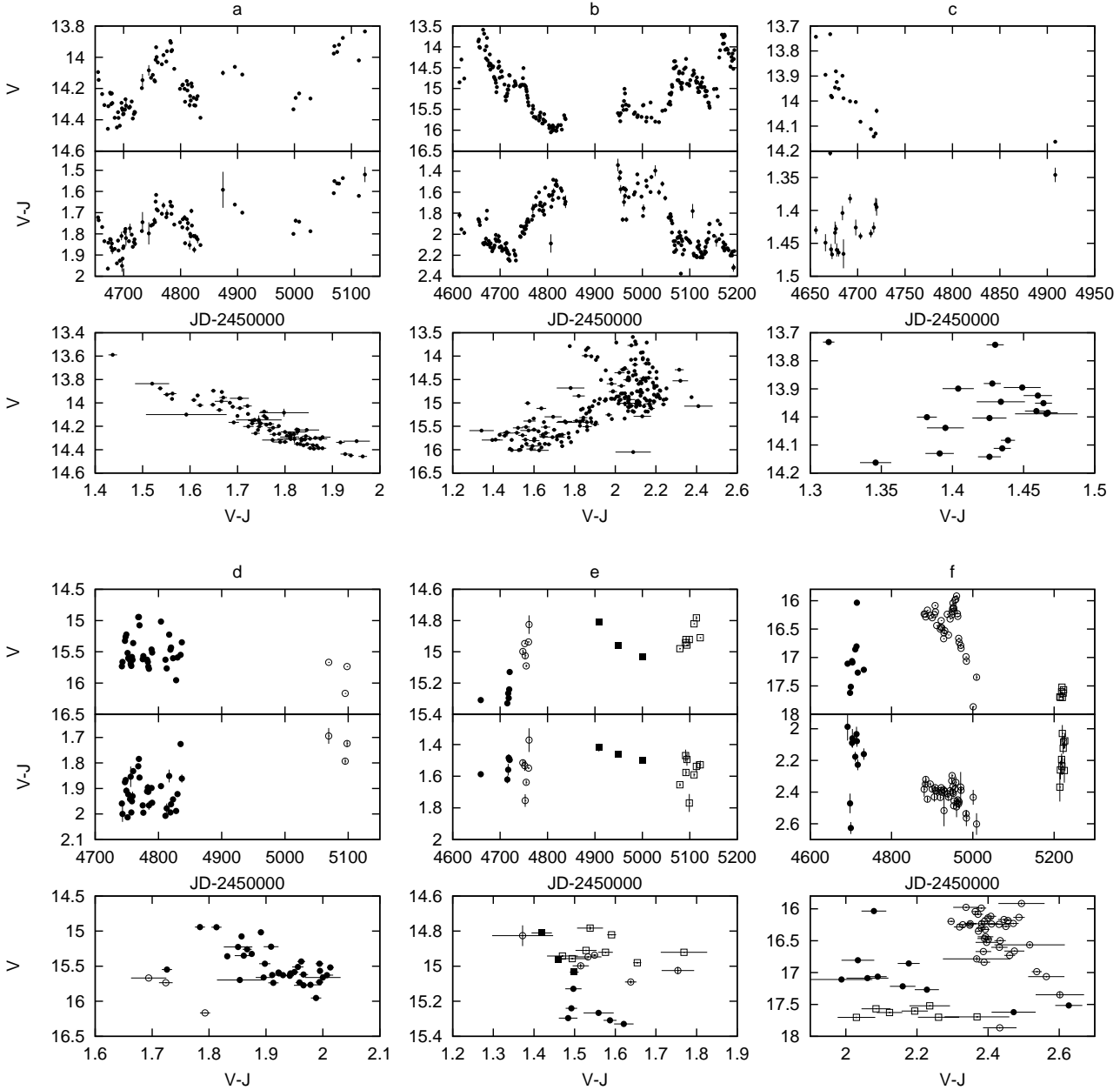


**Fig. 7.** Examples of the V-band light curve (top),  $V - J$  color variation (middle), and their color-magnitude diagram (bottom) of blazars. Panel a: 3C 371, b: 3C 454.3, c: PG 1553+113, d: PKS 0048-097, e: H 1722+119, and f: PKS 1502+106. In the lower three panels, different symbols represent observations taken in different periods of time.

as 3C 454.3 and PKS 1510–089. No bluer-when-brighter trend was significantly detected in its bright state. Panel (c) of figure 7 shows the color-magnitude diagram of this object. The redder-when-brighter trend in the faint state, however, possibly weakens above  $V = 13.8$ . This weakening of the redder-when-brighter trend may suggest a transition of a bluer-when-brighter trend in a bright state of PG 1553+113.

There are seven blazars that showed no significant correlation between the  $V$ -band magnitude and the  $V - J$  color, in addition to PKS 1510–089 and PG 1553+113. The numbers of observations are quite small for two objects: PKS 0215+015 and S4 0954+65. Only 6 and 5 observations were made, respectively. They are too small to conclude anything about the correlation. There are five blazars that was observed for  $> 10$  d and showed no significant correlation of the light curve and color: QSO 0454–234, MisV1436, S5 1803+784, PKS 0048–097, and H 1722+119.

Even in these five objects, bluer-when-brighter trends were occasionally seen in a short period of time. Panel (d) of figure 7 shows the variation in the magnitude and the color for PKS 0048–097. Our observation of PKS 0048–097 covered two seasons in 2008 (JD 2454741–2454851) and 2009 (JD 2455068–2455097). A significant bluer-when-brighter trend was detected in the 2008 observation shown in the filled circles in panel (d). A possible bluer-when-brighter trend can be seen also in the 2009 observation shown in the open circles, while the number of observations is too small to conclude it. It is important to note that, in the color-magnitude diagram, the 2009 data apparently shows a different bluer-when-brighter slope from the 2008 data. This is the reason why no significant correlation was detected when we performed a correlation analysis using all data.

A similar behavior can also be seen in H 1722+119 [panel e of figure 7]. We divided our observation period into four periods of time (JD 2454659–2454720, JD 2454747–2454760, JD 2454908–2455001, and JD 2455079–2455121), and show them by different symbols in panel (e). Bluer-when-brighter trends are apparently seen in the first (filled circles), second (open circles), and third (filled squares) epochs, while the number of observations is small. A sign of bluer-when-brighter trends can also be seen in QSO 0454–234, MisV 1436, and S5 1803+784 in their bright states (see figure 22, 25, and 27, respectively). QSO 0454–234 exhibited a significant bluer-when-brighter trend in its bright state ( $V < 16.0$ ), while the trend is not statistically significant in MisV 1436 and S5 1803+784.

We found that PKS 1502+106 also exhibited a flux-color behavior similar to those of PKS 0048–097 and H 1722+119, although a redder-when-brighter trend was detected in this object in its whole data from 2008 to 2010. Panel (f) of figure 7 shows the variations in the magnitude and color of PKS 1502+106. We calculated correlation coefficients for each year, and found significant bluer-when-brighter trends in both the 2008 and 2009 data sets. In 2010, this object remained faint ( $V > 17.2$ ) and showed no

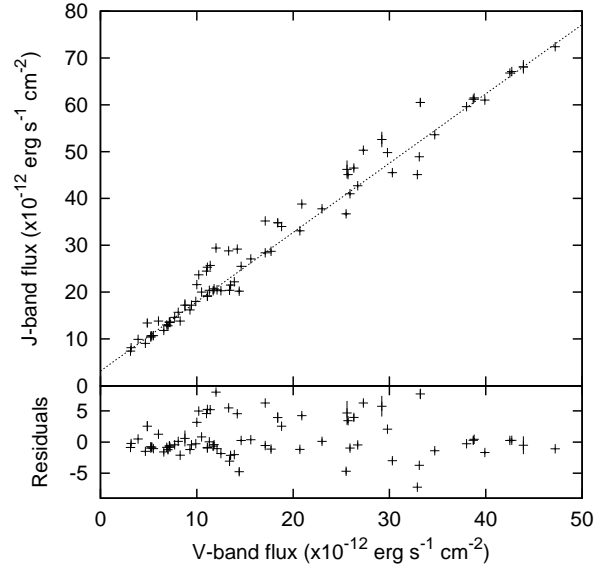


**Fig. 8.** Upper panel:  $J$ - and  $V$ -band flux variations observed in PKS 1749+096. The lower panel: Residuals of the  $J$ -band flux from the best-fitted linear model.

significant correlation between the light curve and color.

The sample reduces to 32 blazars once we exclude 10 objects, in which the number of  $V - J$  observations is  $< 10$ . In these 10 objects, observations are too few to conclude whether there is a significant correlation between the light curve and color. Among those 32 blazars, in summary, 23 blazars showed significant bluer-when-brighter trends in their total data. Five blazars showed temporary significant bluer-when-brighter trends in short periods of time (QSO 0454–234, PKS 1510–089, PKS 1502+106, 3C 454.3, and PKS 0048–097). Then, we conclude that a total of 28 blazars, corresponding to 88 % of the well-observed sample, had the bluer-when-brighter trend. Four blazars (PG 1553+113, H 1722+119, S5 1803+784, and MisV 1436) possibly showed a sign of bluer-when-brighter trends, although the trends were not statistically significant in our data.

### 3.2.3. $J$ - and $V$ -band Flux Diagram

Most blazars exhibited the bluer-when-brighter trend, as mentioned in the last subsection. Two scenarios can be considered to generate the bluer-when-brighter trend. The first scenario is that the variation component, itself, had a bluer-when-brighter trend. The second scenario is that the color of the variation component was constant with time, while an underlying component was redder than the flare component. We can evaluate those two scenarios using the  $F_J - F_V$  diagrams, where  $F_J$  and  $F_V$  denote the  $J$ - and  $V$ -band fluxes, respectively. Examples of the  $F_J - F_V$  diagrams are presented in figures 8, 9, and 10. In these figures, achromatic variations are described in a form of  $F_J = cF_V$ , where  $c$  is a constant.

$F_J$  can be described with a linear function of  $F_V$  in most objects. A typical example is PKS 1749+096, as shown in figure 8. The linear relationship holds over one order of

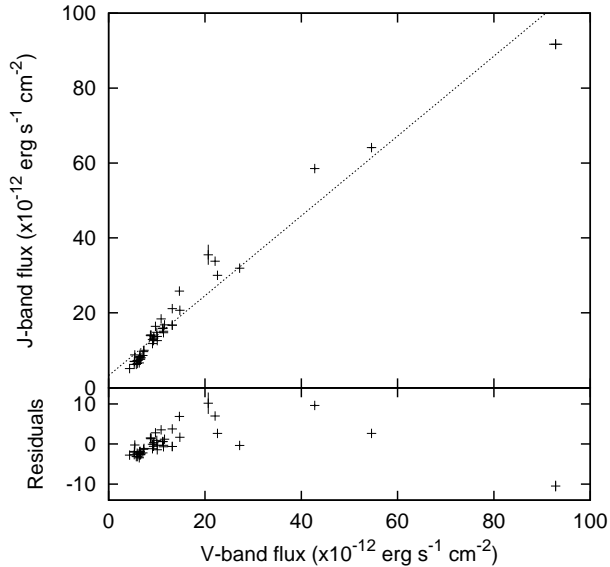


Fig. 9. As for figure 8, but for PKS 1510–089.

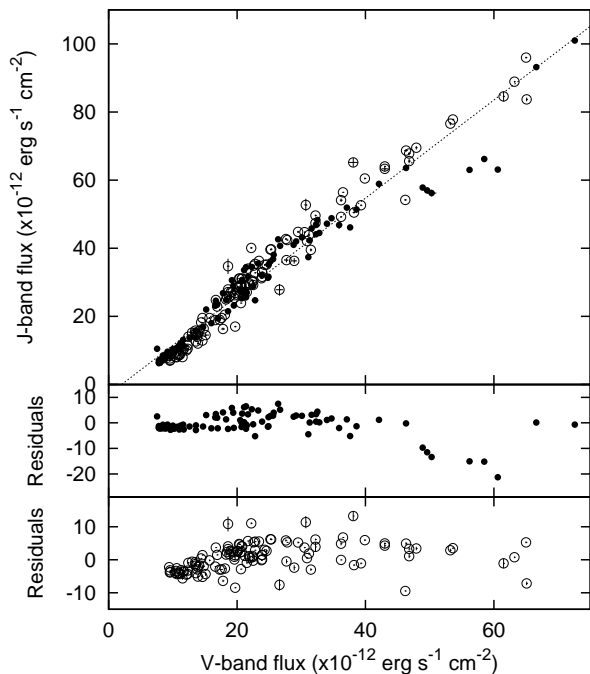


Fig. 10. Top panel: As for figure 8, but for 3C 454.3. The filled and open circles represent the observations in 2008 and 2009, respectively. The middle and bottom panels: Residuals of the 2008 and 2009 data, respectively.

magnitude of the flux. We confirmed that linear regression models for  $F_J$  and  $F_V$  yielded significant positive intersections of  $F_J$  at  $F_V = 0$  in all bluer-when-brighter objects. These results support that there was an underlying component which was redder than the variation components and the color of the variation components was roughly constant.

We note that there are two possible exceptions of our 28 bluer-when-brighter blazars in terms of the  $F_J$ – $F_V$  relation: PKS 1510–089 and 3C 454.3. Their  $F_J$ – $F_V$  diagrams are shown in figures 9 and 10, respectively. In both objects, we can see a sign of systematic deviations from their best-fitted linear models; the slope is steep in a low flux regime, but shallow in a high flux one. The 2008 and 2009 observations of 3C 454.3 are represented by the filled and open circles, respectively. PKS 1510–089 and 3C 454.3 had a common feature that they showed redder-when-brighter trends when they were faint, as mentioned in sub-subsection 3.2.2. The low-flux regimes in the  $F_J$ – $F_V$  diagram correspond to the redder-when-brighter phase.

Next we focus on the behavior of short-term flares on time scales of days–weeks in the  $F_J$ – $F_V$  diagram. In sub-subsection 3.2.1, we describe our search for spectral hysteresis associated with flares through time-lags between different band fluxes, or between the flux and the color. This approach could be effective if the observed colors directly represent the color of the variation components. However, as mentioned above, the observed color is probably a composition of an underlying red component and variable ones. It could be better to search for a sign of hysteresis using the  $F_J$ – $F_V$  diagram.

Figure 11 shows the  $F_J$ – $F_V$  diagram (lower panels) and the  $V$ -band light curves (upper panels) for three short-term flares (flare a, b, and c) observed in PKS 1749+096. Flares a, b, and c are shown in left, middle, and right panels, respectively. In flare a, the rising phase appears to draw a different path from the decay phase in the  $F_J$ – $F_V$  diagram. As a result, we can see hysteresis in this diagram. The object appears to draw a “loop” in the  $F_J$ – $F_V$  diagram, moving in the anti-clockwise direction in the loop during the flare. This behavior means that the rising phase of the flare was bluer than the decay phase around the flare maximum. We can also see similar hystereses in flares b and c, while the hysteresis in flare c may be just an erroneous one because a detailed behavior was overlooked around the peak of flare c.

We searched for such hystereses for all short-term flares that we observed. It is expected that a hysteresis of a small flare in the  $F_J$ – $F_V$  diagram is disturbed by the superposition of other small flares. Hence, we again used the 17 prominent flare events that are selected in sub-subsection 3.2.1. Then, we calculated the slopes in the  $F_J$ – $F_V$  diagram for rise and decay phases of those flares. The slopes were defined as:

$$(\Delta F_J / \Delta F_V)_{\text{rise}} = (F_{J,p} - F_{J,p-1}) / (F_{V,p} - F_{V,p-1}) \quad (4)$$

$$(\Delta F_J / \Delta F_V)_{\text{decay}} = (F_{J,p} - F_{J,p+1}) / (F_{V,p} - F_{V,p+1}), \quad (5)$$

where  $F_{J(V),p}$  and  $F_{J(V),p\pm 1}$  denote the  $J$ -( $V$ )-band fluxes



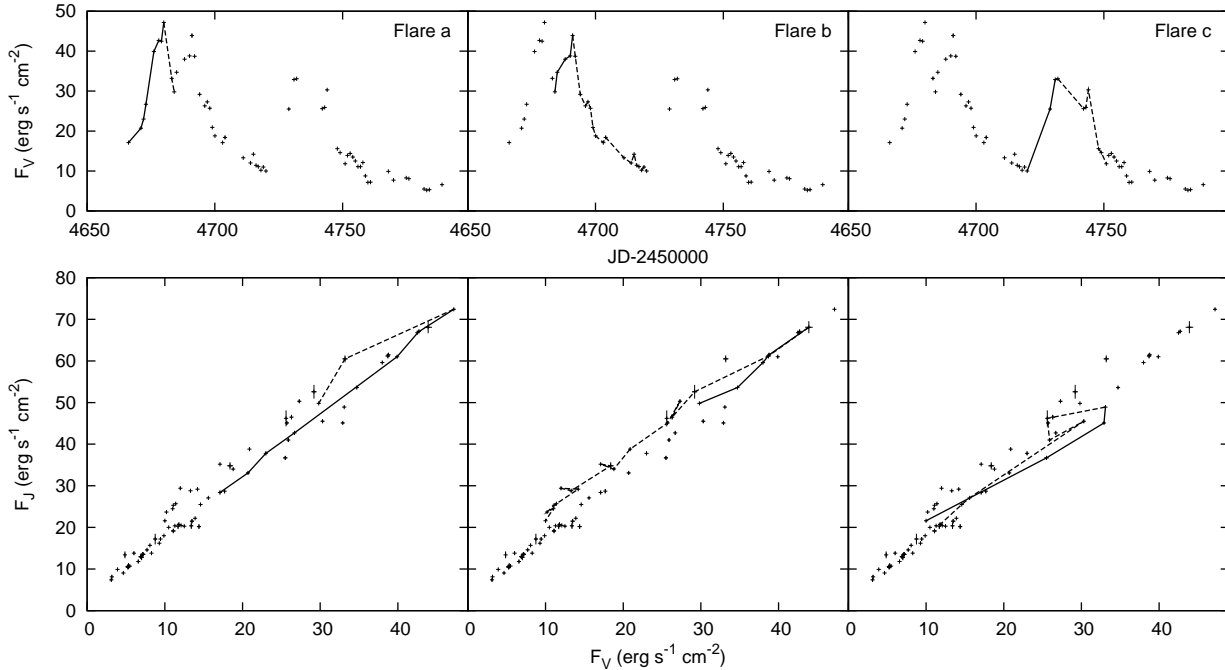


**Fig. 11.**  $V$ -band light curves (upper panels) and the  $F_J$ – $F_V$  diagrams (lower panels) of PKS 1749+096. The rise and decay phases of three flares (flare a, b, and c) are represented by the solid and dashed lines in each panel, respectively.

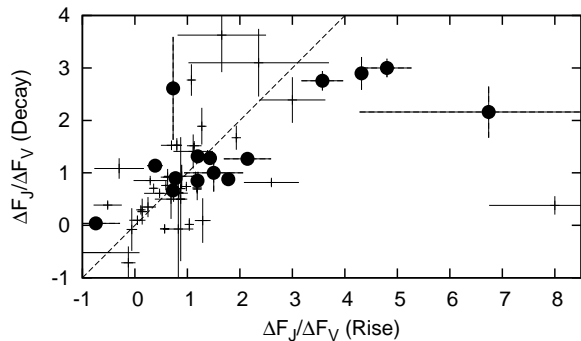


**Fig. 12.** Slope in the  $F_J$ – $F_V$  diagram of the rise and decay phases around the maxima of short-term flares. The filled circles and crosses represent the flares which were selected with peak-to-peak amplitudes of  $> 1.0$  mag and  $> 0.1$  mag, respectively. The dashed line represents  $(\Delta F_J / \Delta F_V)_{\text{rise}} = (\Delta F_J / \Delta F_V)_{\text{decay}}$ .

at the flare maximum and its neighboring observations. The case of  $(\Delta F_J / \Delta F_V)_{\text{rise}} = (\Delta F_J / \Delta F_V)_{\text{decay}}$  means that there is no hysteresis. The case of  $(\Delta F_J / \Delta F_V)_{\text{rise}} > (\Delta F_J / \Delta F_V)_{\text{decay}}$  indicates that a rising phase is bluer than a decay phase, as can be seen in figure 11. The case of  $(\Delta F_J / \Delta F_V)_{\text{rise}} < (\Delta F_J / \Delta F_V)_{\text{decay}}$  indicates that a rising phase is redder than a decay phase.

Figure 12 shows  $\Delta F_J / \Delta F_V$  of the rise and decay phases of the 17 flares, as indicated by the filled circles. There are 11 flares showing  $(\Delta F_J / \Delta F_V)_{\text{rise}} > (\Delta F_J / \Delta F_V)_{\text{decay}}$ , five flares showing  $(\Delta F_J / \Delta F_V)_{\text{rise}} < (\Delta F_J / \Delta F_V)_{\text{decay}}$ , and

one flare showing no significant hysteresis. This result suggests that the spectral hysteresis of  $(\Delta F_J / \Delta F_V)_{\text{rise}} > (\Delta F_J / \Delta F_V)_{\text{decay}}$  was more preferable for the prominent short-term flares. The crosses in the figure represent  $\Delta F_J / \Delta F_V$  for small flares selected with a peak-to-peak amplitude of 0.1–1.0. The fraction of these small flares showing  $(\Delta F_J / \Delta F_V)_{\text{rise}} > (\Delta F_J / \Delta F_V)_{\text{decay}}$  was comparable to that showing  $(\Delta F_J / \Delta F_V)_{\text{rise}} < (\Delta F_J / \Delta F_V)_{\text{decay}}$ . This is probably due to the superposition of multiple flares that disturb the hysteresis pattern of each flare.

The spectral hysteresis was detected in the sample of prominent flares whose peaks were recorded within 5 d after and before the neighboring observations (see subsection 3.2.1). Together with the time-lag analysis described in subsection 3.2.1, the time-scale of the hysteresis events that we detected is, hence, less than a few days. This is comparable with or possibly shorter-than-average sampling rate of our monitoring. It is possible that short-term hysteresis events could be overlooked in the flares of  $(\Delta F_J / \Delta F_V)_{\text{rise}} \leq (\Delta F_J / \Delta F_V)_{\text{decay}}$ .

### 3.3. Light Curve and Polarization

#### 3.3.1. Time lag between variations in the light curve and the polarization degree

We searched for time lags between the light curve and the polarization degree ( $PD$ ) using the  $DCF$  method, as described in sub-subsection 3.2.1. Figure 13 presents an example of  $DCF$ , which was calculated with all data of the  $V$ -band flux and  $PD$  of BL Lac. As shown in this figure, we found no significant time-lag between them. We calculated  $DCF$  for all blazars that we observed, and con-

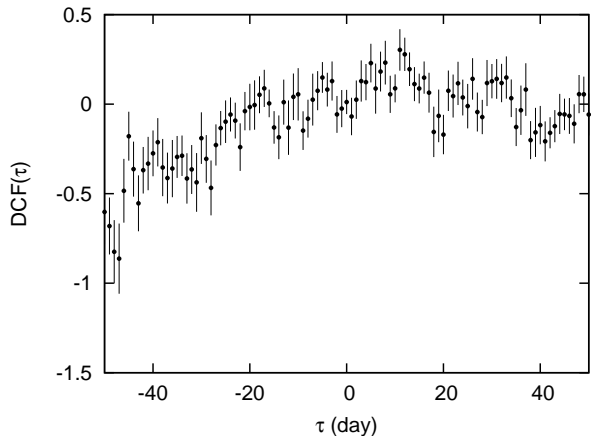


**Fig. 13.** *DCF* calculated with the *V*-band light curve and the polarization degree of BL Lac.

firmed that no objects exhibited a significant time-lag between the light curve and *PD*. As mentioned in the next subsection, the correlation, itself, was weak between the flux and *PD*.

We selected 17 prominent flare events in subsection 3.2.1. The peak timings of their light curves were coincident with those of *PD*, or there was no correlation between them at all, except for the flares observed in PKS 1510–089, AO 0235+164, and PKS 1502+106. Sasada et al. (2011) report that the increases in *PD* were associated with prominent flares in PKS 1510–089 and AO 0235+164 using the same data as that in the present paper. The *PD* peaks preceded the flux peaks by 1 d in PKS 1510–089 and 4 d in AO 0235+164. On the other hand, figure 14 shows the cases that the *PD* maximum lagged the flux one. The upper panel shows the light curve and *PD* in PKS 1502+106. A large flare having double peaks can be seen in JD 2454940–2454970. The double-peaked feature was also seen in the variation in *PD*, while both peaks of *PD* lagged behind those of the light curve by 3 d. Similar events were also found in 3C 454.3. A large flare in  $\sim$ JD 2455170 was followed by a subsequent increase in *PD*, as shown in the lower panel of figure 14. The lag was about 5 d. All of those time-lags were not universal in each object; there were flares showing no or shorter time-lags in all objects.

Thus, there was no universal time-lag between the flux and *PD*. As well as the flux–color correlation, the flux–*PD* correlation is also discussed without respect to time lags in the next subsection.

### 3.3.2. Correlation between the *V*-band light curve and the polarization degree

We report on the correlation of the flux and *PD* in this subsection. We present examples of the light curves and variations in *PD* in figure 15. Panel (a) of figure 15 shows those of AO 0235+164. *PD* of this object became higher when it was brighter. As described in subsection 3.2.2, we calculated the Pearson correlation coefficients with the *V*-band flux and *PD*, and tested them using the Student’s

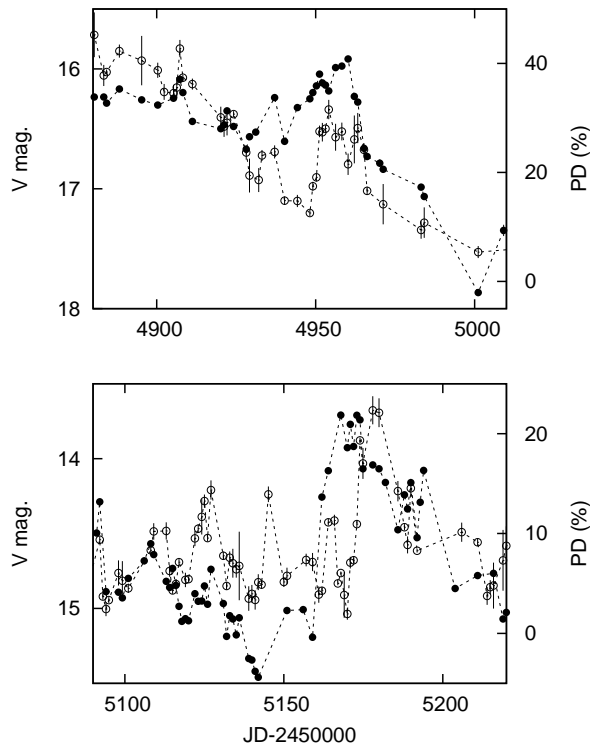


**Fig. 14.** *V*-band light curves and *PD* variations of flares in PKS 1502+106 (upper panel) and 3C 454.3 (lower panel). The filled and open circles represent the light curve and *PD*, respectively.

*t*-test. The correlation coefficients are presented as  $r_{\text{pol}}$  in table 2. We identified that 10 blazars exhibited significant positive correlations between the *V*-band flux and *PD*.

The flux–*PD* correlation was not simple in several objects, even for  $r_{\text{pol}} > 0$ . For example, panel (b) of figure 15 shows the *V*-band light curve and *PD* of MisV 1436. This is one of objects that showed a significant positive correlation between the flux and *PD*. However, *PD* in JD 2454817–2454901 were much lower than those in JD 2455034–2455085, although the *V*-band magnitudes in these periods were comparable. Similar behavior was also observed in PKS 1749+096. Significant positive correlations between the flux and *PD* were detected when we analyzed the flares between JD 2454720–2454760 and JD 2454894–2455084 in PKS 1749+096 (figure 23). However, no significant correlation was detected when we used all data. This is due to the presence of flares without an increase in *PD*. Hence, the correlation was not universal in those objects.

We identified that four blazars (OJ 49, ON 231, 3C 66A, and ON 325) showed a significant negative correlation of the flux and *PD*, namely  $r_{\text{pol}} < 0$ . Panel (c) of figure 15 shows the light curve and *PD* of OJ 49. *PD* were lower when the object was brighter. In addition to those four blazars, OJ 287 and BL Lac also exhibited flares in which negative correlations between the flux and *PD* were observed: A flare of OJ 287 in JD 2454612–2454983 and a

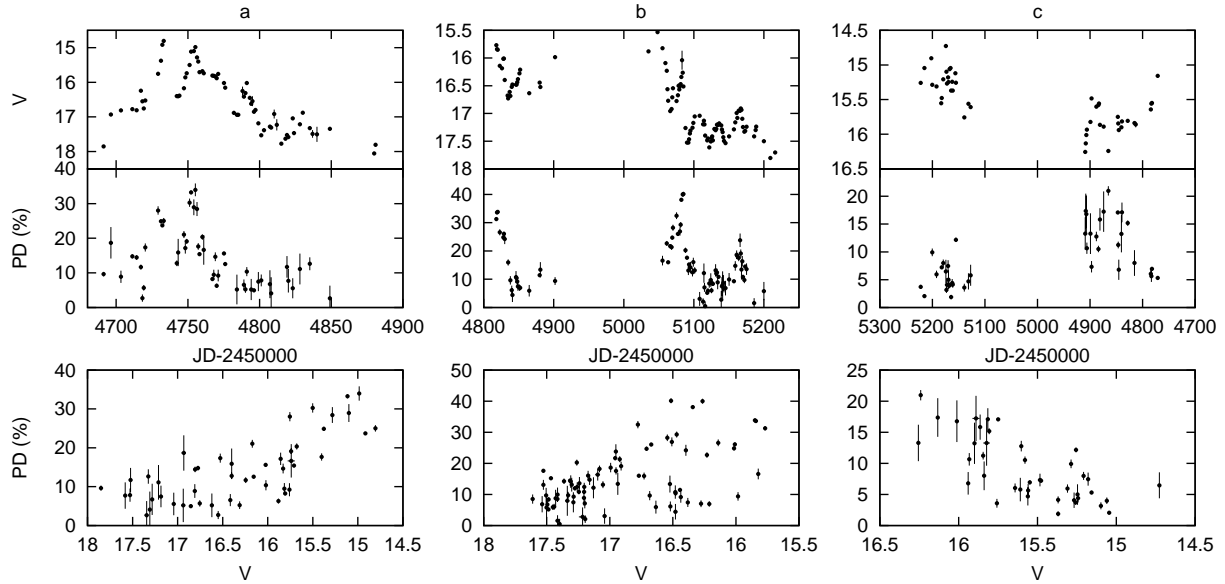


**Fig. 15.** Examples of the time variation in the  $V$ -band magnitude (top) and polarization degree (middle), and the flux–polarization degree diagram (bottom). Panel a: AO 0235+164, b: MisV1436, and c: OJ 49.

flare of BL Lac in JD 2454612–2454864 (figures 23 and 26).

The sample reduces to 33 blazars once we exclude the objects in which available polarization data were less than 10. The numbers of objects with significant positive and negative correlation correspond to 30 % and 12 % of the sample, respectively.

In addition, we calculated the correlation coefficients between the  $V - J$  color and  $PD$ . The results are shown in table 2 as  $r_{\text{col.}-\text{pol.}}$ . A positive (or negative)  $r_{\text{col.}-\text{pol.}}$  means that an object becomes redder (or bluer) when  $PD$  increases (or decreases). The numbers of objects with significant positive and negative correlation, and non-significant correlation are, 2, 3, and 29, respectively. The correlation between  $V - J$  and  $PD$  was quite weak.

### 3.3.3. Rotation of polarization angle

Possible rotations of polarization angle ( $PA$ ) have been reported and discussed both in optical and radio observations. However, a part of them was so sparsely sampled that it can be explained by a result of a random walk in the Stokes  $QU$  plane (e.g. Aller et al. 1981; Jones et al. 1985; Kikuchi et al. 1988). Hence, polarimetric observations with high observation density are required to establish real rotation events of polarization. Recently, smooth rotations of optical polarization have been reported in several blazars based on long-term polarimetric observations (Marscher et al. 2008; Sasada et al. 2010; Marscher et al. 2010; Abdo et al. 2010c; Jorstad et al. 2010). Our polarimetric observation allowed us to perform a systematic search for such rotations.

A search for polarization rotation events is, however, not straightforward. Two issues should be taken into account; one is an ambiguity of  $180^\circ$  in  $PA$ , and the other is the presence of multiple polarization components. First, we resolved the  $180^\circ$  ambiguity by assuming that objects

favor gradual changes in  $PA$  rather than rapid changes. In other words, a difference in  $PA$  between neighboring two observations should be smaller than  $90^\circ$ . We added  $-180^\circ$  (or  $+180^\circ$ ) to the observed  $PA$  in the case that  $PA_n > PA_{n-1} + 90^\circ$  (or  $PA_n < PA_{n-1} - 90^\circ$ ), where  $PA_i$  is the  $i$ -th observation. The corrected  $PA$  by this method is shown in the left-bottom panel in the figures in Appendix.

Second, there are blazars in which a stationary or long-term variation component of polarization has been proposed (e.g. Moore et al. 1982; Villforth et al. 2010). Polarization rotations in such objects should be discussed for each component, i.e., long- or short-term ones. In this paper, we define the average  $QU$  as a stationary polarization component. The averages of  $Q$  and  $U$  were calculated iteratively; we first calculated an average of  $Q$  (or  $U$ ) using all data, and after discarding outliers ( $> 3\sigma$ ) from the sample, re-calculated it. The iteration continued until no outliers remained.

Even after those two-types of corrections were performed, we could not find any clear universal correlations between the light curve and any sets of corrected  $PA$ . However, we found several noteworthy objects or flares in which possible rotations of polarization were seen. We describe them below.

Figure 16 shows the temporal variation in the observed and corrected  $PA$  and the  $QU$  distribution of PKS 1510–089. The observed  $PA$ , shown in panel (b), apparently varies randomly. However, as shown in panel (c), we can see an increasing trend in the  $180^\circ$ -ambiguity corrected  $PA$  during an active phase of the object. This rotation event has also been reported in Marscher et al. (2010), and confirmed in Sasada et al. (2011). The rotation event continued for  $\sim 90$  d and its amplitude in  $PA$  was over  $700^\circ$ . The long duration and large amplitude of the ro-

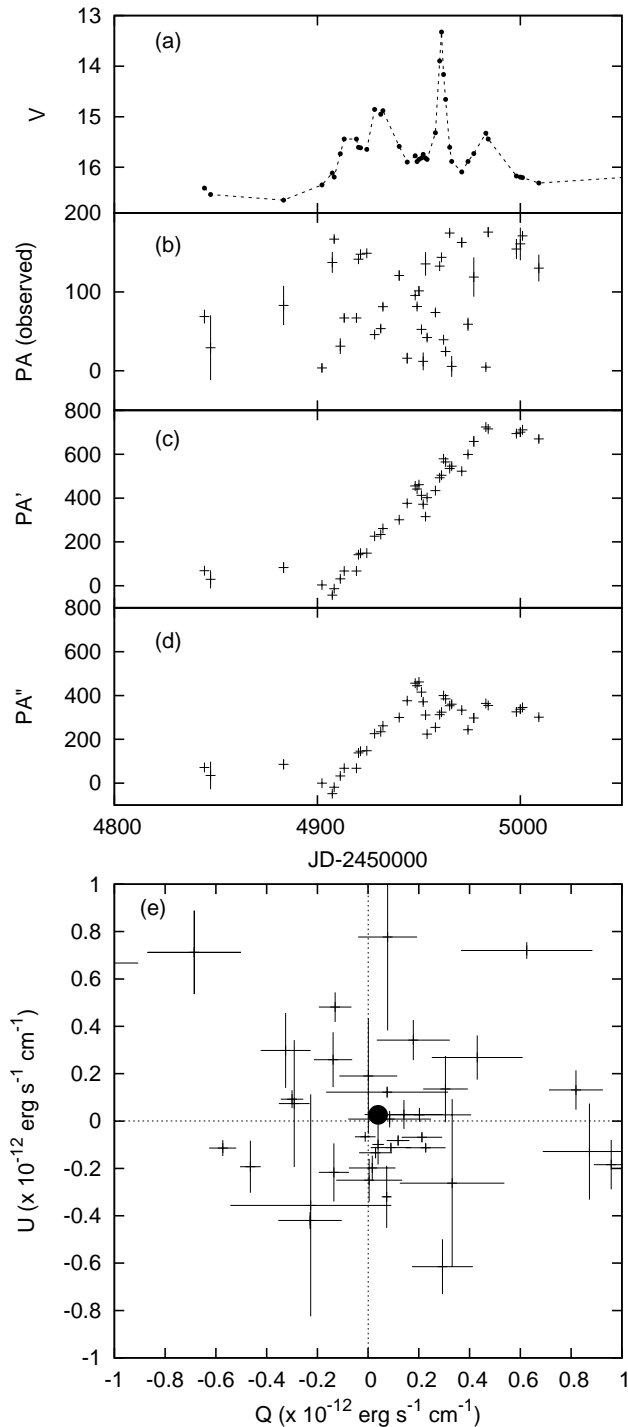


**Fig. 16.** Variation in  $PA$  of PKS 1510–089 observed in 2009. Panels (a) the  $V$ -band light curve, (b) observed  $PA$ , (c) corrected  $PA$  for the  $180^\circ$  ambiguity, (d)  $PA$  measured from the average  $(Q, U)$ , and (e) the  $QU$  plane around the origin of  $QU$ . In panel (e), the average  $(Q, U)$  is indicated by the filled circle.

tation event are definitely difficult to be explained by the result of a random walk in the  $QU$  plane (e.g. Moore et al. 1982).

Similar rotation events having a long duration and a large amplitude were seen only in two objects: 3C 454.3 (figure 25) and PKS 1749+096 (figure 23). All of those rotation events have a common feature, that they were associated with active phases or flares. This implies that the rotation events were related to the variation in the magnetic field direction in the emitting region of the flares. Another possible rotation event can be seen in S5 0716+714 (figure 29). The change in  $PA$  of this object was, however, not as smooth as observed in the above three objects, but rather had a step-like profile. It continued for a very long time of  $\sim 400$  d.

It should be noted that the  $180^\circ$ -ambiguity correction is sensitive to the sampling density of observations. Furthermore, the results should be considered carefully if there are multiple polarization components. The behavior of  $PA$  in PKS 1510–089 apparently changes if the origin of  $(Q, U)$  is shifted to their observed averages, as shown in panel (d) of figure 16. The increasing trend in  $PA$  is terminated earlier than that shown in panel (c). The average  $(Q, U)$  was  $(3.9 \times 10^{-14}, 2.6 \times 10^{-14})$  (in  $\text{erg s}^{-1} \text{cm}^{-1} \text{Hz}^{-1}$ ), indicated by the filled circle in the  $QU$  plane (panel e). This average  $(Q, U)$  corresponds to a  $PD$  of  $\sim 0.6\%$  at  $V = 16.0$ . This result demonstrates that the  $180^\circ$ -ambiguity correction could be affected by another polarization component, even if it has a quite small contribution to the total flux. The polarization rotation in PKS 1510–089 probably started at the onset of the active phase. It was then interrupted by a sharp spike-like flare in  $\sim \text{JD } 2454960$ . After this spike, it is unclear whether the rotation continued or not.

Another noteworthy case is 3C 66A. Figure 17 is the same as figure 16, but for 3C 66A. Our  $180^\circ$ -ambiguity correction yields a short-term rotation event between JD 2454840–2454850, as can be seen in panel (c). However, this feature cannot be seen in panel (d), in which  $PA$  are measured from the observed average of  $(Q, U)$ . As shown in the  $QU$  plane in panel (e), the observed  $QU$  are distributed not around the origin of  $(Q, U)$ , but around the average point indicated by the filled circle. Hence, this observation suggests that the observed polarization in 3C 66A can be interpreted as a composition of two polarization components, namely, long- and short-term variation components. If this is the case, the apparent  $PA$  variation in panel (c) means no real variation in the magnetic field direction in the emitting area. A long-term component should be subtracted from observed polarization when the rotation of polarization is discussed for objects like 3C 66A.

Similar cases to 3C 66A can be found in RX J1542.8+612 (figure 27) and QSO 0454–234 (figure 24); short-term rotation events appeared in their corrected  $PA$ . Furthermore, their average  $(Q, U)$  were significantly deviated from their origin of  $(Q, U)$ . Marscher et al. (2008) have reported the detection of a polarization rotation in BL Lac. The rotation event was



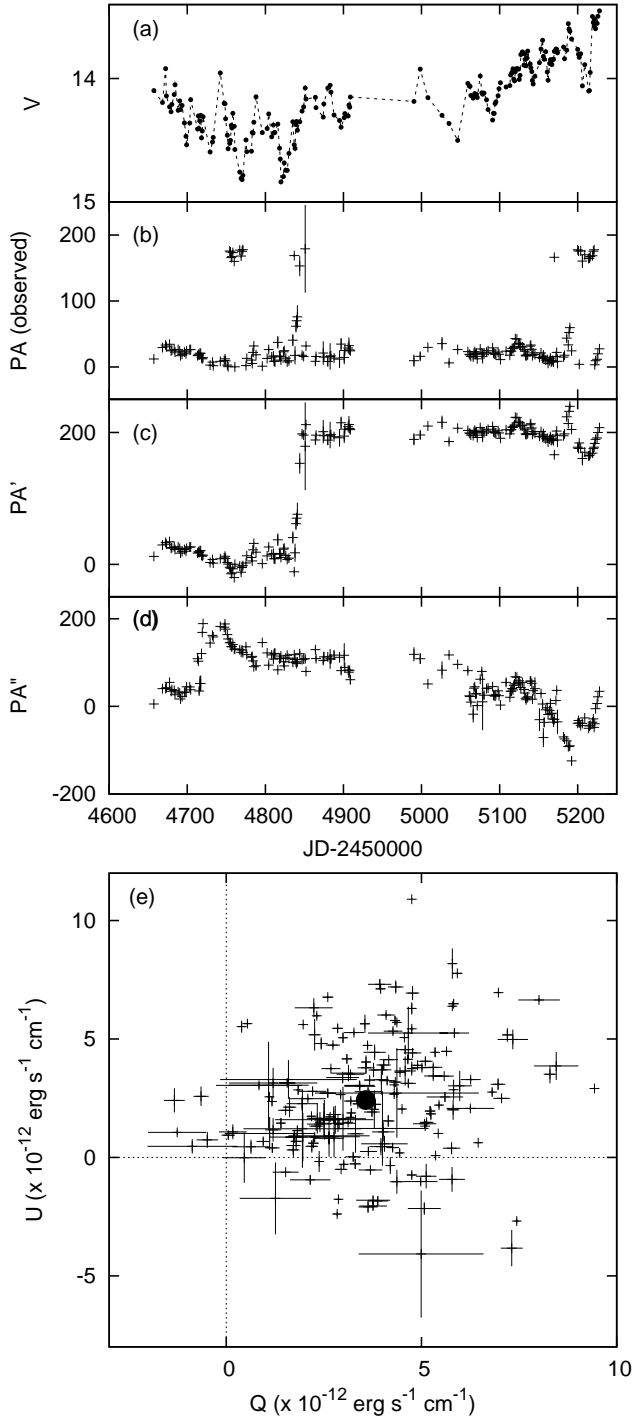


**Fig. 17.** Variation in  $PA$  of 3C 66A. Panels (a) the  $V$ -band light curve, (b) observed  $PA$ , (c) corrected  $PA$  for the  $180^\circ$  ambiguity, (d)  $PA$  measured from the average  $(Q, U)$ , and (e) the  $QU$  plane in which all observations are included. In panel (e), the average  $(Q, U)$  is indicated by the filled circle.

well sampled, continuing for about one week and having an amplitude in  $PA$  of  $240^\circ$ . This object has, however, been proposed to have two polarization components. It is known that the observed average of  $(Q, U)$  is significantly deviate from the origin of  $(Q, U)$  (Hagen-Thorn et al. 2008). Our observation confirmed it, as can be seen in figure 26. If short-term variation components are superimposed on the stationary or long-term polarization component, the model for the rotation event reported in Marscher et al. (2008) should be reconsidered.

Finally, we show the case for PKS 1502+106 in figure 18. A rotation of polarization is not seen in the observed and  $180^\circ$ -ambiguity corrected  $PA$  [panels (b) and (c)], but can be seen in the origin-shifted  $PA$  [panel (d)]. The validity of this correction is, however, brought into question. The observed  $(Q, U)$  is expected to be distributed centered around the stationary component in the two-component picture. However, there is only few points at the vicinity of the average  $(Q, U)$ , as shown in panel (e). This result is inconsistent with the picture of the two-component model. This example tells us that the shift of the origin of  $(Q, U)$  could generate false variations in  $PA$  in some cases.

In summarizing this subsection, we offer several cautions to avoid misinterpretation of observed  $PA$  variations in terms of the polarization rotations. First, it is required that a rotation episode is well sampled when it is proposed to be a real one. A rotation episode indicated by only a few data points, cannot be distinguished from results of a random walk in the  $QU$  plane. Second, a rotation event would more likely to be real when it has a larger variation amplitude in  $PA$ . An apparent rotation having a small amplitude of  $< 180^\circ$  can be readily produced by a composition of a few flares having different  $PA$ . Third, the appearance of a rotation event should not be changed by a small shift of the origin of  $(Q, U)$ . As mentioned above, a part of the rotation event in PKS 1510–089 is quite sensitive to a small change of the origin of  $(Q, U)$ . Finally, the temporal behavior in the  $QU$  plane should be carefully checked not only during the rotation event, but also before and after it. If the observed average of  $(Q, U)$  is significantly deviated from the origin, a stationary or long-term variation component in polarization could be present. Then, polarization variations should be discussed after the long-term component is subtracted from the observation.

### 3.4. The $\nu_{\text{peak}}$ and luminosity dependence of variability

In this subsection, we report on the dependence of the degree of variability in the flux, color, and  $PD$  on  $\nu_{\text{peak}}$ . The  $\nu_{\text{peak}}$  is related to the luminosity of the blazars in our sample (see subsection 3.1). We note that variation amplitudes may be underestimated because blazars generally have a variation time-scale longer than our observation period. To minimize this observation bias, we calculated the slope in the color-magnitude diagram,  $dV/d(V - J)$ , as well as ordinary peak-to-peak amplitudes. We estimated the slope,  $dV/d(V - J)$ , by fitting a linear function to the observed  $V$  and  $V - J$ .  $dV/d(V - J)$  can be considered as

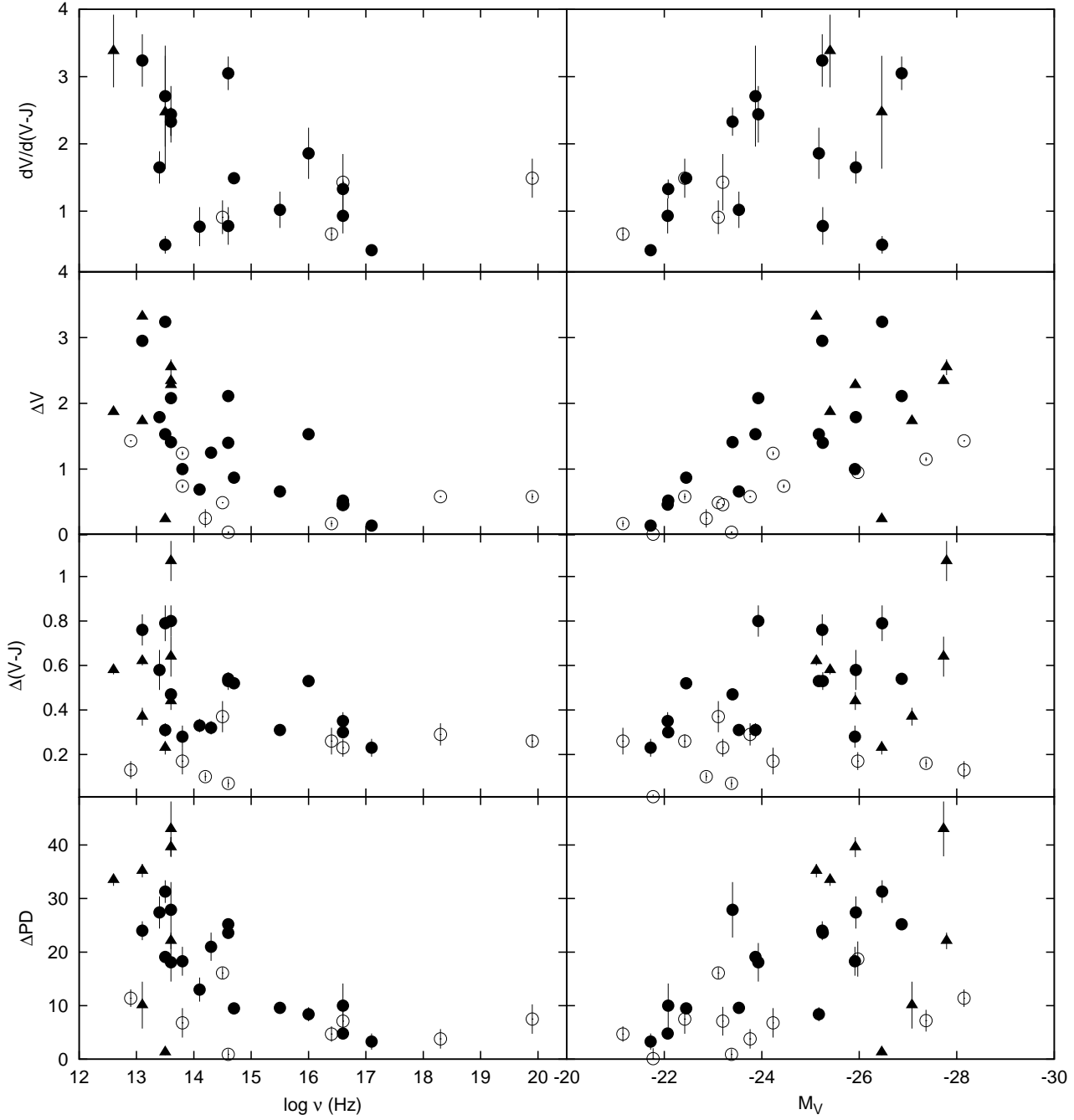


**Fig. 19.** The  $\nu_{\text{peak}}$  and  $M_V$  distribution of the degree of variability. From top to bottom, the panels show  $dV/d(V-J)$ , the peak-to-peak variation amplitudes of the  $V$ -band flux ( $\Delta V$ ), the  $V-J$  color [ $\Delta(V-J)$ ], and the  $V$ -band  $PD$  ( $\Delta PD$ ). The filled circles, triangles, and open circles represent BL Lac objects, FSRQs, and poorly observed objects in which the number of observations are less than 20, respectively.

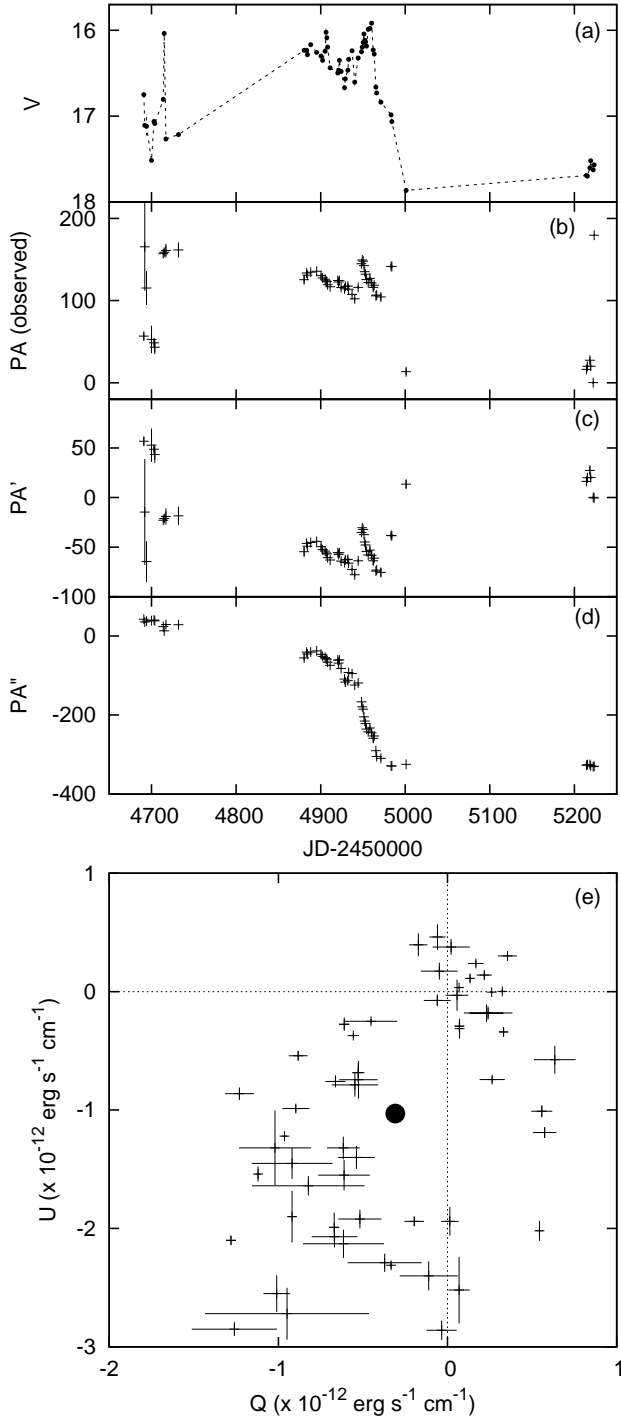


Fig. 18. As for figure 17, but for PKS 1502+106.

an index of the degree of the flux variability against the color variation.

Figure 19 shows the dependence of the degree of variations on  $\nu_{\text{peak}}$  and the average absolute magnitude,  $M_V$ , in the left and right panels, respectively. From top to bottom, the panels show  $dV/d(V-J)$ , the peak-to-peak variation amplitudes of the V-band flux ( $\Delta V$ ), the V-J color [ $\Delta(V-J)$ ], and the V-band PD ( $\Delta PD$ ). In the case of 3C 454.3 and PKS 1510-089,  $dV/d(V-J)$  were calculated using the data in their bright states ( $V < 15$  for 3C 454.3 and  $< 15.5$  for PKS 1510-089). This is for eliminating the redder-when-brighter stage (see, sub-subsection 3.2.2).

All panels in figure 19 suggest that the degrees of variation were low in high  $\nu_{\text{peak}}$ , or faint objects. They can be high in low  $\nu_{\text{peak}}$ , or bright objects. The poorly observed objects represented by the open circles tend to be distributed in low variability regions compared with the others. This is naturally interpreted as underestimations of the variation amplitudes in those objects due to the short period of observations. Several FSRQs, particularly, 3C 273 and QSO 0454-234, exhibit a small variation amplitude, although they have a quite low  $\nu_{\text{peak}}$ . This atypical feature can be understood by large contamination of the thermal emission from accretion disks. Those invariable component probably made the variability of the jet component small, apparently. Thus, the variation amplitudes of poorly observed objects (the open circles) and FSRQs (the filled triangles) can be considered as lower limits of the amplitudes. Then, we can see good correlations of  $dV/d(V-J)$ ,  $\Delta V$ ,  $\Delta(V-J)$ , and  $\Delta PD$  with  $\nu_{\text{peak}}$  and  $M_V$ . Those characteristics of the degree of variation suggest that the variability is stronger in a low  $\nu_{\text{peak}}$  object, and hence in the emission from higher energy electrons.

The fact that the variability in the flux and color is larger in lower  $\nu_{\text{peak}}$  objects has been reported in previous studies (e.g. Ulrich et al. 1997). The present study confirmed this feature with a large sample. In addition, the same feature can be also seen in the variability of PD. This implies that the flares in blazars are generally associated with the variation of PD (see also, Sasada et al. 2011).

## 4. Discussion

### 4.1. “Bluer-When-Brighter”, as a Universal Aspect of Blazars

Our V- and J-band photometric observation showed that the “bluer-when-brighter” trend was detected in a high fraction of blazars we observed: 28/32 well-observed sources. The fraction of bluer-when-brighter objects is quite high compared with those reported in previous studies: Gu et al. (2006) investigated variations in  $V-I$  of three FSRQs and five BL Lac objects. They found that three BL Lac objects exhibited significant bluer-when-brighter trends, while two FSRQs exhibited redder-when-brighter trends. Rani et al. (2010) performed an analogous analysis for six FSRQs and six BL Lac objects. They found that three BL Lac objects exhibited signif-

icant bluer-when-brighter trends, and four FSRQs exhibited redder-when-brighter trends. Those studies thus provide lower fractions of bluer-when-brighter objects than our results. On the other hand, several studies have indicated that the bluer-when-brighter trend is common in BL Lac objects: D’Amicis et al. (2002) have investigated variations in the optical spectral index of eight BL Lac objects, and found that all objects showed bluer-when-brighter trends. Fiorucci et al. (2004) report on their photometric study of 37 blazars, and propose that bluer-when-brighter trends are more prominent in objects showing stronger variability. In those two studies, no evaluation of the significance of the correlation has been given. Vagnetti et al. (2003) also analyzed the spectral slope variability for eight BL Lac objects, and reported that all objects showed bluer-when-brighter trends. However, the sampling rate of their data was  $\sim 25$  d, and it is too large to study variability on a time scale of days. Thus, our present study, for the first time, yields an unambiguous confirmation that the bluer-when-brighter trend is a common feature in variations on time scales of days–months in blazars.

We propose that there are two factors that can disturb the general bluer-when-brighter trend. First, a strong contribution of a blue thermal emission from the accretion disk leads to a redder-when-brighter trend. A typical case is 3C 454.3, as shown in panel (b) of figure 7. The observed color variation suggests that the redder-when-brighter trend was observed only when the objects were faint. This color behavior is consistent with the scenario that the contribution of the thermal emission from the accretion disk becomes strong when the synchrotron emission from the jet weakened (Villata et al. 2006a). Even in the redder-when-brighter objects, our observation revealed that the bluer-when-brighter trend appeared when they were bright.

Second, the bluer-when-brighter trend could be hidden if there are multiple variation components having different bluer-when-brighter sequences. We see the color behavior of long-term variation components, taking the case of PKS 1502+106 as an example. Panel (f) of figure 7 shows the light curve, color, and color-magnitude diagram of PKS 1502+106. A bluer-when-brighter trend was not detected in the whole data of this object, but significantly detected in each year, as reported in sub-subsection 3.2.2. Figure 20 shows the  $F_J$ – $F_V$  diagram of PKS 1502+106. The filled circles and crosses represent data obtained in 2008 and 2009, respectively. As can be seen in this figure,  $F_J$  can be described with a linear function of  $F_V$  both in the 2008 and 2009 data. The dashed lines in the figure represents the best-fitted linear regression models for each year. The slope of the 2008 data in the  $F_J$ – $F_V$  diagram is clearly different from that of 2009; a steep slope in the 2009 data compared with the 2008 one. As can be seen from figure 7, short-term flares are apparently superimposed on a long-term outburst component in the 2009 light curve. The long-term component reached the maximum at the beginning of our 2009 observation, and then started a gradual decay through that year. Hence, the

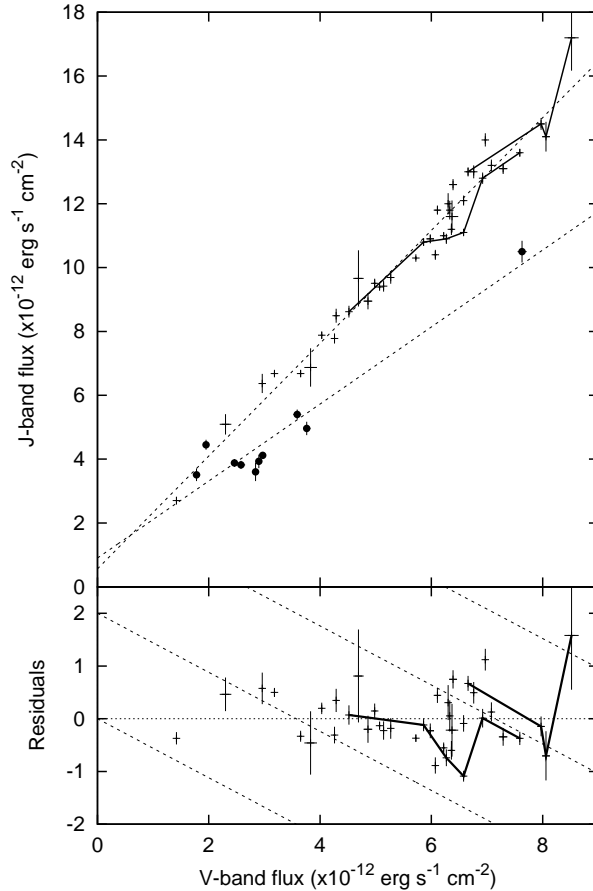


**Fig. 20.** Upper panel:  $J$ - and  $V$ -band flux observed in PKS 1502+106. The filled circles and crosses represent the observations in 2008 and 2009, respectively. The dashed lines indicate the best-fitted linear regression models for each year. The thick solid lines represent rising phases of large flares. Lower panel: Residuals of the  $J$ -band flux from the best-fitted model for the 2009 data. The dashed lines represent the slope of the best-fitted model for the 2008 observations.

general trend seen in the  $F_J$ – $F_V$  diagram of the 2009 data actually originates from the long-term outburst component. In contrast, the object almost remained fainter than  $V = 17$  in 2008, while several short-term flares brighter than  $V = 17$  were observed. There was no prominent outburst component in 2008.

It is interesting to note that, in the 2009 season, the  $F_J$ – $F_V$  slopes of the early phase of the short-term flares were possibly analogous to those in 2008. The thick solid lines in figure 20 represent the rising phases of the prominent short-term flares peaked at JD 2454951 and 2454960. The lower panel shows the residuals of  $F_J$  from the best-fitted model for the 2009 data. The dashed line in the lower panel indicates the  $F_J$ – $F_V$  slope of the 2008 data. The figure suggests that there were stages of shallow  $F_J$ – $F_V$  slopes during the early rising phases of the flares in 2009. After these stages, the slope appears to become very steep near the flare peaks. This may be a sign of spectral hysteresis, which was frequently observed in short-term flares, as mentioned in sub-subsection 3.2.3. The early shallow



$F_J$ – $F_V$  slopes look close to the slope of the short-term flare in 2008.

Those observations give us an idea that the color behavior of the short-term flares in 2008 was the same as that in 2009. In addition, the color of the outburst component in 2009 was probably redder than the short-term flares. As well as PKS 1502+106, PKS 0048–097 and H 1722+119 clearly showed different color behavior in each year, as shown in the lower panels of figure 7. Those phenomena may also be due to the presence of a long-term component, whose color was different from that of short-term flares, and moreover, variable with time. This idea is supported by the fact that correlation coefficients were low even in the bluer-when-brighter sources; as shown in table 2,  $r_{\text{col}}$  was less than 0.70 in more than half of objects. The low correlation-coefficients can be interpreted by the scenario that the observed color is a composition of short- and long-term components that have different bluer-when-brighter sequences. The two-component scenario has also been proposed to explain the color behavior of BL Lac (Villata et al. 2002; Villata et al. 2004).

The above two factors, namely the presence of the thermal disk emission and multiple synchrotron variation components, can disturb the general bluer-when-brighter trend in blazar variability. Our observation overcomes those factors by covering a wide range of wavelengths, namely, the simultaneous optical and NIR observations and a high sampling rate. Those two advantages of our observation led to the high fraction of bluer-when-brighter objects compared with previous studies. In other words, one should carefully discuss apparent redder-when-brighter trends or achromatic variations observed in blazars, while taking into account the above two factors that can disturb the universal bluer-when-brighter trend.

It has been suspected that the bluer-when-brighter trend is common in BL Lac objects, but not in FSRQs because of a large contribution of thermal emission in FSRQs (Gu et al. 2006; Rani et al. 2010). Our objects that were observed more than 10 times include seven FSRQs and seven LBLs. The correlation analysis with all data sets showed that significant bluer-when-brighter trends were detected in two FSRQs and six LBLs (see table 2). This result confirms the previous studies, which suggest that the color–flux correlation of FSRQs is different from that of BL Lac objects. However, the bluer-when-brighter trend was significantly detected even in the other four FSRQs when they were bright (3C 454.3, PKS 1510–089, PKS 1502+106, and QSO 0454–234), as mentioned in sub-subsection 3.2.2. Hence, the jet emission in FSRQs presumably has the same color behavior as that in BL Lac objects.

The relationships of  $F_J$  and  $F_V$  of 3C 454.3 and PKS 1510–089 suggest that their variation components did not have a constant color, but a blueing trend with an increase in flux (see figure 9 and 10). Alternatively, it can be interpreted with the scenario that two variation components had different time-scales and colors, as proposed above. A red and long-term outburst component would be dominant in their low flux regime. The redder-when-

brighter trend was observed probably because an underlying source was the blue thermal emission. The emission from short-term flares would be dominant in the high-flux regime, resulting in the standard bluer-when-brighter trend. This scenario is supported by the light curve structure; short-term flares, making the objects brightest, were superimposed on long-term outburst components (see figures 25 and 23).

In general, variations on time-scales of months–years are expected to have larger amplitudes than those of days–weeks in blazars (Hufnagel, Bregman 1992; Takahashi et al. 2000; Kataoka et al. 2001; Chatterjee et al. 2008). Hence, the variation amplitudes reported in subsection 3.4 are considered to be those of the long-term variation component. In subsection 3.2.3, we reported that the color of the variation component was constant in most objects. Since this constant-color feature is a result from the whole data set obtained during our observation period, it is probably a feature of the long-term variation component.

Thus, the implications for the blazar variability obtained from our observation are summarized below: The short-term flares on time scales of days–weeks tended to exhibit spectral hysteresis; their rising phase was bluer than the decay phase around the flare maxima. They were occasionally superimposed on the long-term variations on time scales of months–years. The color of the long-term component was apparently constant. In addition to those short- and long-term synchrotron components, a stationary component was probably embedded. The bluer-when-brighter trend is commonly observed because this stationary component had a redder color than the variation components. A part of FSRQs has a blue and thermal emission as an underlying component.

#### 4.2. *Physical Implication from the Bluer-When-Brighter Trend*

Several models have been proposed to explain the bluer-when-brighter trend in blazars. When we consider two distinct synchrotron components, the bluer-when-brighter trend could be explained if a flare component has a higher  $\nu_{\text{peak}}$  than an underlying component. Even when we consider a single synchrotron component, it could be explained by a shift of its  $\nu_{\text{peak}}$  to a higher region. In either case, high  $\nu_{\text{peak}}$  can be obtained by the injection of energy into emitting regions, and thereby, the increase of the number of high energy electrons. The most plausible scenario for the origin of the energy injection is internal shocks in relativistic shells (e.g. Spada et al. 2001; Zhang et al. 2002). Besides the energy injection scenario, the bluer-when-brighter trend can be explained by a change in the beaming factor,  $\delta$ , of the emitting region. This is because it leads to not only an apparent increase in the observed flux,  $\nu f_\nu \propto \delta^4$ , but also a shift of the observed frequency,  $\nu_{\text{obs}} \propto \delta$  (e.g. Villata et al. 2004; Papadakis et al. 2007; Larionov et al. 2010).

The short-term variations on a time scale of days–weeks tended to exhibit the spectral hysteresis in the  $F_J$ – $F_V$  diagram, as reported in sub-subsection 3.2.3. This hysteresis presumably has the same nature as the hysteresis which

have been seen between the flux and color, or spectral index (Kataoka et al. 2000; Ciprini et al. 2003; Wu et al. 2007b). Kirk et al. (1998) reproduce the hysteresis between the flux and spectral index using their model for the acceleration of electrons in a shock region. The fact that the short-term variations tended to exhibit the spectral hysteresis supports the energy injection scenario. It is difficult to explain such a hysteresis pattern with a change in  $\delta$ .

The long-term variation components on a time scale of months–years apparently had a constant color. The bluer-when-brighter trend was observed because the underlying source was redder than the variation component, as mentioned in sub-subsection 3.2.3 and the last subsection. The emission of the underlying source is presumably synchrotron emission, because the thermal emission from AGN should be much bluer than the synchrotron emission of the long-term variation component. The red color of the underlying source suggests that its  $\nu_{\text{peak}}$  is lower than that of the long-term component.

In subsection 3.4, we showed that a higher  $\nu_{\text{peak}}$  objects exhibited smaller variations all in the flux, color, and  $PD$ . Based on the discussions in the last subsection, it suggests that the variation amplitude of the long-term component was small in a region of  $\nu < \nu_{\text{peak}}$  and vice versa. This is preferable for the scenario that the long-term variation is also attributed to the energy injection events. If changes in  $\delta$  would be the major cause, it means an eccentric situation that  $\delta$  changes only occur in components having high  $\nu_{\text{peak}}$ . Otherwise, large variations would be observed in a region of  $\nu < \nu_{\text{peak}}$  when low  $\nu_{\text{peak}}$  components are amplified by an increase in  $\delta$ . The energy injection scenario can explain the  $\nu_{\text{peak}}$  dependence of the variation amplitude without such an eccentric situation.

#### 4.3. Implications from Polarization Variations

The high fraction of bluer-when-brighter objects implies that there is a major mechanism common to blazar variations. The most plausible explanation is the energy injection scenario, as mentioned in the last subsection. The internal shock is a promising candidate for the mechanism of the energy injection to the emitting region. If the internal shock results in an aligned magnetic field in the emitting region, a universal aspect of polarization variations can be expected.

In contrast to the strong correlation between the flux and color, the correlation between the flux and  $PD$  was weak; 30 % and 12 % of the sample exhibited significant positive and negative correlations, respectively. On the other hand, these fractions of objects are too high to conclude that the polarization variations are completely random. It is possible that there is no universal law of polarization associated with blazar variations. If this is the case, our observation indicates that flares could occur independent of the structure of the magnetic field in the flaring source.

Alternatively, a universal law could be hidden in the observed polarization, although it was present. Polarization can be described with two parameters, for example,  $PD$

and  $PA$ . It can also be treated like a two-dimension vector with Stokes  $QU$  parameters. This property of polarization is an important difference from that of color. The weak correlation of the flux and  $PD$  may be caused by the presence of two or more polarization components. Even if a flare has specific  $PD$  and  $PA$ , they would disappear in the observed  $PD$  and  $PA$  variations because of the superposition of other flares having different  $PD$  and  $PA$ . Based on this picture, we have developed a method to separate the observed polarization into two components: A short-term variation component having a positive correlation between the total and polarized fluxes, and a long-term one (Uemura et al. 2010). Applying this method to our blazar data, we found that the behavior of polarization in OJ 287 and S2 0109+224 can be explained with this two-component picture. The two-component picture is also supported by the color behavior as described in subsections 4.1 and 4.2.

There are three well-observed blazars in our sample which showed a significant negative correlation between the flux and  $PD$ : OJ 49, ON 231, and 3C 66A. In addition, temporary negative correlations were observed in BL Lac and OJ 287, as mentioned in subsection 3.3.2. It is noteworthy that the observed  $QU$  of all those five objects do not center at the origins of  $QU$ , but concentrate around regions significantly apart from the origins. Such distributions are also seen in their  $(Q/I, U/I)$  plane. These distributions strongly suggest the presence of long-term polarization components. The negative correlation means that the flux variations were associated with the systematic changes in polarization. If the long-term component is subtracted, the variations might change to those showing positive correlation. Hence, the negative correlation can also be explained by the two-component scenario.

## 5. Summary

We performed photopolarimetric monitoring of 42 blazars in the optical and near-infrared band using the Kanata telescope. Our findings are summarized below:

- The bluer-when-brighter trend was observed in 28 blazars, which correspond to 88 % of our well-observed sample. Our observation unambiguously confirmed that it is a universal aspect in blazars.
- The redder-when-brighter trend was observed in three objects (3C 454.3, PKS 1510–089, and PG 1553+113) when they were faint. Even in those three objects, the bluer-when-brighter trends can be seen when they were bright.
- The bluer-when-brighter trend was, in general, generated by a variation source apparently having a constant color and an underlying red source.
- Prominent short-term flares tended to exhibit a spectral hysteresis; their rising phase was bluer than their decay phase around the flare maxima.
- Significant correlations of the flux and the polarization degree were observed only in 10 blazars, which correspond to 30 % of our well-observed sample.

The correlation was weak compared with that between the flux and color.

- The rotations of polarization were observed in PKS 1510–089, 3C 454.3, and PKS 1749+096, and possibly in S5 0716+714. We demonstrated that false events of polarization rotations could be detected in the case that multiple polarization components are present.
- We found that the variation amplitudes were smaller in low  $\nu_{\text{peak}}$  objects all in the flux, color, and polarization degree.

Based on those results, we propose that there are several distinct variation sources on different time-scales, colors, and polarizations in blazars. Both short- and long-term variation components are probably attributed to the energy injection into emitting sources, for example, with the internal shock in relativistic shells.

This work was partly supported by a Grand-in-Aid from the Ministry of Education, Culture, Sports, Science, and Technology of Japan (22540252 and 20340044).

## Appendix 1. Temporal Variations in Flux, Color, and Polarization

Figures 21–34 show temporal variations in flux, color, and polarization of blazars obtained by our observation. The left panels are temporal variations in five parameters. From top to bottom, the panels show the  $V$ -band light curve, the  $V - J$  color, the polarization degree ( $PD$ ) in percent, the polarization angle ( $PA$ ) in degree, and the corrected  $PA$ . The last one was corrected for the  $180^\circ$  ambiguity of  $PA$  (for a detail, see sub-subsection 3.3.3). The upper and lower middle panels show the color-magnitude diagram and the  $PD$ -magnitude diagram, respectively. The upper and lower right panels show the distribution of  $(Q/I, U/I)$  and  $(Q, U)$ , respectively.

## References

- Abdo, A. A., Ackermann, M., Agudo, I., Ajello, M., Aller, H. D., Aller, M. F., Angelakis, E., Arkharov, A. A., et al. 2010a, *ApJ*, 716, 30
- Abdo, A. A., Ackermann, M., Ajello, M., Allafort, A., Antolini, E., Atwood, W. B., Axelsson, M., Baldini, L., et al. 2010b, *ApJ*, 715, 429
- Abdo, A. A., Ackermann, M., Ajello, M., Axelsson, M., Baldini, L., Ballet, J., Barbiellini, G., Bastieri, D., et al. 2010c, *Nature*, 463, 919
- Adelman-McCarthy, J. K., Agüeros, M. A., Allam, S. S., Allende Prieto, C., Anderson, K. S. J., Anderson, S. F., Annis, J., Bahcall, N. A., et al. 2008, *ApJS*, 175, 297
- Aharonian, F., Akhperjanian, A. G., Bazer-Bachi, A. R., Beilicke, M., Benbow, W., Berge, D., Bernlöhr, K., Boisson, C., et al. 2006, *A&A*, 448, L19
- Aller, H. D., Hodge, P. E., & Aller, M. F. 1981, *ApJL*, 248, L5
- Angel, J. R. P. & Stockman, H. S. 1980, *ARA&A*, 18, 321
- Antón, S. & Browne, I. W. A. 2005, *MNRAS*, 356, 225
- Bambieri, C., Capaccioli, M., Cristiani, S., Nardòn, G., & Omizzolo, A. 1983, *Memorie della Societa Astronomica Italiana*, 54, 601
- Blandford, R. D. & Rees, M. J. 1978, in *BL Lac Objects*, ed. A. M. Wolfe (Pittsburgh: University of Pittsburgh Press), 328
- Bloom, S. D., Dale, D. A., Cool, R., Dupczak, K., Miller, C., Haugsjaa, A., Peters, C., Tornikoski, M., Wallace, P., & Pierce, M. 2004, *AJ*, 128, 56
- Bramel, D. A., Carson, J., Covault, C. E., Fortin, P., Gingrich, D. M., Hanna, D. S., Jarvis, A., Kildea, J., et al. 2005, *ApJ*, 629, 108
- Brissenden, R. J. V., Tuohy, I. R., Remillard, R. A., Schwartz, D. A., & Hertz, P. L. 1990, *ApJ*, 350, 578
- Buckley, J. H., Akerlof, C. W., Biller, S., Carter-Lewis, D. A., Catanese, M., Cawley, M. F., Connaughton, V., Fegan, D. J., et al. 1996, *ApJL*, 472, L9
- Burbidge, E. M. & Kinman, T. D. 1966, *ApJ*, 145, 654
- Caccianiga, A. & Marchã, M. J. M. 2004, *MNRAS*, 348, 937
- Carini, M. T., Miller, H. R., Noble, J. C., & Goodrich, B. D. 1992, *AJ*, 104, 15
- Carini, M. T., Noble, J. C., & Miller, H. R. 1998, *AJ*, 116, 2667
- Chatterjee, R., Jorstad, S. G., Marscher, A. P., Oh, H., McHardy, I. M., Aller, M. F., Aller, H. D., Balonek, T. J., et al. 2008, *ApJ*, 689, 79
- Chiang, J. & Böttcher, M. 2002, *ApJ*, 564, 92
- Ciprini, S., Tosti, G., Raiteri, C. M., Villata, M., Ibrahimov, M. A., Nucciarelli, G., & Lanteri, L. 2003, *A&A*, 400, 487
- Clements, S. D. & Carini, M. T. 2001, *AJ*, 121, 90
- Condon, J. J., Hicks, P. D., & Jauncey, D. L. 1977, *AJ*, 82, 692
- Corso, G. J., Harris, R., Ringwald, F., Schultz, J., & Mikolajczyk, D. 1988, *PASP*, 100, 70
- Costamante, L., Ghisellini, G., Giommi, P., Tagliaferri, G., Celotti, A., Chiaberge, M., Fossati, G., Maraschi, L., et al. 2001, *A&A*, 371, 512
- D’Amicis, R., Nesci, R., Massaro, E., Maesano, M., Montagni, F., & D’Alessio, F. 2002, *Publications of the Astronomical Society of Australia*, 19, 111
- Dermer, C. D., Schlickeiser, R., & Mastichiadis, A. 1992, *A&A*, 256, L27
- Doroshenko, V. T., Sergeev, S. G., Merkulova, N. I., Sergeeva, E. A., Golubinsky, Y. V., Pronik, V. I., & Okhmat, N. N. 2005, *Ap*, 48, 304
- Edelson, R. A. & Krolik, J. H. 1988, *ApJ*, 333, 646
- Falomo, R. & Treves, A. 1990, *PASP*, 102, 1120
- Fan, J. H. & Lin, R. G. 2000a, *ApJ*, 537, 101
- Fan, J. H. & Lin, R. G. 2000b, *A&A*, 355, 880
- Fan, J. H., Xie, G. Z., Pecontal, E., Pecontal, A., & Copin, Y. 1998, *ApJ*, 507, 173
- Feigelson, E. D., Bradt, H., McClintock, J., Remillard, R., Urry, C. M., Tapia, S., Geldzahler, B., Johnston, K., et al. 1986, *ApJ*, 302, 337
- Fiorucci, M., Ciprini, S., & Tosti, G. 2004, *A&A*, 419, 25
- Fossati, G., Maraschi, L., Celotti, A., Comastri, A., & Ghisellini, G. 1998, *MNRAS*, 299, 433
- Gaskell, C. M. 1982, *ApJ*, 252, 447
- Ghisellini, G., Celotti, A., Fossati, G., Maraschi, L., & Comastri, A. 1998, *MNRAS*, 301, 451
- Ghisellini, G., Villata, M., Raiteri, C. M., Bosio, S., de Francesco, G., Latini, G., Maesano, M., Massaro, E., et al. 1997, *A&A*, 327, 61
- Ghosh, K. K., Ramsey, B. D., Sadun, A. C., & Soundararajaperumal, S. 2000, *ApJS*, 127, 11
- Giommi, P., Padovani, P., Perri, M., Landt, H., & Perlman, E. 2002, in *Blazar Astrophysics with BeppoSAX and Other*

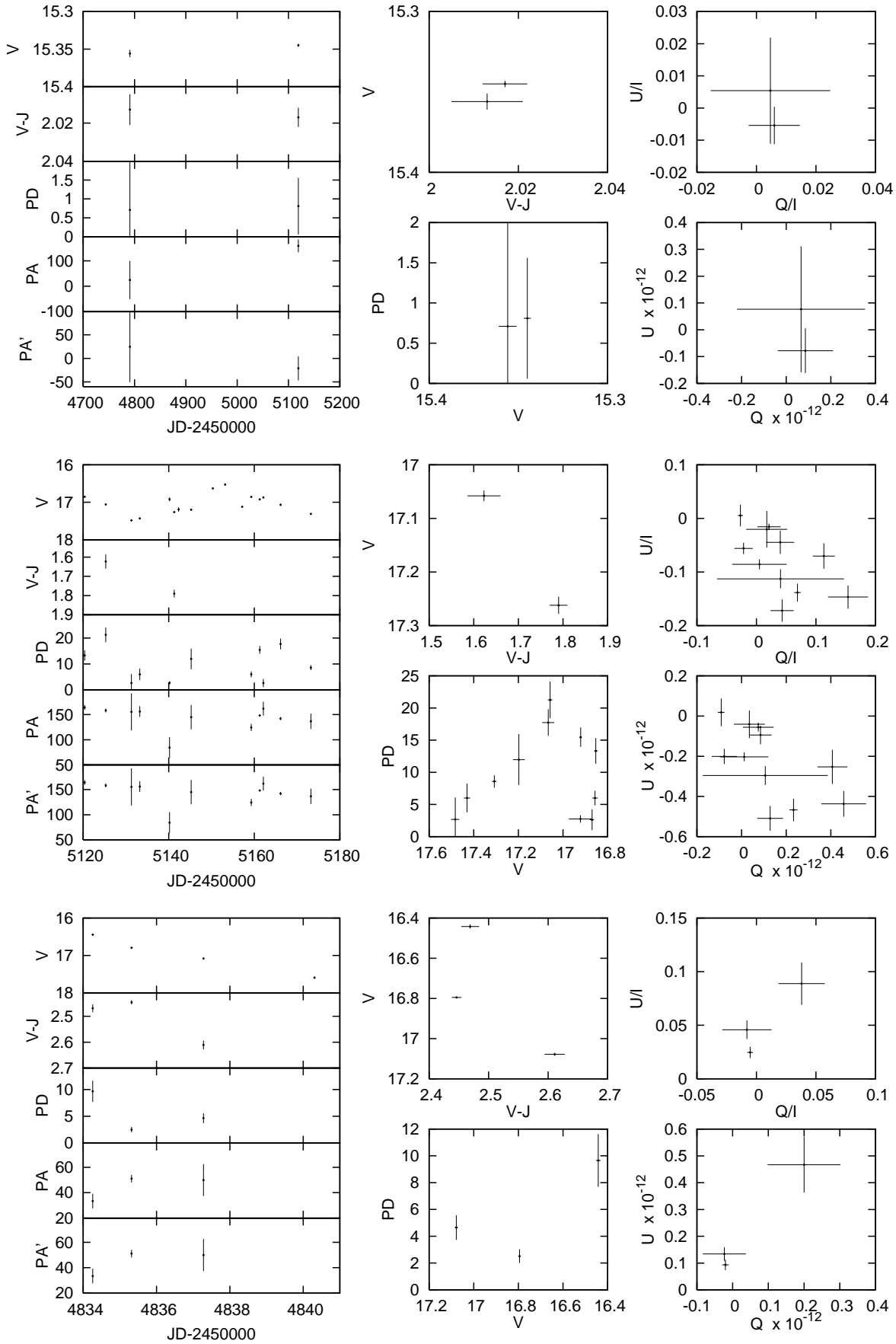


Fig. 21. QSO 0324+341 (top), 4C 14.23 (middle), and QSO 1239+044 (bottom).



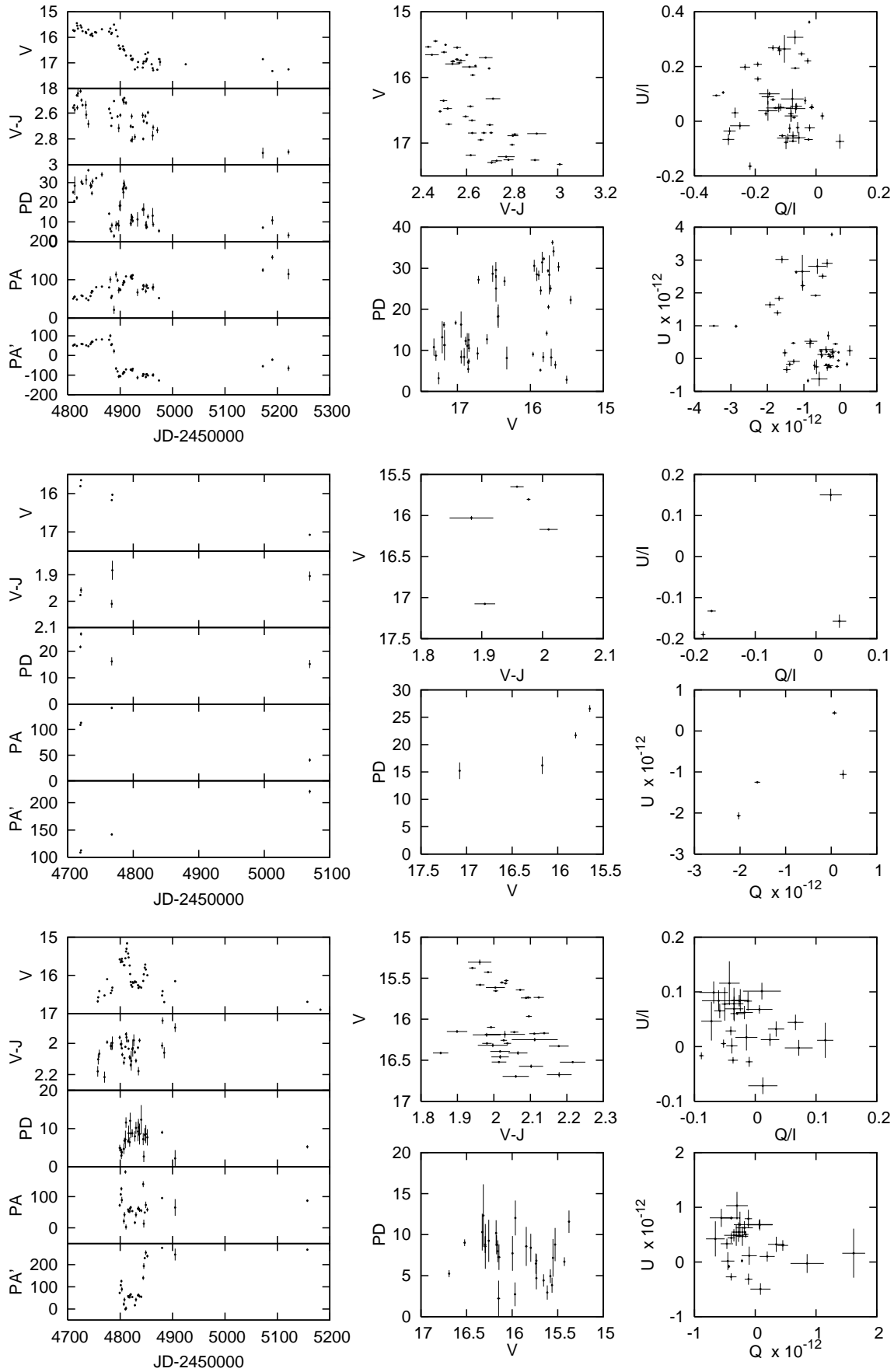


Fig. 22. 3C 279 (top), PKS 0215+015 (middle), and QSO 0454-234 (bottom).

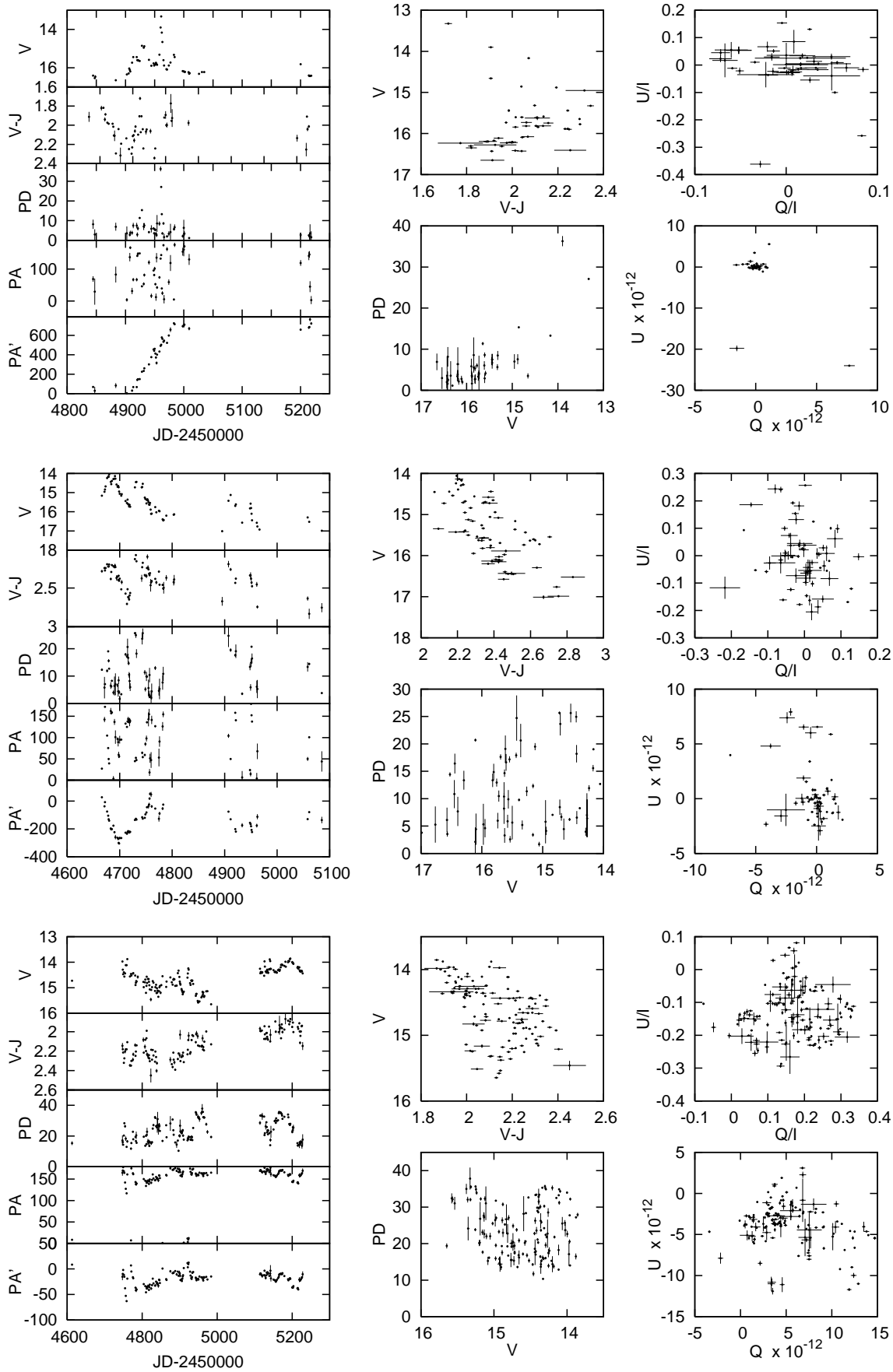


Fig. 23. PKS 1510-089 (top), PKS 1749+096 (middle), and OJ 287 (bottom).

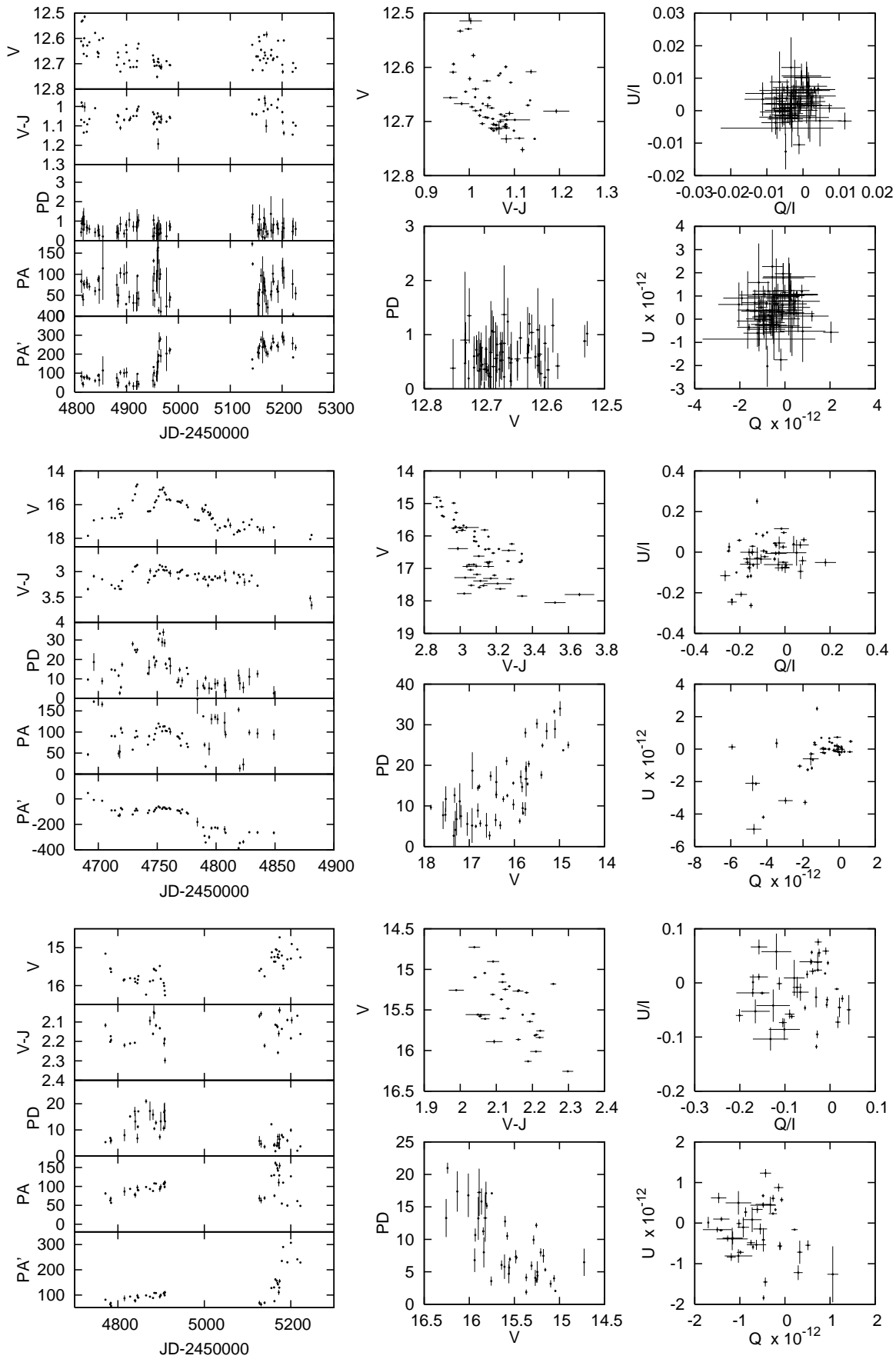


Fig. 24. 3C 273 (top), AO 0235+164 (middle), and OJ 49 (bottom).

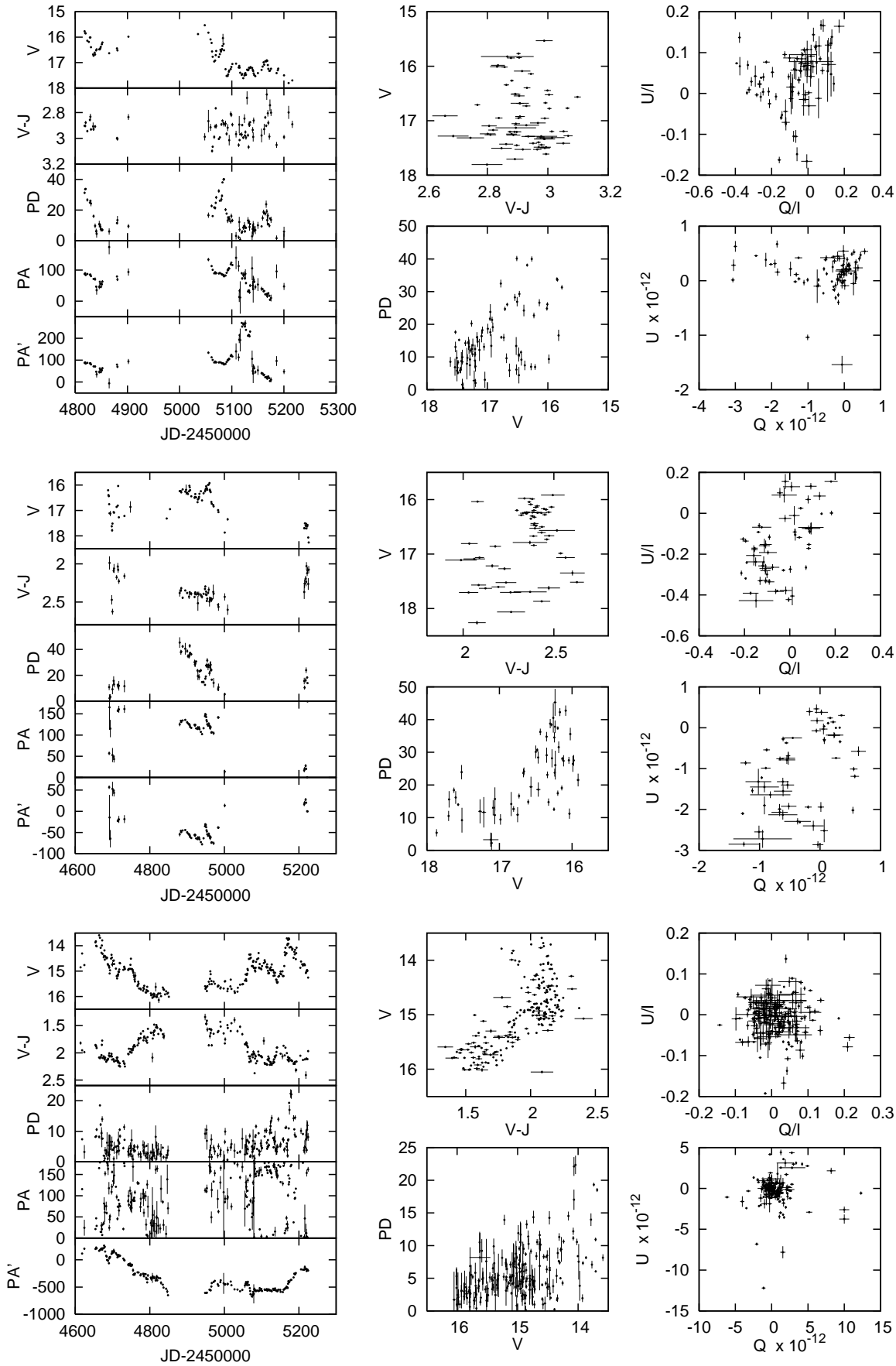


Fig. 25. MisV1436 (top), PKS 1502+106 (middle), and 3C 454.3 (bottom).

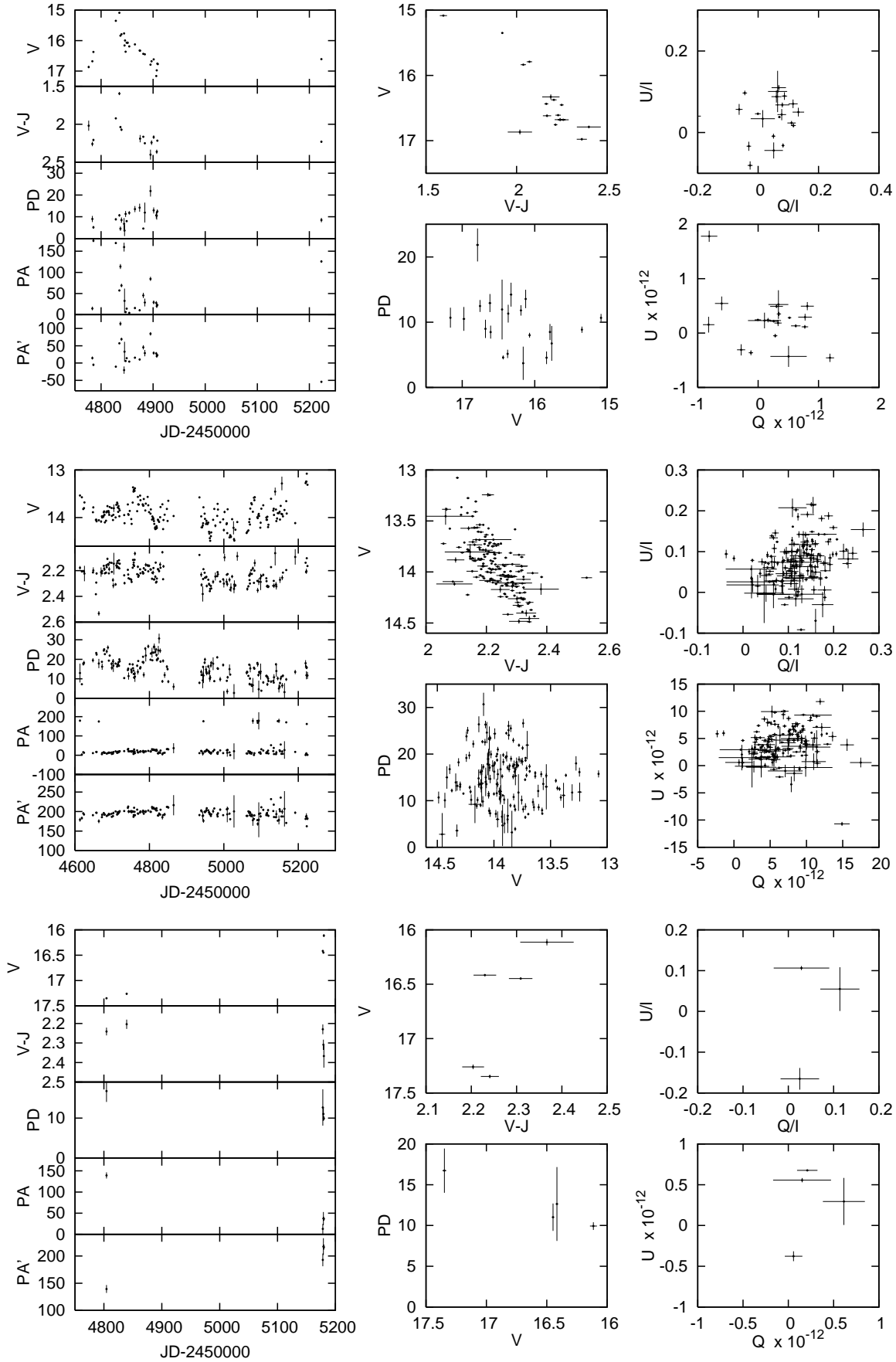


Fig. 26. PKS 0754+100 (top), BL Lac (middle), and S4 0954+65 (bottom).



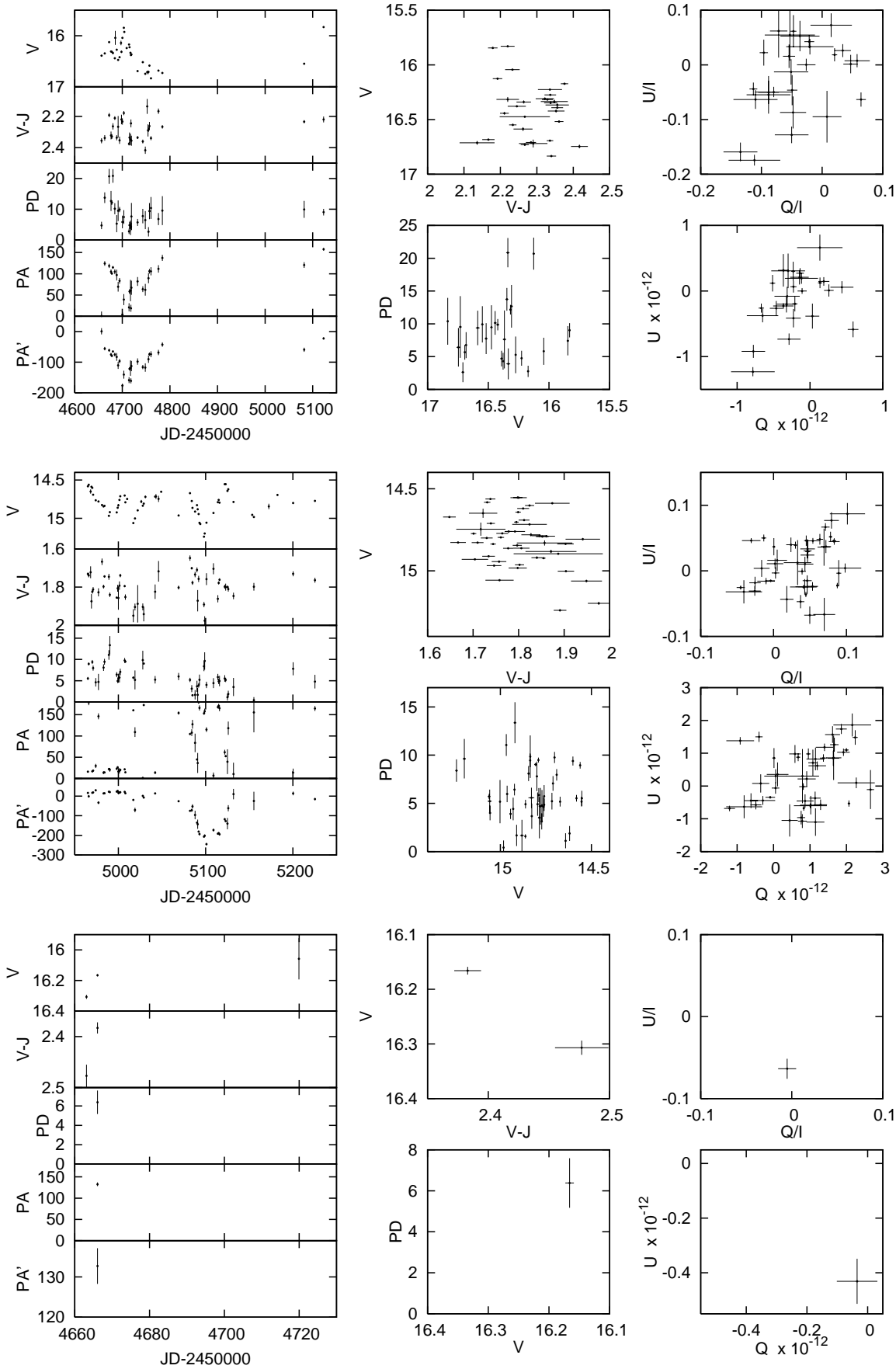


Fig. 27. S5 1803+784 (top), RX J1542.8+612 (middle), and OQ 530 (bottom).

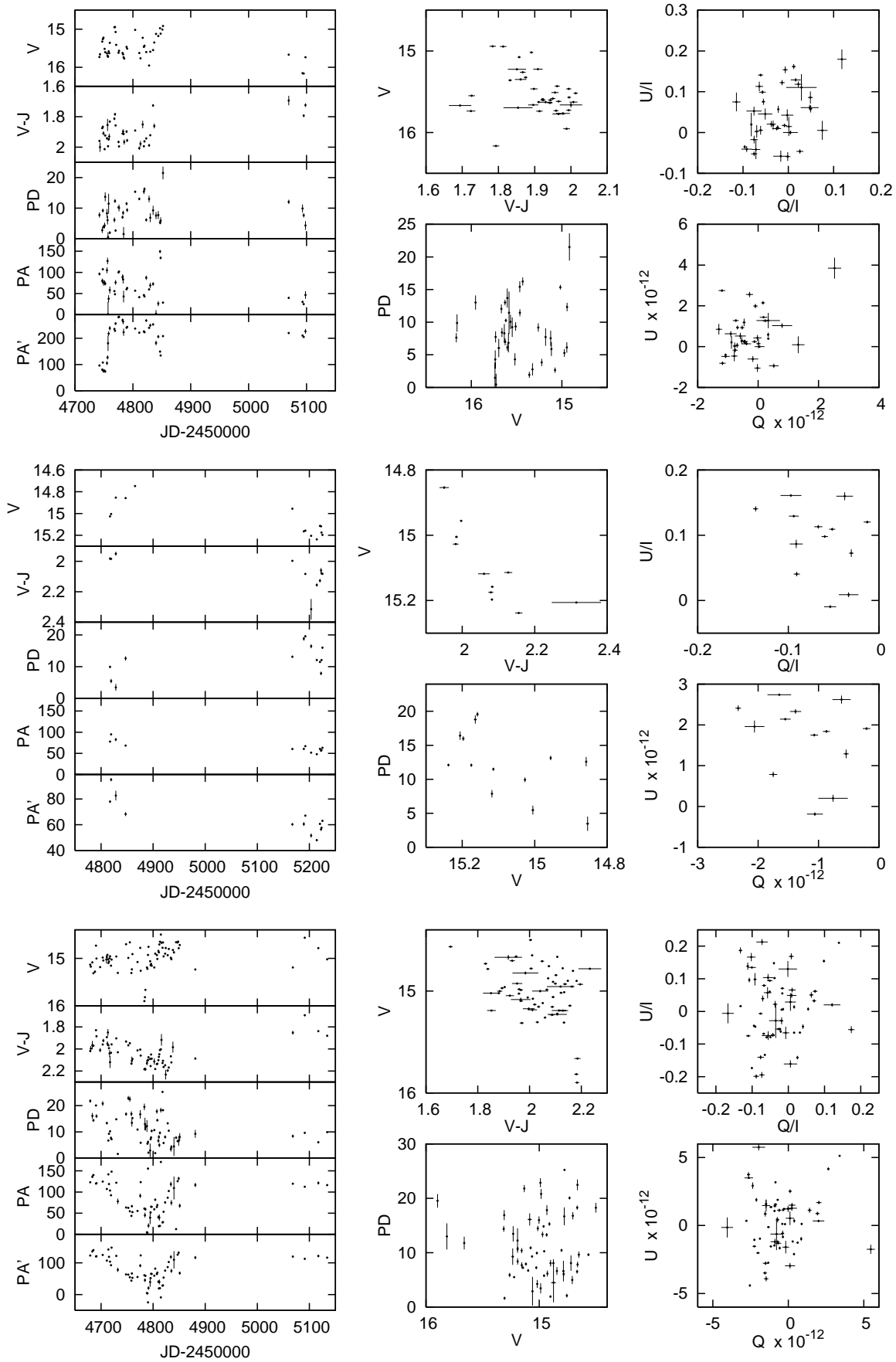


Fig. 28. PKS 0048-097 (top), ON 231 (middle), and S2 0109+224 (bottom).

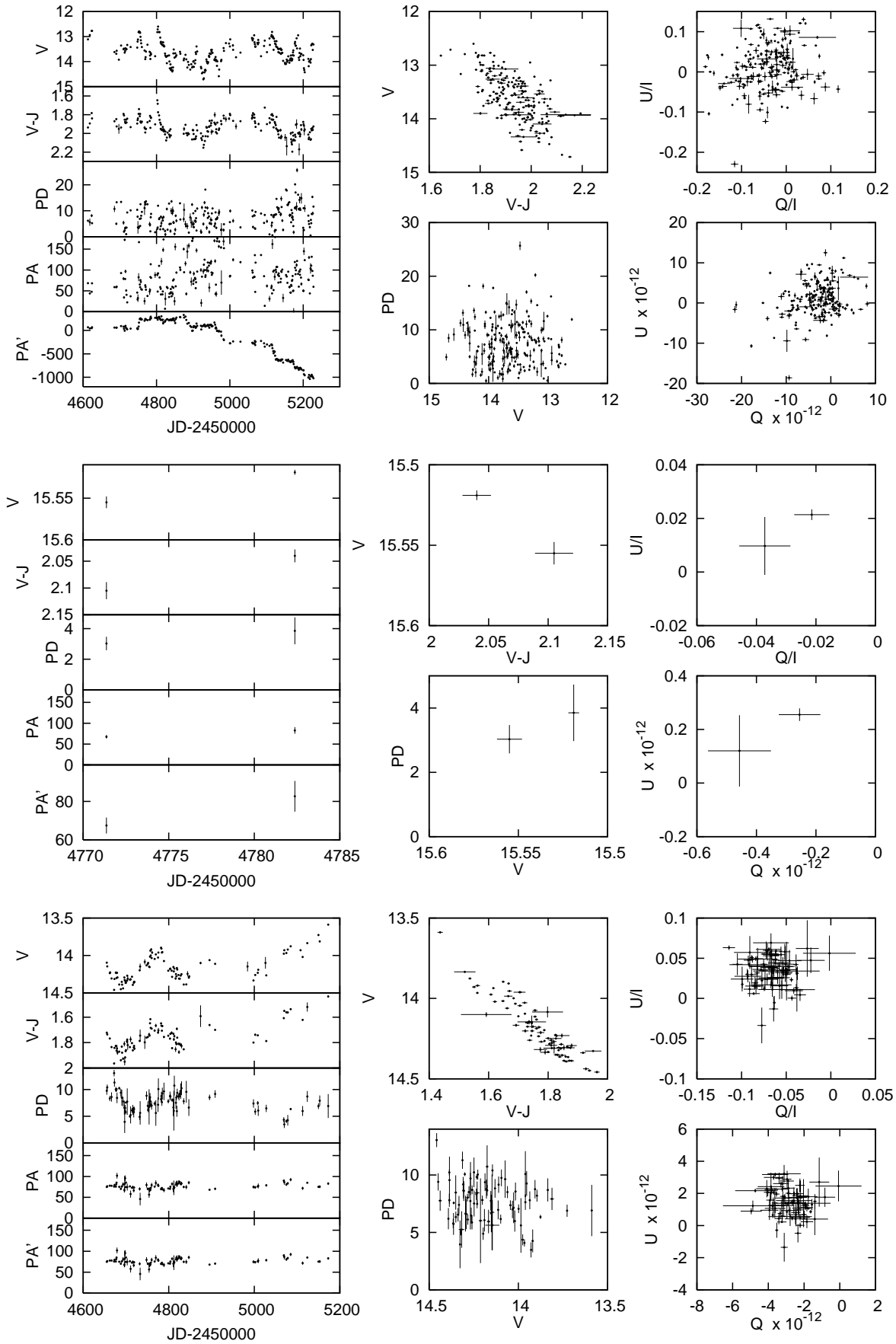


Fig. 29. S5 0716+714 (top), 3EG 1052+571 (middle), and 3C 371 (bottom).

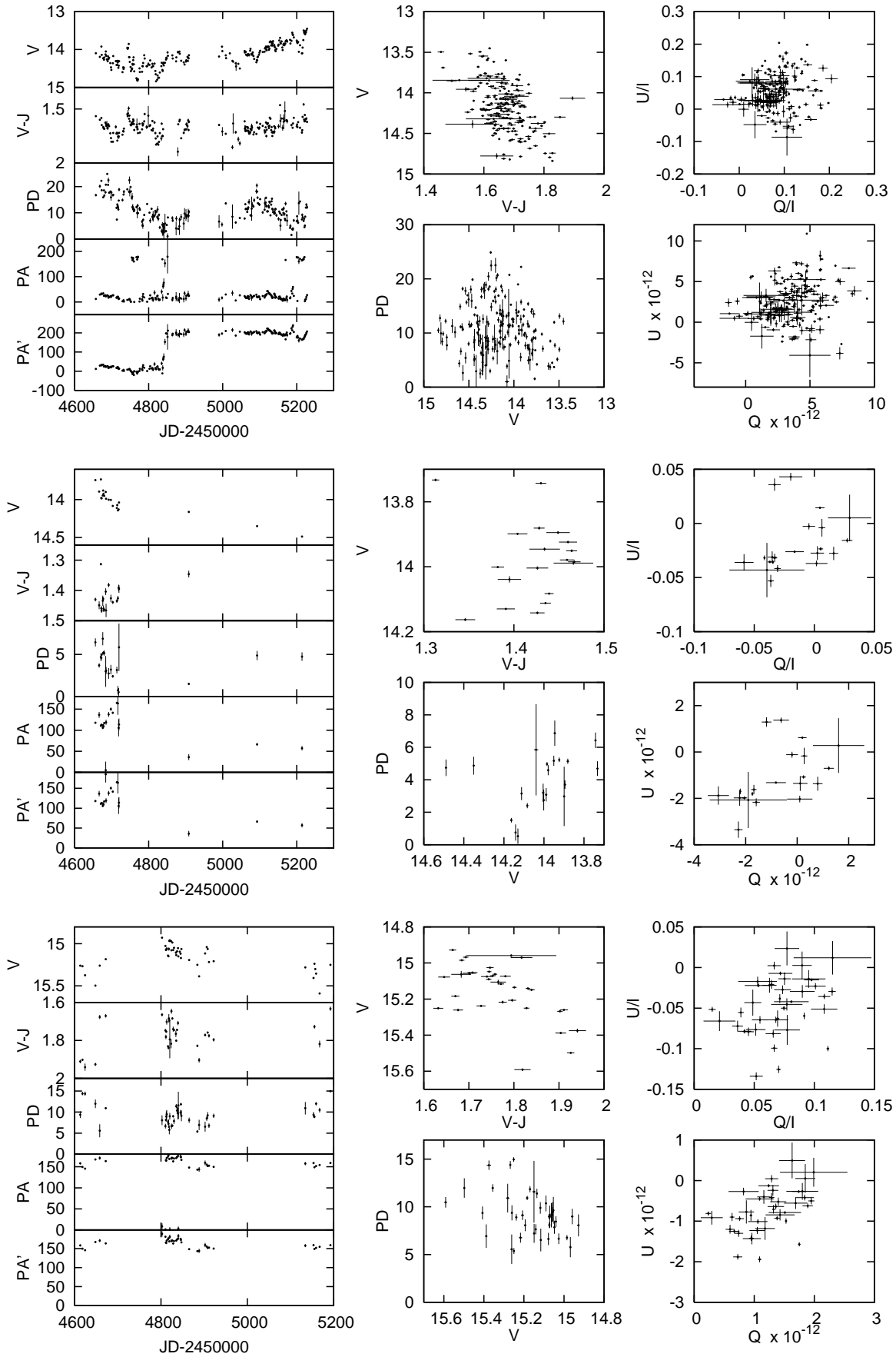


Fig. 30. 3C 66A (top), PG 1553+113 (middle), and ON 325 (bottom).

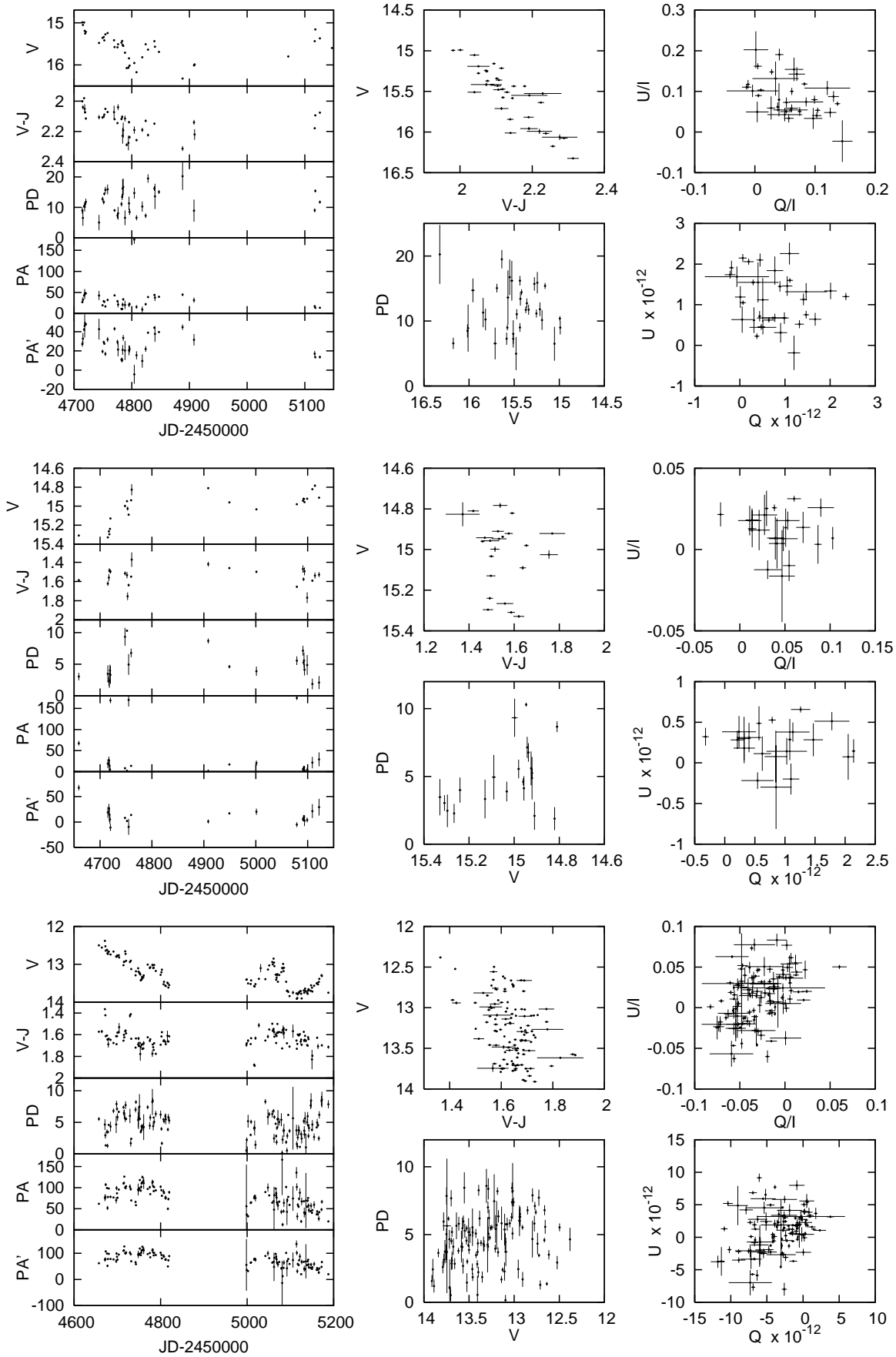


Fig. 31. PKS 0422+004 (top), H 1722+119 (middle), and PKS 2155-304 (bottom).



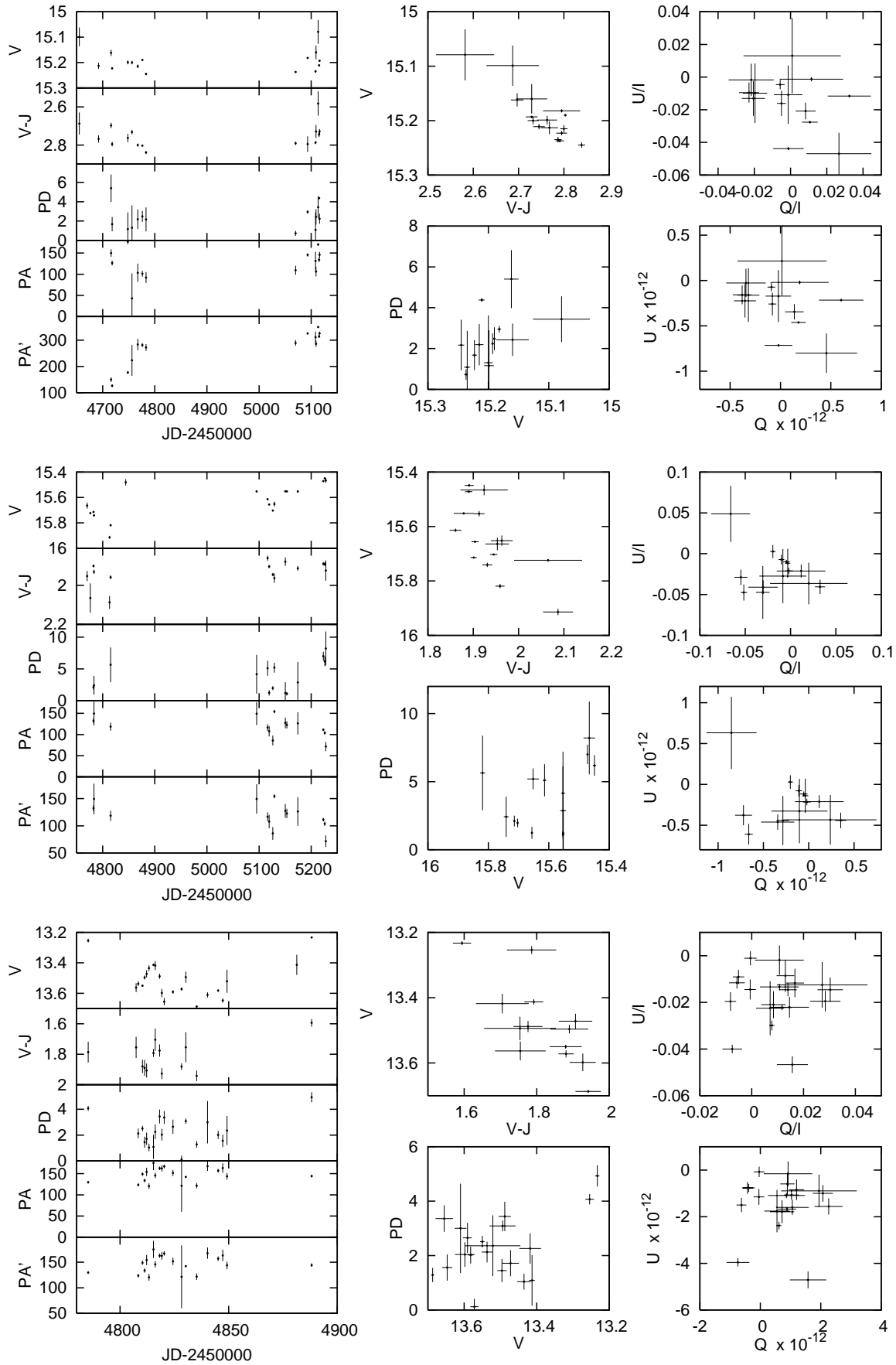


Fig. 32. 1ES 2344+514 (top), 1ES 0806+524 (middle), and Mrk 421 (bottom).

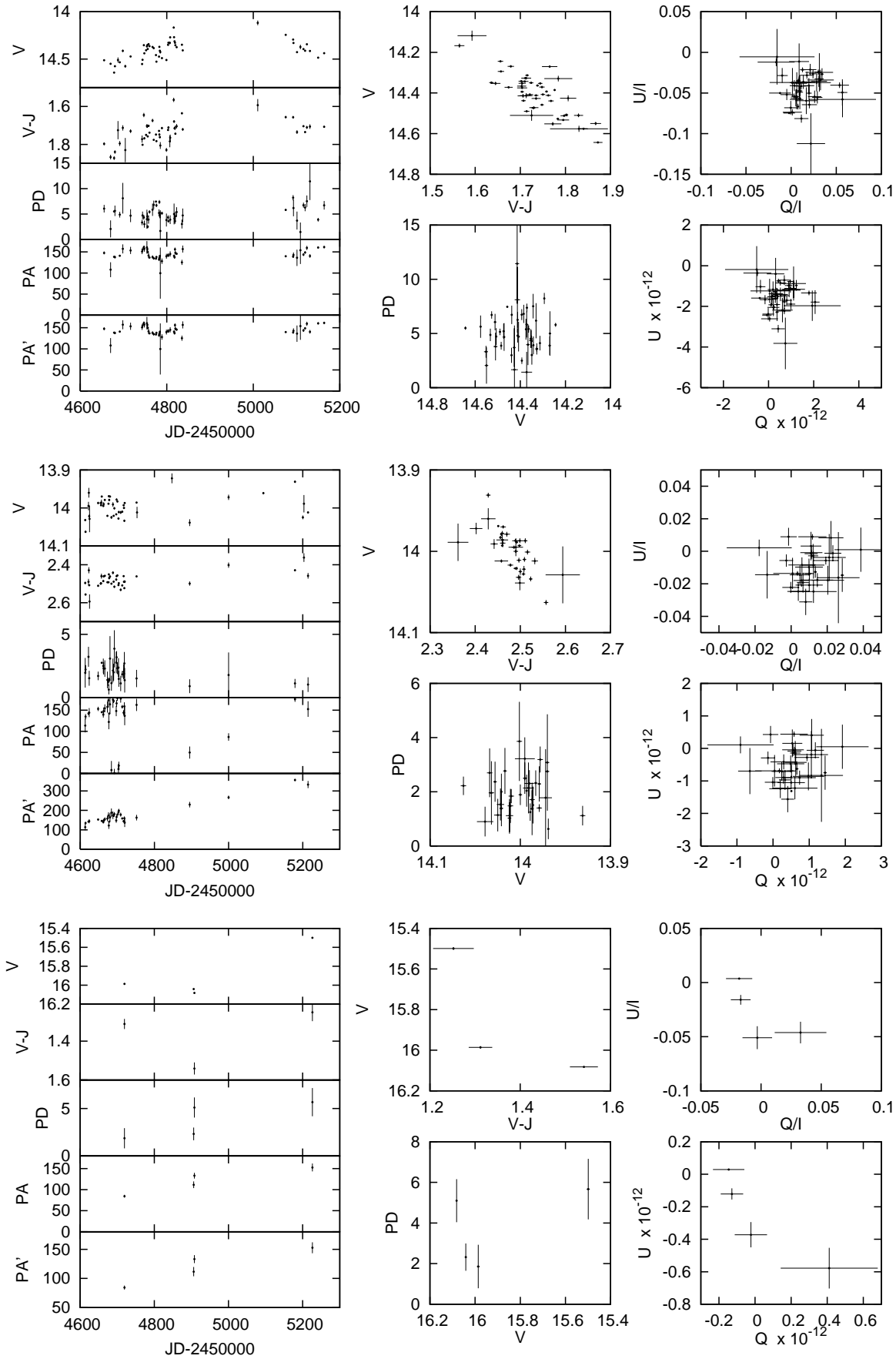


Fig. 33. 1ES 1959+650 (top), Mrk 501 (middle), and 1ES 0647+250 (bottom).

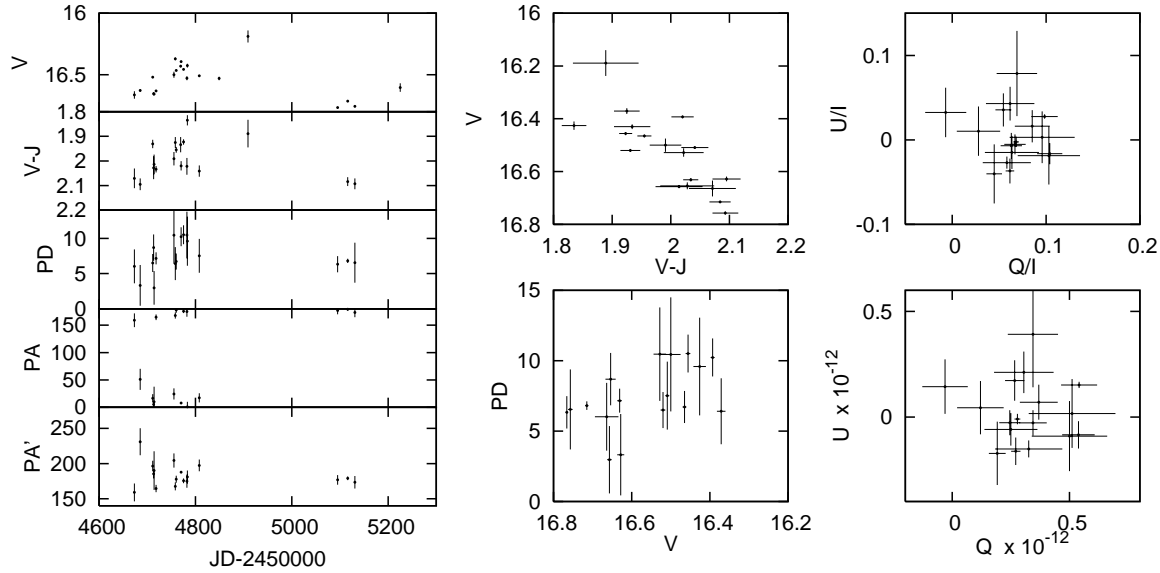


Fig. 34. 1ES 0323+022.

- Observatories, ed. P. Giommi, E. Massaro, & G. Palumbo (ASI Science Data Center), 133
- Giommi, P., Piranomonte, S., Perri, M., & Padovani, P. 2005, *A&A*, 434, 385
- González-Pérez, J. N., Kidger, M. R., & Martín-Luis, F. 2001, *AJ*, 122, 2055
- Griffiths, R. E., Wilson, A. S., Ward, M. J., Tapia, S., & Ulvestad, J. S. 1989, *MNRAS*, 240, 33
- Gu, M. F., Lee, C., Pak, S., Yim, H. S., & Fletcher, A. B. 2006, *A&A*, 450, 39
- Hagen-Thorn, V. A., Larionov, V. M., Jorstad, S. G., Arkharov, A. A., Hagen-Thorn, E. I., Efimova, N. V., Larionova, L. V., & Marscher, A. P. 2008, *ApJ*, 672, 40
- Hagen-Thorn, V. A. & Yakovleva, V. A. 1994, *MNRAS*, 269, 1069
- Halpern, J. P., Eracleous, M., & Mattox, J. R. 2003, *AJ*, 125, 572
- Hauser, M., Wagner, S., & Hagen, H. 2010, *The Astronomer's Telegram*, 2436, 1
- Healey, S. E., Romani, R. W., Cotter, G., Michelson, P. F., Schlafly, E. F., Readhead, A. C. S., Giommi, P., Chaty, S., Grenier, I. A., & Weintraub, L. C. 2008, *ApJS*, 175, 97
- Høg, E., Fabricius, C., Makarov, V. V., Urban, S., Corbin, T., Wycoff, G., Bastian, U., Schwekendiek, P., & Wicenec, A. 2000, *A&A*, 355, L27
- Hufnagel, B. R. & Bregman, J. N. 1992, *ApJ*, 386, 473
- Ikejiri, Y., Uemura, M., Sasada, M., Sakimoto, K., Ito, R., Yamanaka, M., Arai, A., Fukazawa, Y., Ohsugi, T., & Kawabata, K. S. 2009, arXiv 0912.3664
- Impey, C. D., Malkan, M. A., & Tapia, S. 1989, *ApJ*, 347, 96
- Impey, C. D. & Tapia, S. 1988, *ApJ*, 333, 666
- Jones, T. W., Rudnick, L., Fiedler, R. L., Aller, H. D., Aller, M. F., & Hodge, P. E. 1985, *ApJ*, 290, 627
- Jorstad, S. G., Marscher, A. P., Larionov, V. M., Agudo, I., Smith, P. S., Gurwell, M., Lähteenmäki, A., Tornikoski, M., et al. 2010, *ApJ*, 715, 362
- Kapanadze, B. Z. 2009, *MNRAS*, 398, 832
- Kataoka, J., Madejski, G., Sikora, M., Roming, P., Chester, M. M., Grupe, D., Tsubuku, Y., Sato, R., et al. 2008, *ApJ*, 672, 787
- Kataoka, J., Takahashi, T., Makino, F., Inoue, S., Madejski, G. M., Tashiro, M., Urry, C. M., & Kubo, H. 2000, *ApJ*, 528, 243
- Kataoka, J., Takahashi, T., Wagner, S. J., Iyomoto, N., Edwards, P. G., Hayashida, K., Inoue, S., Madejski, G. M., et al. 2001, *ApJ*, 560, 659
- Katarzyński, K., Sol, H., & Kus, A. 2001, *A&A*, 367, 809
- Kikuchi, S. 1988, *PASJ*, 40, 547
- Kikuchi, S., Mikami, Y., Inoue, M., Tabara, H., & Kato, T. 1988, *A&A*, 190, L8
- Kirk, J. G., Rieger, F. M., & Mastichiadis, A. 1998, *A&A*, 333, 452
- Kotilainen, J. K., Falomo, R., & Scarpa, R. 1998, *A&A*, 336, 479
- Larionov, V. M., Villata, M., & Raiteri, C. M. 2010, *A&A*, 510, A93
- Liu, F. K., Liu, B. F., & Xie, G. Z. 1997, *A&AS*, 123, 569
- Liu, F. K., Xie, G. Z., & Bai, J. M. 1995, *A&A*, 295, 1
- Marcha, M. J. M., Browne, I. W. A., Impey, C. D., & Smith, P. S. 1996, *MNRAS*, 281, 425
- Marscher, A. P., Jorstad, S. G., D'Arcangelo, F. D., Smith, P. S., Williams, G. G., Larionov, V. M., Oh, H., Olmstead, A. R., et al. 2008, *Nature*, 452, 966
- Marscher, A. P., Jorstad, S. G., Larionov, V. M., Aller, M. F., Aller, H. D., Lähteenmäki, A., Agudo, I., Smith, P. S., et al. 2010, *ApJL*, 710, L126
- Massaro, E., Giommi, P., Leto, C., Marchegiani, P., Maselli, A., Perri, M., Piranomonte, S., & Sclavi, S. 2009, *A&A*, 495, 691
- Massaro, E., Nesci, R., Maesano, M., Montagni, F., Trevese, D., Fiorucci, M., Tosti, G., Ghisellini, G., et al. 1996, *A&A*, 314, 87
- McGimsey, B. Q. & Miller, H. R. 1977, *AJ*, 82, 453
- Mead, A. R. G., Ballard, K. R., Brand, P. W. J. L., Hough, J. H., Brindle, C., & Bailey, J. A. 1990, *A&AS*, 83, 183
- Mickaelian, A. M., Hovhannisyan, L. R., Engels, D., Hagen, H., & Voges, W. 2006, *A&A*, 449, 425
- Miller, H. R. 1978, *ApJL*, 223, L67
- Moore, R. L., Angel, J. R. P., Duerr, R., Lebofsky, M. J., Wisniewski, W. Z., Rieke, G. H., Axon, D. J., Bailey, J.,

- Hough, J. M., & McGraw, J. T. 1982, *ApJ*, 260, 415
- Morton, T., Drake, A. J., Djorgovski, S. G., Glikman, E., Mahabal, A., Nugent, P., Baltay, C., Rabinowitz, D., et al. 2008, *The Astronomer's Telegram*, 1661, 1
- Nesci, R., Massaro, E., Maesano, M., Montagni, F., Sclavi, S., Venturi, T., Dallacasa, D., & D'Alessio, F. 2002, *AJ*, 124, 53
- Nieppola, E., Tornikoski, M., & Valtaoja, E. 2006, *A&A*, 445, 441
- Nilsson, K., Pasanen, M., Takalo, L. O., Lindfors, E., Berdyugin, A., Ciprini, S., & Pforr, J. 2007, *A&A*, 475, 199
- Nilsson, K., Pursimo, T., Sillanpää, A., Takalo, L. O., & Lindfors, E. 2008, *A&A*, 487, L29
- Padovani, P. 2007, *Ap&SS*, 309, 63
- Padovani, P., Perlman, E. S., Landt, H., Giommi, P., & Perri, M. 2003, *ApJ*, 588, 128
- Papadakis, I. E., Villata, M., & Raiteri, C. M. 2007, *A&A*, 470, 857
- Pian, E., Urry, C. M., Maraschi, L., Madejski, G., McHardy, I. M., Koratkar, A., Treves, A., Chiappetti, L., et al. 1999, *ApJ*, 521, 112
- Pica, A. J., Smith, A. G., Webb, J. R., Leacock, R. J., Clements, S., & Gombola, P. P. 1988, *AJ*, 96, 1215
- Qian, B., Tao, J., & Fan, J. 2002, *AJ*, 123, 678
- Raiteri, C. M., Villata, M., Aller, H. D., Aller, M. F., Heidt, J., Kurtanidze, O. M., Lanteri, L., Maesano, M., et al. 2001, *A&A*, 377, 396
- Raiteri, C. M., Villata, M., Ibrahimov, M. A., Larionov, V. M., Kadler, M., Aller, H. D., Aller, M. F., Kovalev, Y. Y., et al. 2005, *A&A*, 438, 39
- Raiteri, C. M., Villata, M., Larionov, V. M., Aller, M. F., Bach, U., Gurwell, M., Kurtanidze, O. M., Lähteenmäki, A., et al. 2008a, *A&A*, 480, 339
- Raiteri, C. M., Villata, M., Larionov, V. M., Gurwell, M. A., Chen, W. P., Kurtanidze, O. M., Aller, M. F., Böttcher, M., et al. 2008b, *A&A*, 491, 755
- Raiteri, C. M., Villata, M., Tosti, G., Fiorucci, M., Ghisellini, G., Takalo, L. O., Sillanpää, A., Valtaoja, E., et al. 1999, *A&A*, 352, 19
- Rani, B., Gupta, A. C., Strigachev, A., Bachev, R., Wiita, P. J., Semkov, E., Ovcharov, E., Mihov, B., et al. 2010, *MNRAS*, 404, 1992
- Sandage, A. 1972, *ApJ*, 178, 25
- Sasada, M., Uemura, M., Arai, A., Fukazawa, Y., Kawabata, K. S., Ohsugi, T., Yamashita, T., Isogai, M., et al. 2010, *PASJ*, 62, 645
- Sasada, M., Uemura, M., Arai, A., Fukazawa, Y., Kawabata, K. S., Ohsugi, T., Yamashita, T., Isogai, M., Sato, S., & Kino, M. 2008, *PASJ*, 60, L37
- Sasada, M., Uemura, M., Fukazawa, Y., Kawabata, K. S., Y., I., Itoh, R., Yamanaka, M., Sakimoto, K., et al. 2011, *PASJ*, in press (arXiv:1102.1856)
- Sbarufatti, B., Treves, A., Falomo, R., Heidt, J., Kotilainen, J., & Scarpa, R. 2006, *AJ*, 132, 1
- Scarpa, R., Urry, C. M., Falomo, R., Pesce, J. E., & Treves, A. 2000, *ApJ*, 532, 740
- Schlegel, D. J., Finkbeiner, D. P., & Davis, M. 1998, *ApJ*, 500, 525
- Sikora, M., Begelman, M. C., & Rees, M. J. 1994, *ApJ*, 421, 153
- Sillanpää, A., Teerikorpi, P., Haarala, S., Korhonen, T., Efimov, I. S., & Shakhovskoi, N. M. 1985, *A&A*, 147, 67
- Skiff, B. A. 2007, *VizieR Online Data Catalog*, 2277, 0
- Skrutskie, M. F., Cutri, R. M., Stiening, R., Weinberg, M. D., Schneider, S., Carpenter, J. M., Beichman, C., Capps, R., et al. 2006, *AJ*, 131, 1163
- Smith, P. S., Balonek, T. J., Elston, R., & Heckert, P. A. 1987, *ApJS*, 64, 459
- Smith, P. S., Balonek, T. J., Heckert, P. A., & Elston, R. 1986, *ApJ*, 305, 484
- Smith, P. S., Schmidt, G. D., & Allen, R. G. 1993, *ApJ*, 409, 604
- Soldi, S., Türler, M., Paltani, S., Aller, H. D., Aller, M. F., Burki, G., Chernyakova, M., Lähteenmäki, A., et al. 2008, *A&A*, 486, 411
- Souchay, J., Andrei, A. H., Barache, C., Bouquillon, S., Gontier, A., Lambert, S. B., Le Poncin-Lafitte, C., Taris, F., et al. 2009, *A&A*, 494, 799
- Spada, M., Ghisellini, G., Lazzati, D., & Celotti, A. 2001, *MNRAS*, 325, 1559
- Takahashi, T., Kataoka, J., Madejski, G., Mattox, J., Urry, C. M., Wagner, S., Aharonian, F., Catanese, M., et al. 2000, *ApJL*, 542, L105
- Takahashi, T., Tashiro, M., Madejski, G., Kubo, H., Kamae, T., Kataoka, J., Kii, T., Makino, F., Makishima, K., & Yamasaki, N. 1996, *ApJL*, 470, L89
- Takalo, L. O., Kidger, M., de Diego, J. A., Sillanpää, A., Pirola, V., & Terasranta, H. 1990, *A&AS*, 83, 459
- Takalo, L. O., Sillanpää, A., Valtaoja, E., Katajainen, S., Nilsson, K., Pursimo, T., Heinaemaeki, P., Villata, M., et al. 1998, *A&AS*, 129, 577
- Tapia, S., Craine, E. R., Gearhart, M. R., Pacht, E., & Kraus, J. 1977, *ApJL*, 215, L71
- Tosti, G., Fiorucci, M., Luciani, M., Efimov, Y. S., Shakhovskoy, N. M., Valtaoja, E., Terasranta, H., Sillanpää, A., et al. 1998, *A&A*, 339, 41
- Tramacere, A. & Rea, N. 2009, *The Astronomer's Telegram*, 1888, 1
- Uemura, M., Kawabata, K., Sasada, M., Ikejiri, Y., Sakimoto, K., Itoh, R., Yamanaka, M., Ohsugi, T., Sato, S., & Kino, M. 2010, *PASJ*, 62, 1
- Ulrich, M., Maraschi, L., & Urry, C. M. 1997, *ARA&A*, 35, 445
- Urry, C. M., Scarpa, R., O'Dowd, M., Falomo, R., Pesce, J. E., & Treves, A. 2000, *ApJ*, 532, 816
- Urry, C. M., Treves, A., Maraschi, L., Marshall, H. L., Kii, T., Madejski, G., Penton, S., Pesce, J. E., et al. 1997, *ApJ*, 486, 799
- Vagnetti, F., Treves, D., & Nesci, R. 2003, *ApJ*, 590, 123
- Véron-Cetty, M. & Véron, P. 2010, *A&A*, 518, A10+
- Villata, M., Raiteri, C. M., Balonek, T. J., Aller, M. F., Jorstad, S. G., Kurtanidze, O. M., Nicastro, F., Nilsson, K., et al. 2006a, *A&A*, 453, 817
- Villata, M., Raiteri, C. M., Balonek, T. J., Aller, M. F., Jorstad, S. G., Kurtanidze, O. M., Nicastro, F., Nilsson, K., et al. 2006b, *A&A*, 453, 817
- Villata, M., Raiteri, C. M., Kurtanidze, O. M., Nikolashvili, M. G., Ibrahimov, M. A., Papadakis, I. E., Tosti, G., Hroch, F., et al. 2004, *A&A*, 421, 103
- Villata, M., Raiteri, C. M., Kurtanidze, O. M., Nikolashvili, M. G., Ibrahimov, M. A., Papadakis, I. E., Tsinganos, K., Sadakane, K., et al. 2002, *A&A*, 390, 407
- Villata, M., Raiteri, C. M., Lanteri, L., Sobrito, G., & Cavallone, M. 1998, *A&AS*, 130, 305
- Villata, M., Raiteri, C. M., Popescu, M. D., Sobrito, G., De Francesco, G., Lanteri, L., & Ostorero, L. 2000, *A&AS*, 144, 481

- Villforth, C., Nilsson, K., Heidt, J., Takalo, L. O., Pursimo, T., Berdyugin, A., Lindfors, E., Pasanen, M., et al. 2010, *MNRAS*, 402, 2087
- Watanabe, M., Nakaya, H., Yamamuro, T., Zenno, T., Ishii, M., Okada, M., Yamazaki, A., Yamanaka, Y., et al. 2005, *PASP*, 117, 870
- Webb, J. R., Carini, M. T., Clements, S., Fajardo, S., Gombola, P. P., Leacock, R. J., Sadun, A. C., & Smith, A. G. 1990, *AJ*, 100, 1452
- Wills, B. J., Wills, D., Breger, M., Antonucci, R. R. J., & Barvainis, R. 1992, *ApJ*, 398, 454
- Wu, J., Zhou, X., & Ma, J. 2007a, in *The Central Engine of Active Galactic Nuclei*, ed. L. C. Ho & J.-W. Wang Vol. 373 of *Astronomical Society of the Pacific Conference Series*(. *ASP Conference Series*, Vol. 373), 199
- Wu, J., Zhou, X., Ma, J., Wu, Z., Jiang, Z., & Chen, J. 2007b, *AJ*, 133, 1599
- Xie, G. Z., Zhou, S. B., Dai, B. Z., Liang, E. W., Li, K. H., Bai, J. M., Xing, S. Y., & Liu, W. W. 2002, *MNRAS*, 329, 689
- Yanny, B., York, D. G., & Gallagher, J. S. 1989, *ApJ*, 338, 735
- Yoshida, S., Ohkura, N., Nakashima, Y., Greaves, J., & Bouma, R. J. 2008, *Central Bureau Electronic Telegrams*, 1249, 1
- Zekl, H., Klare, G., & Appenzeller, I. 1981, *A&A*, 103, 342
- Zhang, X., Zheng, Y. G., Zhang, H. J., & Hu, S. M. 2008, *ApJS*, 174, 111
- Zhang, Y. H., Treves, A., Celotti, A., Chiappetti, L., Fossati, G., Ghisellini, G., Maraschi, L., Pian, E., Tagliaferri, G., & Tavecchio, F. 2002, *ApJ*, 572, 762
- Zhou, H., Wang, T., Yuan, W., Shan, H., Komossa, S., Lu, H., Liu, Y., Xu, D., Bai, J. M., & Jiang, D. R. 2007, *ApJL*, 658, L13